

MSc Thesis

Uncertainty in aviation emissions inventories:
Sources and improvements

Harry Aldridge

MSc Thesis

Uncertainty in aviation emissions inventories: Sources and improvements

by

Harry Aldridge

to obtain the degree of Master of Science
at the Delft University of Technology,
to be defended publicly on Monday April 11, 2022 at 9:30 AM.

Student number: 4490452
Project duration: September 7, 2020 – April 11, 2022
Thesis committee: Dr. ir. I. Dedoussi, TU Delft, Supervisor
Prof. dr. ir. M. Snellen, TU Delft, Chair
Dr. ir. R. Vos, TU Delft, Examiner

An electronic version of this thesis is available at <http://repository.tudelft.nl/>.

Acknowledgements

This report represents the culmination of my academic career at TU Delft. Being able to conclude my studies with a thesis on aviation emissions has been important to me, as the reduction of our environmental impact may be one of the most important themes in engineering of my generation. Working full-time on this thesis for over a year has required the application of all of the skills and knowledge acquired throughout my BSc and MSc in aerospace engineering. It has not been an easy journey by any means, and the COVID-19 pandemic of the past two years has only made it more of a challenge. However, there are some people I would like to acknowledge, without whom I would not have made it to where I am now.

First of all I would like to thank my supervisor, Dr. Irene Dedoussi, for your guidance and patience. Your advice and feedback has been indispensable in giving direction to my research. Our weekly Zoom meetings were also my most consistent social interactions for a period during lockdown. I would also like to thank Flavio Quadros for answering all of my AEIC-related questions, as well as Jin Maruhashi for always being available to help me troubleshoot my issues with Cartesius or Snellius: This work was carried out on the Dutch national e-infrastructure with the support of SURF Cooperative.

I next want to thank my family – Mum, Dad and James – for the support from afar. This thesis is ultimately a product of all of the opportunities you have afforded me to develop myself. It has been a long process, but thank you for trusting it, and reminding me to enjoy being a student. I am looking forward to finally coming home.

Of course I need to express my gratitude to all of the friends who have been close to me during my time here – you know who you are. You have all made Delft genuinely feel like home. Special shout out to Mauritz and Thibaud, Flores, Val and the rest of the boys and girls at the library for knowing not to ask about my thesis, and always being up for a beer or three. Lastly, an extended thank you to Edouard and Chris for being the closest thing to family out here in Europe. It is safe to say I have a network of friends for life.

Finally, I want to thank Noor, for being tirelessly motivational and understanding, and whose contribution to the completion of this thesis cannot be overstated. Watching you progress through your thesis, and subsequently establish your career has been nothing short of inspiring. Above all, thank you for putting up with me, feeding me and for being an absolute comfort.

*Harry Aldridge
Delft, April 2022*

Abstract

Despite the contraction in global air traffic due to the COVID-19 pandemic, the aviation sector has otherwise experienced constant growth over the last few decades. The growth of the aviation sector is closely linked with both global economic growth and increasing environmental impact. Curbing emissions thus becomes a challenge; policymakers are tasked with mitigating aviation's environmental impacts without totally constraining its growth.

The approach to sustainable aviation requires effective policy and regulation, informed by accurate environmental research. Aviation emissions inventories develop an account of the emissions of pollutant species due to aviation, thus forming the basis of any environmental assessment. However, due to the complex physical processes being modelled, the calculation methodologies of existing emissions inventories are based on engineering and operational assumptions that introduce some degree of inherent uncertainty. In terms of robust policy-making, it is especially necessary to quantify this uncertainty.

The Aviation Emissions Inventory Code (AEIC) was developed as an open source tool capable of rapid estimation of global aviation emissions. To reduce computational complexity, simplifications are made, which are accounted for by uncertainty distributions. The rapid nature of AEIC's modelling lends itself to methods of uncertainty quantification that the high computational intensity of traditional models prohibit. This study aims to investigate the sources of uncertainty in global, full-flight estimates of fuelburn, NO_x, HC and CO, using AEIC, with the ultimate goal of improving the uncertainty of the input space.

This process begins with an uncertainty propagation, to understand quantify the uncertainty in the outputs. From here a global sensitivity analysis in the form of a Sobol analysis is conducted to identify the sources of uncertainty. The results of this show that uncertainty can largely be attributed to a few key inputs. The Base of Aircraft Data (BADA) Drag and Fuel Flow corrective multipliers contribute significantly to uncertainty across fuelburn and emissions estimates. Across the emitted species, variance is driven by the uncertainty around their respective Emissions Index (EI). Fuelburn and NO_x are highly sensitive to uncertainty in Takeoff Weight (TOW), while the sensitivity to low thrust of CO and HC make them susceptible to the uncertainties in Taxi Thrust and Arrival Inefficiency.

Identifying key sources of uncertainty allows for a targeted approach to improving input uncertainty modelling. Recent publication of flight track data by EUROCONTROL presents the opportunity to perform a focused revision of lateral flight inefficiencies. Based on the method of Reynolds (2008), EU flight inefficiencies in departure, enroute and arrival are reassessed, with the addition of intercontinental enroute inefficiencies. Compared, the nominal figures for departure and arrival are 15% and 40% lower than original values, respectively. The revised intra-EU enroute inefficiency demonstrates lower inefficiencies for enroute flight shorter than 370 NM, and higher inefficiencies for longer enroute flight. The intercontinental enroute study suggests an average inefficiency of 2.2% of the flight's enroute Great Circle distance, plus 37.41 NM. Most significantly, the resulting distributions demonstrate the same positive skew of the Reynolds (2008) study, which could not be accurately approximated from literature. Thus, curve fitting the data, and implementing the revised distributions results in a more realistic stochastic description of variation in inefficiency.

Finally, global fuelburn and emissions were estimated for each updated variable, keeping all others constant, to isolate and investigate the impact of each. The nominal case, the lower values of EU departure and arrival inefficiencies logically resulted in a decrease in fuelburn and emissions. This effect was largest in CO and HC where their sensitivity to arrival inefficiency saw reductions in nominal EU emissions of 3.92% and 7.51%, respectively. Both enroute inefficiencies served to increase estimates of fuelburn and emissions. In terms of uncertainty propagation, the effect of accurately modelling the distributions becomes apparent. The positively skewed distributions serve to shift output distributions left: EU departure and arrival inefficiencies demonstrate a larger decrease in fuelburn and emissions, while the increase due to enroute inefficiencies is reduced (in some cases negated). Despite not reducing uncertainty, input uncertainty is more accurately modelled which should improve the reliability of AEIC's output, without sacrificing computational expense.

Ultimately, this process demonstrates the identification and improvement of a key source of uncertainty in an aviation emissions inventory. The other significant contributors to uncertainty identified in this study naturally lead to recommendations for future studies.

List of Figures

3.1	Overview of the AEIC emissions modelling process	8
4.1	Uncertainty Quantification framework	15
4.2	Scatterplots of fuelburn versus drag and CO ₂ EI	17
4.3	The mean values of fuelburn along the x-axis	17
5.1	Flowchart of Monte Carlo process	21
5.2	Results of Monte Carlo uncertainty propagation	23
6.1	Flowchart of Sobol analysis process	26
6.2	Flowchart of Sobol analysis process	26
6.3	First-order Sobol indices for CO ₂ -equivalent from Stettler et al. (2011) [1]	27
6.4	First-order Sobol indices for total PM _{2.5} from Stettler et al. (2011) [1]	27
6.5	Total-order Sobol indices for CO ₂ -equivalent from Stettler et al. (2011) [2]	27
6.6	Total-order Sobol indices for total PM _{2.5} from Stettler et al. (2011) [2]	27
6.7	First- and total-order Sobol indices for CO ₂ -eq	27
6.8	First- and total-order Sobol indices for non-volatile PM	27
6.9	First and total-order Sobol indices for Fuelburn	29
6.10	First and total-order Sobol indices for NO _x	29
6.11	First and total-order Sobol indices for CO	30
6.12	First and total-order Sobol indices for HC	30
7.1	Departure, enroute and arrival inefficiencies compared to the great circle path [3]	32
7.2	Distribution of EU arrival inefficiencies from AEIC, based on results of Reynolds (2008)	32
7.3	EU arrival inefficiencies from Reynolds (2008) [3]	32
7.4	Region in which AEIC applies EU inefficiencies	33
7.5	Flowchart of stochastic mapping of inefficiency across EU and US variables	33
7.6	Comparison of flight point data and Great Circle route between Amsterdam Schiphol and London Heathrow	35
7.7	Illustration of Terminal Area (TA) radius range	35
7.8	Ground tracks of Swiss A320-family flights analysed by Reynolds (2008) [3]	36
7.9	Ground tracks of Swiss A320-family flights from the EUROCONTROL R&D data archive	36
7.10	European departure inefficiencies from Reynolds (2008) [3]	37
7.11	Swiss Airlines A320-family departure inefficiencies from March 2015	37
7.12	Intra-EU Enroute inefficiencies from Reynolds (2008) [3]	37
7.13	Swiss Airlines A320-family enroute inefficiencies from March 2015	37
7.14	European arrival inefficiencies from Reynolds (2008) [3]	38
7.15	Swiss Airlines A320-family arrival inefficiencies from March 2015	38
7.16	Ground tracks of domestic flights originating from 9 major US airports [3]	38
7.17	Ground tracks of flights originating or arriving at the 9 major US airports	38
7.18	Distance from departure airport to first flight point in the US	39
7.19	Flight level of the first flight point after departure in the US	39
7.20	Distance from last flight point to destination airport in the US	39
7.21	Flight level of the last flight point before arrival in the US	39
7.22	Flights with sufficient TA data outside of the European bounding box	39
7.23	Actual trajectories between LHR-GEN from Enhanced Flight Efficiency Indicators (EFEI) (2004) [4]	40
7.24	Actual trajectories between LHR-GEN from March 2015	40
7.25	Actual trajectories between ORY-NCE from EFEI (2004) [4]	40

7.26	Actual trajectories between ORY-NCE from March 2015	40
7.27	Actual trajectories between BHX-CPH from EFEI (2004) [4]	41
7.28	Actual trajectories between BHX-CPH from March 2015	41
7.29	Distribution of extra distance flown during EU departures	42
7.30	Extra distance flown enroute against great circle routes for intra-EU flights	43
7.31	Extra distance flown against great circle routes for intercontinental flights	43
7.32	Distribution of extra distance flown during EU arrivals	44
7.33	Sensitivity of departure inefficiencies to TA radius window	45
7.34	Sensitivity of arrival inefficiencies to TA radius window	45
7.35	Sensitivity of intra-EU enroute inefficiencies	46
7.36	Sensitivity of intercontinental enroute inefficiencies	46
7.37	Probability distribution fitting to departure inefficiencies	47
7.38	Probability distribution fitting to arrival inefficiencies	48
7.39	Comparison of updated and original departure inefficiency distributions	48
7.40	Comparison of updated and original arrival inefficiency distributions	48
7.41	Probability distribution fitting to Intra-EU Enroute inefficiencies	49
7.42	Probability distribution fitting to intercontinental enroute inefficiencies	49
7.43	Comparison of updated and original Intra-EU Enroute inefficiency distributions	50
7.44	Comparison of updated and original intercontinental enroute inefficiency distributions	50
8.1	Distribution comparing the Baseline and Total estimates of global fuelburn, NO _x , CO and HC	52
9.1	Distribution of intercontinental FL cruise using 1 month of EUROCONTROL flight data	60
B.1	Second-order Sobol indices for Fuelburn	63
B.2	Second-order Sobol indices for NO _x	64
B.3	Second-order Sobol indices for CO	65
B.4	Second-order Sobol indices for HC	66

List of Tables

3.1	Overview of LTO, TIMs and thrust levels	10
3.2	LTO fuel flow uncertainty multiplier	10
3.3	TOW and cruise altitude uncertainty distributions	11
3.4	Overview EI uncertainty distributions for different emissions species	12
3.5	Overview of lateral inefficiency uncertainty distributions, per region	13
3.6	BADA drag and SFC uncertainty distributions	13
3.7	Summary of global aviation fuelburn and emissions estimated by AEIC, as published by Simone et al. (2013) [5]	13
5.1	Summary of global civil aviation fuelburn and emissions estimated by AEIC	22
6.1	Summary of first-order indices for fuelburn, NO _x CO and HC	28
7.1	Overview of lateral inefficiency uncertainty distributions, per region	32
7.2	Comparison between values calculated in the EFEI (2004) study and this study	41
7.3	Number of departures and arrivals analysed in each case	45
7.4	Number of enroute flight portions analysed in each case	46
7.5	Comparison of original and updated nominal values for inefficiency variables	46
7.6	Comparison of original and updated distributions of inefficiency variables	47
8.1	Overview of inefficiencies used per simulation case	51
8.2	Relative difference to EU fuelburn estimates due to updated EU inefficiencies	53
8.3	Relative difference to rest-of-world fuelburn estimates due to updated intercontinental enroute inefficiency	53
8.4	Relative difference to EU NO _x estimates due to updated EU inefficiencies	54
8.5	Relative difference to rest-of-world NO _x estimates due to updated intercontinental enroute inefficiency	54
8.6	Relative difference to EU CO estimates due to updated EU inefficiencies	55
8.7	Relative difference to rest-of-world CO estimates due to updated intercontinental enroute inefficiency	55
8.8	Relative difference to EU HC estimates due to updated EU inefficiencies	55
8.9	Relative difference to rest-of-world HC estimates due to updated intercontinental enroute inefficiency	56
9.1	Summary of first-order indices for fuelburn, NO _x CO and HC	58
9.2	Summary of revised lateral flight inefficiency variables	58
C.1	Relative difference to global fuelburn estimates due to all updated inefficiencies	67
C.2	Relative difference to global NO _x estimates for updated inefficiencies	67
C.3	Relative difference to global CO estimates for updated inefficiencies	67
C.4	Relative difference to global HC estimates for updated inefficiencies	68

List of Abbreviations

***.PTF** Performance Table Files.

AEDT Aviation Environmental Design Tool.

AEIC Aviation Emissions Inventory Code.

AFE Above Field Elevation.

AIC Akaike information criterion.

AMS Amsterdam Schiphol Airport.

APU Auxiliary Power Unit.

ATFM Air Traffic Flow Management.

ATM Air Traffic Management.

BADA Base of Aircraft Data.

BFFM2 Boeing Fuel Flow Method 2.

BHX Birmingham Airport.

CAEP Committee on Aviation Environmental Protection.

CCD Climb, Cruise and Descent.

CORSIA Carbon Offsetting and Reduction Scheme for International Aviation.

CPH Copenhagen Airport.

CRCO Central Route Charges Office.

DEL Indira Gandhi International Airport.

EDB Engine Emissions Databank.

EEA European Environmental Agency.

EFEI Enhanced Flight Efficiency Indicators.

EI Emissions Index.

ETMS Enhanced Traffic Management System.

EWR Newark Liberty International Airport.

FAST Future Civil Aviation Scenario Software Tool.

FDR Flight Data Recorder.

FEAT Fuel Estimation in Air Transportation.

FL Flight Level.

FSC Fuel Sulphur Content.

GCD Great Circle distance.

GEN Geneva Airport.

GEOS 5 Goddard Earth Observing System Model 5.

GSE Ground Service Equipment.

ICAO International Civil Aviation Organisation.

IFR Instrument flight rules.

IMPACT Integrated Aircraft Noise and Fuel Burn and Emissions Modelling Platform.

IPCC Intergovernmental Panel on Climate Change.

KDE kernel density estimation.

LHR London Heathrow Airport.

LTO Landing and Take-off.

MLE maximum likelihood estimation.

NCE Nice Cote d'Azur Airport.

NM Network Manager.

NM Nautical miles.

OAG Official Airline Guide.

OEW Operating Empty Weight.

ORY Paris Orly Airport.

PER Perth Airport.

PM Particulate Matter.

ROCD Rate of Climb/Descent.

SAGE System for Assessing Aviation's Global Emissions.

SARPs Standards and Recommended Practices.

SFC Specific Fuel Consumption.

SFO San Francisco International Airport.

SIN Singapore Changi Airport.

TA Terminal Area.

TAS True Airspeed.

TIMs Times-in-mode.

TOW Takeoff Weight.

XD Extra Distance.

Contents

Acknowledgements	iii
Abstract	v
List of Figures	vii
List of Tables	ix
1 Introduction	1
2 Thesis Objective	3
2.1 Motivation	3
2.2 Research Objective	4
2.2.1 Research Question(s)	5
3 Aviation Emissions Inventory Code	7
3.1 Tier 3 Aviation Emissions Inventories	7
3.2 The AEIC	7
3.3 Flight Movements.	9
3.3.1 Flight Scheduling	9
3.3.2 Flight Track Generation	9
3.4 Aircraft Performance	9
3.4.1 LTO	9
3.4.2 CCD	10
3.5 Emissions Calculations	11
3.6 Corrective Adjustments	12
3.6.1 Lateral Inefficiencies.	12
3.6.2 BADA corrections	13
3.7 Application to 2005 Aviation Activity	13
4 Uncertainty Quantification	15
4.1 General Framework	15
4.2 Sensitivity Analysis	16
4.3 Sobol Analysis.	18
4.3.1 Sobol Decomposition	18
4.3.2 Sobol Indices.	18
5 Uncertainty Propagation	21
5.1 Methodology	21
5.1.1 Computational expense	22
5.2 Results	22
6 Sobol Analysis	25
6.1 Methodology	25
6.1.1 Computational Expense	26
6.2 Comparison With Existing Literature	26
6.3 Results	28
6.3.1 Fuelburn.	28
6.3.2 NO _x	29
6.3.3 CO	30
6.3.4 HC.	30

7	Improving Sources of Uncertainty	31
7.1	Improvement Opportunities	31
7.2	Lateral Flight Inefficiencies	31
7.3	Methodology	34
7.3.1	EUROCONTROL R&D data archive	34
7.3.2	Calculating Lateral Inefficiencies	34
7.3.3	Modifications	35
7.4	Comparisons With Existing Literature	36
7.4.1	Reynolds (2008)	36
7.4.2	EUROCONTROL (2004)	40
7.5	Results	41
7.5.1	Departure	42
7.5.2	Enroute	42
7.5.3	Arrival	44
7.6	Sensitivity Analysis	45
7.7	Implementation	46
7.7.1	Departure and Arrival Inefficiencies	47
7.7.2	Enroute Inefficiencies	48
8	Re-propagation of Updated Inputs	51
8.1	Methodology	51
8.2	Results	51
8.2.1	Fuelburn	53
8.2.2	NO _x	54
8.2.3	CO	55
8.2.4	HC	55
9	Conclusions and Recommendations	57
9.1	Conclusions	57
9.2	Recommendations for Future Work	59
A	Variance Identity	61
B	Second-order Sobol Indices	63
B.1	Fuelburn	63
B.2	NO _x	64
B.3	CO	65
B.4	HC	66
C	Re-propagation Results for Global Fuelburn and Emissions Estimates	67
C.1	Fuelburn	67
C.2	NO _x	67
C.3	CO	67
C.4	HC	68
	Bibliography	69

Introduction

In the context of reducing aviation's impact on the environment, the aviation sector faces a significant challenge, summarised in International Civil Aviation Organisation (ICAO)'s environmental goals. Aviation emissions inventories play an intrinsic role in environmental assessments, as well as in the tracking and forecasting of aviation's environmental goals. Ultimately, accurate profiling of aviation's emissions form the basis of the development of effective environmental policies and informed targets. Thus, when considering the need for confident emissions estimates, understanding the sources of uncertainty in aviation emissions inventories is of significant importance.

Uncertainty quantification typically involves computationally expensive methods. When coupled with the high computational complexity of current aviation emissions inventories, the application of uncertainty quantification methods becomes prohibitive. The Aviation Emissions Inventory Code (AEIC) model is a rapid estimation tool for aviation emissions, capable of reproducing global, annual fuelburn and emissions estimates from civil aviation in an hour. It is based on similar methodologies used in traditional "bottom-up" aviation emissions models, however compared to these high-fidelity models, AEIC removes a considerable portion of computational intensity by way of modelling simplifications. As an open source code which does not suffer from computational requirements or data restrictions, it presents itself as an accessible tool for uncertainty quantification methods. This study aims to perform a complete uncertainty quantification cycle of full-flight aviation emissions estimates at a global scale, using the AEIC.

The overall objectives of this thesis are outlined in Chapter 2. This chapter contextualises this research and includes motivation, establishes the research objective, and states the research questions that this thesis ultimately aims to answer. Background on the AEIC model is detailed in Chapter 3, where specific attention is placed on the uncertain input parameters. Chapter 4 presents background on uncertainty quantification, establishes the framework that this thesis will follow, and covers theory on the global sensitivity analysis methodology. From here, each successive chapter represents one process in the uncertainty quantification framework, and effectively builds upon the results of the preceding chapter. Chapter 5 presents the first set of results in this thesis: uncertainty propagation in AEIC is quantified. The results of this chapter set a baseline to which other results can be compared. Chapter 6 outlines the global sensitivity analysis of AEIC, in which inputs which contribute significantly to uncertainty are identified. Identifying key sources of uncertainty allows for a focused revision of their associated distributions: this is performed in Chapter 7, where the uncertainty distributions of key inputs are improved in a data-driven study, and directly implemented into AEIC. To investigate the effects of the revised inputs, Chapter 8 follows the re-propagation of uncertainty in AEIC, thus completing a full iteration of the established uncertainty quantification framework. Finally conclusions will be drawn and recommendations proposed in Chapter 9.

2

Thesis Objective

This chapter will present the space of research that this thesis is concerned with. This will begin with outlining the motivation behind the research, based on a literature review of state-of-the-art aviation emissions inventories, and their associated uncertainty. From this, the research objective is developed. Finally, the research question(s) that this thesis aims to answer are presented.

2.1. Motivation

The aviation sector has been experiencing high growth rates over the past decade. Despite the COVID-19 pandemic, which saw passenger demand fall over 60%, air traffic is forecast to have a full recovery by 2023. The growth of air traffic supports increased connectivity, benefiting the flow of goods, people, and capital, and is therefore closely linked to global economic growth [6–8]. However with increased air traffic, the negative impacts of aviation are also magnified. Aviation is currently responsible for 2-3% of global CO₂ emissions, however when considering all aviation pollutant species, aviation is responsible for 5% of total anthropogenic radiative forcing [9–13]. Coupled with the consistent increase of passenger demand, aviation emissions show no signs of decreasing without policy intervention.

In terms of climate change policy, the emissions of international aviation are excluded from the emission limits set by the Kyoto Protocol. Instead, the responsibility of international aviation emissions lies with the ICAO [14–16].

In 1999 the Intergovernmental Panel on Climate Change (IPCC) produced its first report for a specific industrial subsector; *Aviation and the Global Atmosphere*. This Special Report was produced at the request of the ICAO, with intent to assess the impact of global aviation emissions on the climate. The initial report estimated that total fuel burn in 2050 would be somewhere between 1.6-9.4 times greater than in 1990. Published only 20 years ago, it demonstrated the significant uncertainty associated with emissions estimations, for what was at the time, the most comprehensive study on the subject [17].

ICAO has since established 19 Annexes which outline the Standards and Recommended Practices (SARPs) of international civil aviation. As a result, in 2010 the aviation sector effectively become one of the first transport industries to launch global climate change goals in the context of the Paris Agreement [18]. Environmental protection is addressed in ICAO Annex 16, volumes II-IV, which contains certification standards for aircraft engine emissions, namely NO_x, HC, CO and Particulate Matter (PM) [19]. Most recently ICAO established the Carbon Offsetting and Reduction Scheme for International Aviation (CORSIA). CORSIA is a global market-based environmental solution to attaining carbon neutral growth in the aviation sector from 2020, requiring operators to purchase carbon credits to offset their emissions [16]. The ultimate goal is to halve the aviation carbon emissions of 2005 by 2050 [18].

The approach to sustainable aviation is a challenge which requires ambitious goals, achieved through rational policy, which is informed by environmental assessments. Aviation emissions inventories detail the emissions profile of pollutants discharged into the atmosphere due to aviation, and form the basis of environmental assessments. The aviation emissions inventories that support and inform the policy-making processes of the ICAO's Committee on Aviation Environmental Protection (CAEP), are high-fidelity, physics-based emissions models. These all follow much the same "bottom-up" modelling process, however differ slightly in the sources used to inform input values. Thus, even high-fidelity models are based on assumptions regarding input parameters. These sources of uncertainty manifest themselves as uncertainties in the output [20]. In the context of understanding underlying atmospheric processes, assessing the sector's contribution

to global emissions, and designing emission mitigation approaches, it is especially necessary to have minimal uncertainty in global emissions inventories.

Reducing the uncertainty in any model's output begins with characterising sources of uncertainty and their effect on model response. Understanding key model sensitivities effectively identifies areas within a model where uncertainty can be reduced: these key inputs become priorities for model development and future research [1, 20, 21]. Improving the representation of uncertain variables to more closely reflect actual behaviour aid in the development of more detailed and robust model response [22].

The quantification of uncertainty and sensitivities in aviation emissions inventories is an area that has not been sufficiently explored. The investigations of uncertainty in aviation emissions inventories have typically only been concerned with Landing and Take-off (LTO) emissions, at the local scale [1, 20, 21, 23]. When assessing aviation's global impacts, uncertainty quantification of full-flight emissions estimates becomes especially important. However, full-flight aviation emissions calculations from traditional emissions models are typically too computationally intense to produce the number of samples required by many uncertainty quantification and sensitivity analysis methods. For instance, surrogate modelling of Aviation Environmental Design Tool (AEDT) was required to perform the uncertainty and sensitivity analyses of the tool's LTO emissions estimates [20, 24].

The AEIC was developed as an open-source, rapid estimation tool for simulating global civil aviation emissions. It incorporates many of the same inputs and methodologies of more traditional high-fidelity models where possible. In the order of an hour, the AEIC can reproduce global annual emissions estimates from civil aviation on a single core. As a computationally cheap model, it presents a suitable tool for the uncertainty quantification of global, full flight aviation emissions inventories. Furthermore, as an open-source code, AEIC lends itself to input manipulation where improvements to sources of uncertainty can be investigated.

2.2. Research Objective

The study by Simone et al. (2013), detailing the development of the AEIC, demonstrates AEIC as an appropriate tool to quantify the uncertainty in global full-flight aviation emissions estimates. Building upon the results of Simone et al. (2013), the main research objective of this thesis is:

“To perform an extensive uncertainty quantification of full flight, global civil aviation emissions inventory, using the AEIC”.

The process of uncertainty quantification not only concerns the characterisation of uncertainty in a model's output, but is an iterative process that involves the identification of sensitivities and improvements to the model [25, 26]. This research objective can thus be viewed as a combination of the following project objectives:

1. Perform a baseline uncertainty propagation of AEIC.
2. Identify significant contributors to uncertainty using a global sensitivity analysis.
3. Update the uncertainty distributions of key input variables.
4. Perform another uncertainty propagation of AEIC with updated input parameters.

In order to achieve the overarching research objective, the work must be divided into several smaller, more feasible sub-goals, or work packages. The overall flow of work will start with understanding the input assumptions and calculation methodology used in the AEIC, followed by the establishment of an uncertainty quantification framework. This uncertainty quantification framework is then applied to AEIC to cover each research objective.

First, a replication of the original uncertainty propagation of AEIC will be performed, to serve as a baseline. This will be done for each output of interest: fuelburn, NO_x, CO and HC¹. From here, a global sensitivity analysis will be performed to identify the input variables which have the most significant contributions to uncertainty, with respect to each output. To minimise the uncertainty which these parameters introduce, their uncertainty distributions will be updated given new data-driven insights. Finally, to understand the impact of the updated uncertainty distributions, a further uncertainty propagation will be performed with these parameters isolated.

¹As per Simone et al. (2013)

2.2.1. Research Question(s)

The main goal of this research is to understand, quantify, and ultimately improve the uncertainty that is associated with sources used in aviation emissions inventories, using the AEIC. This goal can be formally formatted as the following central question that this research aims to answer:

“How do sources of uncertainty contribute to the uncertainty in global aviation fuelburn and emissions estimates, and how can they be improved?”

In order to answer this question, it will be important to first identify the most significant sources of uncertainty in the AEIC, and quantify their impact. Thus, the central research question can be split into the following sub-questions:

- (a) Which input(s) lead to the greatest source of uncertainty in global fuelburn and emissions estimates?
- (b) To what extent do these input(s) effect the overall uncertainty in global fuelburn and emissions estimates?

Furthermore, a goal of the thesis is to try to improve the reliability of AEIC’s estimates by incorporating new and up-to-date uncertainty distributions. This leads to the following research sub-question:

- (c) How can a data-driven approach be used to update input uncertainty distributions?

Finally, the impact of updating input uncertainty is to be addressed. This leads to the final research question:

- (d) How do these updated input parameters affect fuelburn and emissions estimates?

Aviation Emissions Inventory Code

An aviation emissions inventory details the spatiotemporal and speciated emissions profile of pollutants discharged into the atmosphere due to aviation. The Aviation Emissions Inventory Code (AEIC) presents one such inventory which is suited to methods of uncertainty and sensitivity analyses. This chapter will outline the AEIC model, and follow the emissions calculation methodology with specific focus on the uncertainty modelling of input variables.

3.1. Tier 3 Aviation Emissions Inventories

The ICAO lists three Tier 3 emissions models and databases which it uses to support and inform the policy-making processes of the ICAO's CAEP; these include the Aviation Environmental Design Tool (AEDT), the Integrated Aircraft Noise and Fuel Burn and Emissions Modelling Platform (IMPACT), and the Future Civil Aviation Scenario Software Tool (FAST) [27].

A Tier 3 emissions model represents the most thorough aviation emissions calculation methods, as per the European Environmental Agency (EEA)'s published guidelines on developing air pollutant emission inventories [28]. In contrast to Tier 1 and 2 methods which are "top-down" approaches to emissions calculations based on total fuel sale figures, Tier 3 emissions inventories take a "bottom-up", flight-by-flight approach to emissions calculations. Making use of full flight trajectory data, emissions are calculated based on the physical modelling of flight performance throughout a flight's trajectory. Performing these calculations requires a significant amount of data, including flight-specific Takeoff Weight (TOW), thrust levels and Times-in-mode (TIMs), aircraft-engine pair-specific flight performance, and engine-specific emissions indices, some of which is often proprietary [29–32].

Emissions inventories produced by these models can be resolved in 4-dimensions: latitude, longitude, altitude and at various temporal levels. Tier 3 models are thus considered to give the most complete picture of aviation emissions. However due to the complex physical processes which are modelled, these methods suffer from high computational complexity and expense, which makes them inaccessible to many research applications [5, 33].

3.2. The AEIC

In contrast to the aforementioned Tier 3 models, the Aviation Emissions Inventory Code (AEIC) was developed as an open source code capable of producing a rapid estimation of global aviation emissions. To allow for such rapid simulations, computational complexity is reduced by way of engineering and operational simplifications and assumptions. To account for these simplifications, inputs are described as random variables, using uncertainty distributions, to capture the full range of possible values [5].

Like other Tier-3 aviation emissions inventories, AEIC follows much the same "bottom-up" approach. However, instead of modelling on a flight-by-flight basis, AEIC emissions are calculated on the basis of each unique 'aircraft–airport directional pair' [5]. This means that AEIC models the emissions of a flight between two airports flown by a specific aircraft once, and multiplies the results by the number of times this aircraft–airport directional pair is flown. The AEIC emissions estimation methodology is outlined in Fig. 3.1.

Very generally, a flight movement inventory is first compiled, where aircraft–airport directional pairs are identified, and the number of times it is flown is calculated. The flight's trajectory is then generated, from which aircraft performance can be derived, and fuelburn along the trajectory is calculated. From fuelburn, the emissions of various species can be calculated. Finally, corrective multipliers on fuelburn (and thus emis-

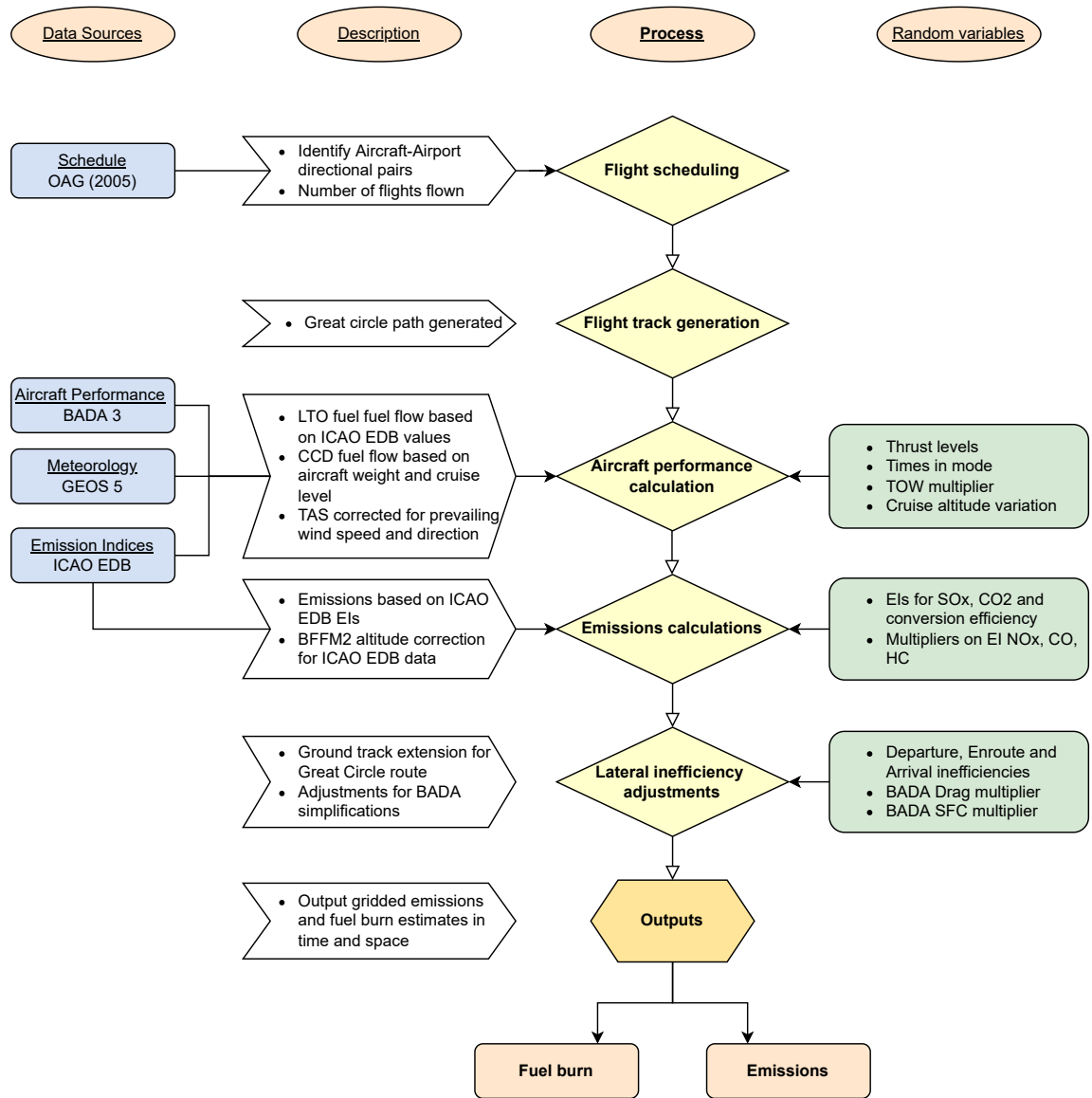


Figure 3.1: Overview of the AEIC emissions modelling process

sions) are applied, and these final results are multiplied by the number of times the flight is flown in the time frame specified. It is important to note that in AEIC, Auxiliary Power Unit (APU) and Ground Service Equipment (GSE) emissions are calculated, but are considered as separate outputs to the aviation fuelburn and emissions sums. As such their impact is not included in this thesis, so as to maintain consistency with the results from Simone et al. (2013).

As mentioned, inputs are described stochastically using uncertainty distributions. AEIC can thus be run for the nominal case, using nominal input values, or a probabilistic case, where inputs are described stochastically. These variables are described either uniformly, $X \sim U(\min, \max)$, or with a triangular distribution, $X \sim Tri(\min, \text{mode}, \max)$. Each variables' uncertainty range is based on the results of empirical studies, and uncertainty distributions are approximated using a triangular distribution. In total, AEIC describes 49 variables stochastically. Each of these random variables contribute to the model uncertainty, which is the focus of this thesis. Each step in the AEIC emissions modelling process is detailed in the following sections, with specific focus on the assumptions which are accounted for with random variables.

3.3. Flight Movements

The typical emissions modelling process begins with the generation of a flight movement inventory. This requires flight track data, which contains information on an aircraft's coordinates, and altitude at various points throughout a flight. This data can be used to develop a full picture of a flight's actual trajectory throughout space and time. However, processing this amount data can become extremely expensive when considering the number of flights that occur throughout a year. AEIC thus generates a flight movement inventory using schedule data.

3.3.1. Flight Scheduling

As mentioned, to simplify data requirements and lower computational costs, AEIC models emissions on the basis of each aircraft–airport directional pair, and multiplies results by the number of times it is flown. This is done using flight schedule data from Official Airline Guide (OAG) to identify each pair and the number of times it is flown. Schedule data covers information on a flight's origin and destination airports, departure and arrival times and aircraft type for all scheduled civil air traffic. Thus, in comparison to flight track data, schedule data does not include any information on the flown trajectory between origin and destination. Furthermore schedule data suffers from the lack of details on flights that were unscheduled, delayed or cancelled, as well as general or military aviation flights. The OAG schedule data used is for the full year of 2005.

Despite apparent limitations, using this approach requires the program to model just 110,000 flights to estimate emissions of the 27 million flights which occurred in 2005. This represents a 99.6% reduction in computational expense [5].

3.3.2. Flight Track Generation

Once an aircraft–airport directional pair is identified, the flight trajectory between departure and arrival must still be generated. The ground track is generated by simply assuming a Great Circle route between the origin and destination airports. The Great Circle route assumes an 'optimal' straight line path, and does not include for any deviations from this course or holding patterns, thus unrepresentative of realistic flight behaviour. This assumption leads to an underestimation of actual flight distance, which is accounted for by the application of lateral flight inefficiencies as corrective adjustments, detailed in Section 3.6.

3.4. Aircraft Performance

Once a ground track has been generated for the aircraft–airport directional pair, the fuel flow along this flight track can be calculated based on aircraft performance metrics. The current version of AEIC as described by Simone et al. (2013) is essentially the Climb, Cruise and Descent (CCD) extension of the Landing and Take-off (LTO) emissions inventory described by Stettler et al. (2011) [34]. Thus the calculation of aircraft performance in the LTO and CCD phases uses two separate methodologies, outlined below. The LTO methodology applies to the portion of flight below 3,000 feet, and above this, the CCD methodology is used.

3.4.1. LTO

The LTO phase of the flight is based on a default LTO cycle which defines the TIMs and respective thrust levels for each mode. These values are derived from empirical studies of LTO cycles at UK airports, which

include some variation around a nominal value [1, 35–37]. Table 3.1 presents both the nominal values, and their respective uncertainty distributions for the stochastic case, for every phase of the LTO. Thrust level is expressed as a percentage of the rated thrust, F_{00} of an engine.

Describing the LTO cycle in terms of TIMs and thrust level allows for straightforward determination of LTO fuelburn for a specific aircraft engine combination using the ICAO Engine Emissions Databank (EDB). The ICAO EDB contains thrust-specific fuel flow rates of all ICAO certified engines [38], as well as thrust-specific emissions indices of NO_x , CO and HC (used later for emissions calculations). This certification information is given in terms of four thrust levels: 7%, 30%, 85%, and 100%. Interpolation is thus required for the given thrust level. Fuelburn is the product of the fuel flow for the given thrust levels, and the respective TIMs.

Empirical evidence suggest deviations in thrust settings result in some uncertainty around the fuel flow values reported in the ICAO EDB [1, 39]. This uncertainty is thus expressed as a multiplier on LTO fuel flow, shown in Table 3.2. AEIC assumes constant engine assignments per aircraft type, however variation is not accounted for probabilistically.

Table 3.1: Overview of LTO, TIMs and thrust levels

Phase	Nominal TIM [s]	TIM uncertainty range	Nominal thrust [F_{00} %]	Thrust uncertainty range
Approach	286	Triangular for all.	25	$\sim U(21-30)$
Landing roll	46	$\pm 10\%$ for airports with empirical data	5.5	$\sim U(4-7)$
Reverse thrust	15	$\pm 20\%$ for airports without empirical data	30	—
Taxi in	371		5.5	$\sim U(4-7)$
Taxiway acceleration	10		10	$\sim Tri(7,10,17)$
Taxi out	780		5.5	$\sim U(4-7)$
Taxiway acceleration	10-20		10	$\sim Tri(7,10,17)$
Hold	341		5.5	$\sim U(4-7)$
Takeoff	29		90	$\sim U(75-99)$ with 10% probability of 100
Initial Climb	38		90	—
Climb out	61		85	—

Table 3.2: LTO fuel flow uncertainty multiplier

Variable	Nominal value	Uncertainty range
LTO fuel flow multiplier [-]	1	$\sim Tri(0.9, 1, 1.1)$

3.4.2. CCD

To calculate fuelburn across the CCD portions of the full flight, AEIC simulates aircraft performance using EUROCONTROL's Base of Aircraft Data (BADA) 3. BADA is an Air Traffic Management (ATM) tool which includes a powerful physics-based fuelburn module to directly simulate the performance of 117 aircraft types, and indirectly supports a total of 338 aircraft through similarity [5].

However, to simplify aircraft performance calculations AEIC makes use of pre-calculated aircraft-specific performance tables from BADA, known as Performance Table Files (*.PTF). *.PTF files includes information on True Airspeed (TAS), fuel flow rates, and Rate of Climb/Descent (ROCD) according to the aircraft's weight and Flight Level (FL). Thus, to generate fuelburn, the aircraft's TOW and FL along the trajectory must be generated.

TOW is a function of the Operating Empty Weight (OEW), the maximum payload, $W_{pl,max}$, and various fuel weights for the enroute flight, W_f , diversion, $W_{f,diversion}$, and hold, $W_{f,hold}$. This expression is presented in Eq. (3.1) [34, 40].

$$TOW = OEW + 0.609W_{pl,max} + 1.05W_f + W_{f,diversion} + W_{f,hold} \quad (3.1)$$

Here, an assumed loading factor of 60.9% is applied to payload weight, and the enroute fuel weight includes 5% reserve fuel. Fuel for diversion includes enough fuel to fly a diversion of 100 Nautical miles (NM) for short haul flights (flights shorter than 3 hours), and 200 NM for long haul flights (flights longer than 3 hours). Hold fuel weight contains enough fuel to maintain a 45 minute holding pattern, and 30 minute holding pattern for short and long haul flights, respectively. Once calculated, a multiplier on TOW is applied to account for uncertainty, specified in Table 3.3, based on a 13% 1σ uncertainty [5, 41].

In terms of altitude, AEIC assumes a constant cruise altitude, which is set at 7,000 feet below the specified aircraft's maximum cruise altitude. Variation in cruise altitude is modelled as an adjustment, specified in Table 3.3, based on a 1σ uncertainty of 3,000 feet [5, 41].

Table 3.3: TOW and cruise altitude uncertainty distributions

Variable	Nominal value	Uncertainty range
TOW multiplier [-]	1	$\sim Tri(0.7075, 1, 1.2925)$
Cruise altitude variation [ft]	0	$\sim Tri(-6750, 0, 6750)$

Having determined a cruise altitude and TOW, AEIC models the trajectory of the CCD between origin and destination airports in a stepwise manner, using the specific *.PTF for the aircraft. Climb and descent portions are defined as between 3,000 feet Above Field Elevation (AFE) (after LTO¹) and cruise altitude, and are divided into altitude steps of 1,000 feet. The cruise portion is between climb and descent, and divided into legs of 125 NM.

For each altitude step in climb and descent, AEIC interpolates for ROCD, TAS and fuel flow rate, based on aircraft weight and FL, and calculates the time step: simply the step size, divided by the ROCD. The horizontal distance is the product of the TAS and time step. Fuelburn is the product of the fuel flow rate and the time step. The starting conditions of the next step take into account the weight of the fuel burned in the previous step. This process is repeated for climb until cruise altitude, or descent to 3,000 feet AFE at the destination.

A similar process is employed for cruise, where TAS and fuel flow rate are interpolated for using aircraft weight and cruise FL. Here, the TAS and step length determine the time step, which is used to calculate fuelburn. Again, the fuel burnt serves to reduce the weight used as input into the next step.

At every stage, prevailing wind data from the Goddard Earth Observing System Model 5 (GEOS 5) data set is applied to correct the relationship between an aircraft's TAS and ground speed, depending on location and heading [5]. Throughout the flight, fuel flow, TAS and atmospheric conditions at each step are stored to be used as inputs for determining emissions. In combination with the LTO method, AEIC efficiently builds a comprehensive account of fuel flow for a specific aircraft-airport directional pair.

3.5. Emissions Calculations

Having calculated fuel flows for each step throughout the flight trajectory, emissions can be calculated. This is straightforward for emissions which scale with fuelburn; for CO₂ and SO_x their constant Emissions Index (EI) is directly applied to the fuel flow value of each step. For species the which do not scale with fuelburn, NO_x, CO and HC, their EIs are taken from the ICAO EDB.

Here the EIs here are expressed in terms of thrust level, which can be applied directly to the LTO model of the flight, in the same method as fuel flow in LTO (Section 3.4.1). In CCD however, some adjustments need to be made to apply the EDB data at altitude, as the certification process of these engines takes places at sea level, with engine uninstalled conditions. Furthermore, as EIs are thrust-specific, they must be converted to be used with the fuel flow determined in the CCD portions.

The Boeing Fuel Flow Method 2 (BFFM2) was developed to estimate NO_x, CO and HC emissions at altitude, using ICAO certification data, where thrust level data is not available. It thus first provides a relationship between thrust and fuel flow to be able to convert EIs from thrust-specific to fuel flow-specific. The BFFM2 then provides a method of altitude correction on the fuel flow calculated at altitude, $W_{f_{alt}}$, to generate a sea level-equivalent fuel flow $W_{f_{SL}}$. This takes into account the ambient temperature, pressure and flight Mach number, as per Eq. (3.2). The resulting expression for the corrected fuel flow at sea level is also corrected for engine install conditions.

$$W_{f_{SL}} = W_{f_{alt}} \cdot \frac{\theta_{amb}^{3.8}}{\delta_{amb}} \cdot e^{0.2M^2} \quad \text{where} \quad \theta_{amb} = \frac{T_{amb}}{T_{SL}} \quad \text{and} \quad \delta_{amb} = \frac{p_{amb}}{p_{alt}} \quad (3.2)$$

The sea level-equivalent fuel flow can then be used in conjunction with the ICAO EDB to determine (sea-level) emissions. These emissions must once again be adjusted for altitude effects using the following relationships [42, 43]:

$$EI(NO_x)_{alt} = EI(NO_x)_{SL} \cdot \sqrt{\frac{\delta_{amb}^{1.02}}{\theta_{amb}^{3.3}}} \cdot e^H \quad (3.3)$$

Here, the e^H term accounts for humidity effects, and a constant humidity of 60% for all flights is assumed [5].

¹Directly above the airport, thus assuming no ground covered during LTO

$$EI(HC)_{alt} = EI(HC)_{SL} \frac{\theta_{amb}^{3.3}}{\delta_{amb}^{1.02}} \quad (3.4)$$

$$EI(CO)_{alt} = EI(CO)_{SL} \frac{\theta_{amb}^{3.3}}{\delta_{amb}^{1.02}} \quad (3.5)$$

Thus, for every flight step in CCD, atmospheric properties and flight speed are used to correct the BADA fuel flow for sea level conditions, and produce emissions at altitude. An emissions profile for the flight is thus generated.

In terms of uncertainty, the EIs of CO₂ and SO_x depend on the ratio of carbon to hydrogen in the fuel, and the Fuel Sulphur Content (FSC), respectively [44, 45]. Thus, uncertainty ranges for these emissions are used to account for variations in fuel type. Furthermore, while the majority of SO_x emissions are in the form of SO^{IV} (SO₂), a percentage is emitted as SO^{VI} (SO₃) [1]. This is accounted for in a conversion efficiency, ϵ , of 2% [5]. Uncertainty ranges for NO_x, CO and HC are derived from comparisons to measured EIs of these species to those in the ICAO EDB. There are centred around 1.0, and are treated as multipliers on the ICAO EDB value. Interestingly, the EI of NO_x is nominally set at 90%, as observed EIs in studies tended to be overestimated by 10% in the EDB [1, 44, 46]. An overview of nominal EI values and their associated uncertainty are presented in Table 3.4.

Table 3.4: Overview EI uncertainty distributions for different emissions species

Species	Nominal Value	Uncertainty Range
EI(CO ₂) [g/kg]	3160	~Tri(3148, 3160, 3173)
EI(SO _x) [g/kg]	0.6	~Tri(0.5, 0.6, 0.7)
SO _x ϵ [%]	2.0	~Tri(0.5, 2.0, 5.0)
EI(NO _x) [-]	0.9	~Tri(0.7, 0.9, 1.3)
EI(CO) [-]	1.0	~Tri(0.4, 1.0, 1.6)
EI(HC) [-]	1.0	~Tri(0.1, 1.0, 1.9)

3.6. Corrective Adjustments

Finally, once a profile of fuelburn and emissions has been developed for the flight, corrective adjustments are made for several underlying assumptions. These are applied as multipliers which serve to increase the calculated fuelburn and emissions values.

3.6.1. Lateral Inefficiencies

As mentioned, fuel flow is calculated along the Great Circle path between airport pairs, ie. a flight is assumed to fly the shortest route to the destination. In reality, flight tracks deviate from this 'fuel-optimum' path due to factors such as noise constraints, weather, separation requirements, airspace restrictions or geopolitical considerations. As such, the Great Circle assumption tends to lead to an underestimate of actual distance flown. Any extension to the ground track over the Great Circle route is considered a routing inefficiency, expressed as Extra Distance (XD) [3]. AEIC thus employs lateral inefficiency factors to increase the ground track of the CCD portions of the flown flight [5].

These inefficiencies are taken from an empirical analysis of flight behaviour in Europe and the US, and are divided into departure, enroute and arrival inefficiencies. Departure and arrival inefficiencies are an extra distance (expressed in NM) applied to the first 50 NM of climb and last 50 NM of descent, respectively. These values are shown in Table 3.5, for each region. Enroute inefficiencies are described in terms of the enroute Great Circle distance, $GCD_{Enroute}$, as per Eqs. (3.6) and (3.7). This is applied to the portion of flight between the first and last 50 NM of the Great Circle route.

$$XD_{Enroute_EU} = 0.020 \cdot GCD_{Enroute} + 12 \quad (3.6)$$

$$XD_{Enroute_US} = 0.029 \cdot GCD_{Enroute} + 22 \quad (3.7)$$

In AEIC the European inefficiencies are applied to all EU² departures, enroutes and arrivals, while flights elsewhere in the world are assumed to use inefficiencies for the US. There is significant variation around the nominal inefficiencies, which can be seen in Table 3.5. Note that enroute inefficiency here factors serve as multipliers on the aforementioned nominal enroute inefficiencies (Eqs. (3.6) and (3.7)).

Table 3.5: Overview of lateral inefficiency uncertainty distributions, per region

Inefficiency	Nominal Inefficiency		Uncertainty Distributions	
	EU	US	EU	US
Departure [NM]	9.0	7.8	$\sim Tri(0, 5, 25)$	$\sim Tri(0, 3, 23)$
Enroute [-]	1.0	1.0	$\sim Tri(0.25, 1.0, 2.5)$	$\sim Tri(0.25, 1.0, 2.0)$
Arrival [NM]	26.9	27.7	$\sim Tri(0, 22, 57)$	$\sim Tri(0, 2, 75)$

3.6.2. BADA corrections

The BADA model itself makes use of two significant simplifying assumptions concerning aircraft drag, and engine Specific Fuel Consumption (SFC). In terms of aircraft drag, the BADA model does not fully capture the dependence of lift/drag performance on altitude and speed. This uncertainty is modelled based on a 14% 1σ uncertainty. Similarly for engine SFC the BADA model does not fully capture the dependence of engine performance on altitude and speed. This uncertainty is modelled based on a 11% 1σ uncertainty [5, 23, 41]. These uncertainties are presented in Table 3.6, and are applied as multipliers on calculated fuelburn and emissions.

Table 3.6: BADA drag and SFC uncertainty distributions

Variable	Nominal value	Uncertainty range
BADA drag multiplier [-]	1	$\sim Tri(0.685, 1, 1.315)$
BADA SFC multiplier [-]	1	$\sim Tri(0.7525, 1, 1.2475)$

3.7. Application to 2005 Aviation Activity

According to the modelling process delineated throughout this chapter, AEIC is capable of generating a gridded emissions inventory of global civil aviation for 2005, within 4% of published inventories of ICAO listed Tier 3 models [5]. These results can be seen in Table 3.7, for both the nominal case and the probabilistic case. The AEIC emissions inventory is generated in approximately one hour on a single 2.4GHz core, without proprietary data or methods, lending itself to methods of uncertainty quantification that are not possible with more computationally complex models.

Table 3.7: Summary of global aviation fuelburn and emissions estimated by AEIC, as published by Simone et al. (2013) [5]

Emission	Nominal (Tg)	Mean (Tg)	Median (Tg)	Coefficient of Variation (%)	5 th -95 th percentile uncertainty range (Tg)
Fuelburn	180.6	180.9	178.5	16.7	136.1–232.9
NOx	2.689	2.631	2.535	23.7	1.761–3.804
CO	0.749	0.760	0.749	28.8	0.422–1.145
HC	0.201	0.203	0.196	42.6	0.072–0.362

²Here EU refers to an arbitrarily defined European bounding box, and not the European Union. This is further explained in Section 7.2

Uncertainty Quantification

As is apparent from the previous chapter, computational models are always abstractions of a physical system. These abstractions can come in the form of errors in input data measurement, approximations of input parameters or imperfect knowledge and simplifications of the physical processes being modelled. Thus, modelling a physical system is never deterministic; there is always inherent randomness in a system's inputs. As a result, a model's output is always subject to inherent uncertainty. Uncertainty quantification is the analysis of this uncertainty in the response of a computational model [25, 47]. This chapter will outline the general approach to uncertainty quantification using AEIC.

4.1. General Framework

Uncertainty quantification is an iterative process, and involves four main steps visualised in Fig. 4.1¹. On top of characterisation of uncertainty in the model response, it is concerned with identification of significant contributors to uncertainty, with the aim of improving and reducing the uncertainty of the model response [25, 26]. This process will be explained in the context of AEIC's probabilistic model.

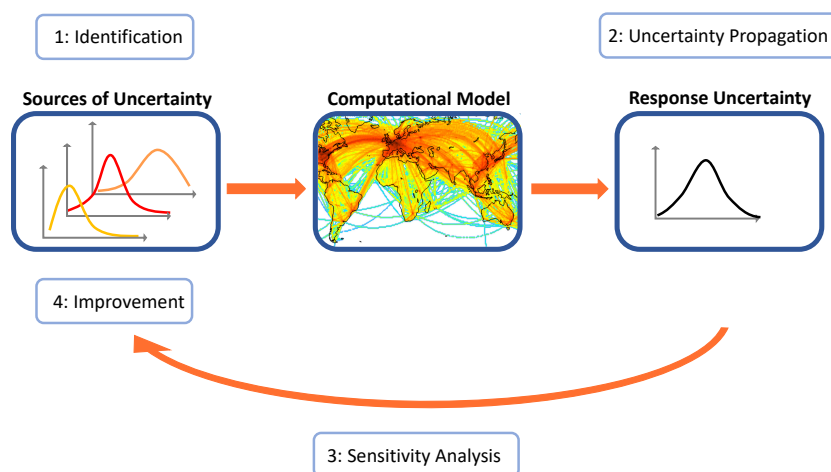


Figure 4.1: Uncertainty Quantification framework

1: Identification

The first step in uncertainty quantification is the identification of the possible sources of uncertainty, and characterising the uncertainty. As a model is a function of various input parameters, one source of uncertainty in the response is the uncertainty in these input parameters; known as parametric uncertainty. This can be accounted for by describing inputs stochastically, using probability distributions. Uncertainty can also be attributed to imperfect representation of the physical process being modelled; known as structural uncertainty [22]. This thesis is only concerned with parametric uncertainty.

¹Computational model image from Stettler et al. (2013)

As mentioned, AEIC makes use of 49 different random variables to describe different parameters across flight track generation, aircraft performance, and emissions calculations. To account for the randomness in these inputs, these input variables are described stochastically. These sources of uncertainty have already been characterised in the AEIC documentation, and contextualised in Chapter 3 [5, 34, 48].

2: Uncertainty Propagation

Stochastic input variables will propagate uncertainty through a model, resulting in uncertainty in the model output. The aim of an uncertainty propagation is to generate probability distributions of the model's output in order to understand the full range of responses [47].

This is done by passing the full space of input values through the model, and recording each response. The Monte Carlo method, which works on the principle of repeated random sampling of the inputs, provides a straightforward way to propagate uncertainty [25, 47]. This generates a range of responses from the model, which can be used to construct a histogram. A histogram approximates a model's solution, and provides the most information about the uncertainty in the solution [22, 49]. Statistical moments and indices can be derived, such as mean and variance, from which general inferences can be made [25]. Although this has already been done by Simone et. al (2013), this process will be repeated in Chapter 5 to form a baseline to which results of this thesis can be compared.

3: Sensitivity Analysis

Once the uncertainty propagation is characterised, a sensitivity analysis is performed. Sensitivity analyses study how the uncertainty of an output of a numerical model can be attributed to sources of uncertainty in the model inputs [25, 50]. There are various methods of performing sensitivity analyses, which are described in-depth in Sections 4.2 and 4.3. Here, the goal is to also identify sources of uncertainty which not only contribute significantly to output uncertainty, but present potential for improvement [22]. A sensitivity analysis of AEIC is performed in Chapter 6.

4: Improvements

Establishing the relative impact of inputs with respect to their contributions to uncertainty effectively identifies areas of the input space which can be improved. Here, key input parameters are the focus of re-calibration or revision with more recent research or data-driven investigations [22]. This is done in Chapter 7. The goal of this step is to improve the descriptions of variable behaviour to increase the reliability of a model's output. Furthermore, the improved understanding of variable uncertainty has potential for more general scientific significance, with applications in other research efforts and model development.

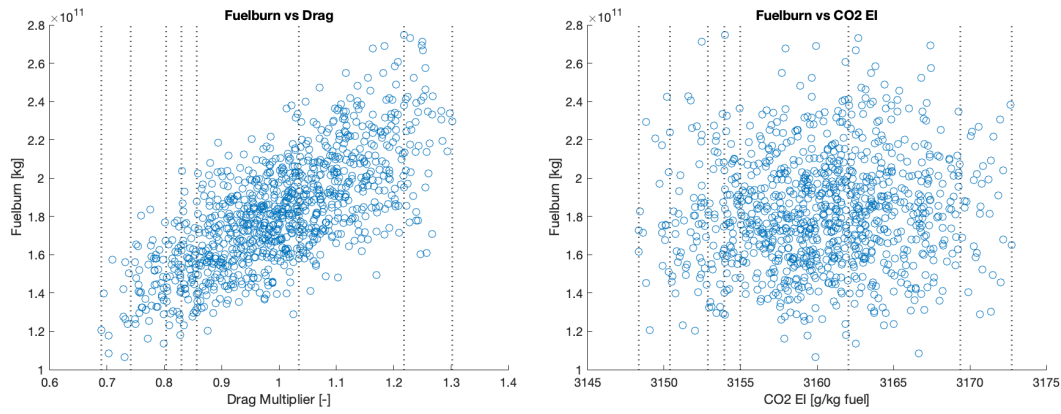
With improved the sources of uncertainty, the uncertainty propagation in the model's response can again be investigated, thus beginning the iterative cycle. Performing the first re-iteration of uncertainty quantification in AEIC with updated inputs is the final objective of this thesis, presented in Chapter 8.

4.2. Sensitivity Analysis

As mentioned, sensitivity analyses assess the contribution of a parameter's uncertainty to the model output's uncertainty. One way to visualise sensitivity is by performing a Monte Carlo simulation, and plotting the model output against the input samples [22, 51]. Fig. 4.2 depicts the results of a Monte Carlo simulation of AEIC's fuelburn, sampled at 1,000 points, against two different input variables: the aircraft drag multiplier, and the CO₂ emissions index.

These two variables were chosen to clearly demonstrate model sensitivity – within AEIC's calculations, fuelburn is a function of aircraft drag, but not a function of the CO₂ emissions index. The influence of an input can be seen directly by the pattern, or shape of the scatterplot. The stronger the shape, the more influence an input has on the output, while a uniform cloud of points indicates a non-influential factor [25, 51]. This is readily apparent in the different scatterplots of Fig. 4.2.

This is however, a purely qualitative analysis of sensitivity. In order to quantify sensitivity, one can look at the vertical variation in fuelburn values, moving along the x-axis. The vertical lines, or 'slices' in Fig. 4.2 represent a sample of fuelburn values at a specific input value. Along a slice, various fuelburn values exist, which can be averaged. Taking these average values for fuelburn over these slices results in the plots in Fig. 4.3. A uniform distribution of fuelburn points will result in largely the same mean value along the x-axis, while a response with a stronger pattern will demonstrate a wider range of mean fuelburn points. Thus, it can be concluded that the sensitivity of a model response to an input can be quantified by the variation of the

Figure 4.2: Scatterplots of fuelburn versus drag and CO₂ EI

expected value of the response, at a specific input value [51].

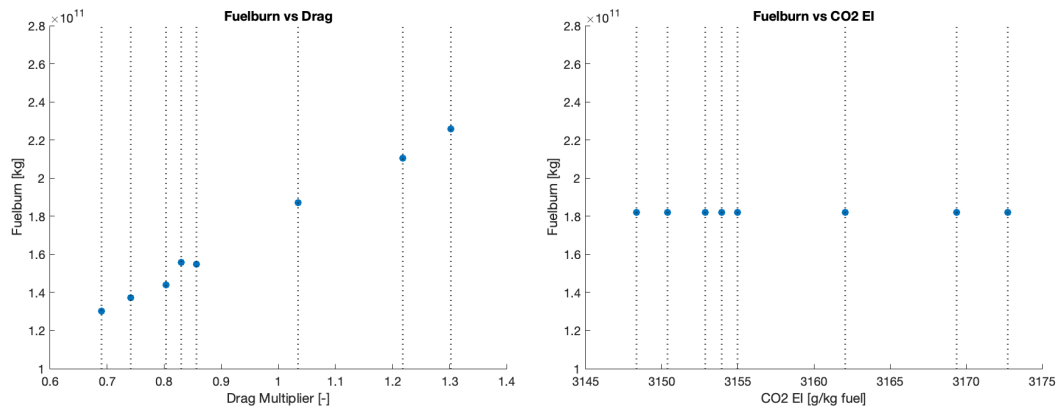


Figure 4.3: The mean values of fuelburn along the x-axis

To put this in terms of a generic model f , with output Y , and input vector \mathbf{X} of the dimension d , consider:

$$Y = f[X_1, X_2, \dots, X_d] \quad (4.1)$$

In the above example, the mean value of fuelburn over a specific point on the x-axis correspond to the expectation of Y , conditional a fixed X_i ², while averaging over all-but- X_i (other input variables are un-fixed): $E_{\mathbf{X}_{-i}}(Y | X_i)$. Thus, when taking the variance of these values for input X_i , the sensitivity of response Y to variable X_i may be expressed as [25, 51, 52]:

$$V_{X_i}(E_{\mathbf{X}_{-i}}(Y | X_i)) \quad (4.2)$$

² i is on the interval $[1, d]$

4.3. Sobol Analysis

The Sobol analysis is a variance-based form of global sensitivity analysis, which seeks to decompose the total variance of the output into partial variances, directly attributable to input variables [25, 51, 52].

4.3.1. Sobol Decomposition

Consider again the generic model:

$$Y = f[X_1, X_2, \dots, X_d] \quad (4.3)$$

The function f may be decomposed into a set of functions increasing in dimensionality (known as a Hoeffding decomposition) [51, 53]:

$$f = f_0 + \sum_i f_i + \sum_i \sum_{j>i} f_{ij} + \dots + f_{12\dots d} \quad (4.4)$$

Here, each term is a function only of the factors in its index ie. $f_i = f_i(X_i)$, and $f_{ij} = f_{ij}(X_i, X_j)$ ³. Russian mathematician I. M. Sobol proved that if each term in Eq. (4.4) has zero mean, then all terms of the decomposition are orthogonal in pairs. ie. $\int f(x_i) dx_i = 0$ then $\int f(x_i) f(x_j) dx_i dx_j = 0$. It follows from the property of orthogonality that each term in the decomposition can be calculated using the conditional expectations of model output Y [51, 53].

$$f_0 = E(Y) \quad (4.5)$$

$$f_i = E_{\mathbf{X}_{-i}}(Y | X_i) - E(Y) \quad (4.6)$$

$$f_{ij} = E_{\mathbf{X}_{-ij}}(Y | X_i, X_j) - f_i - f_j - E(Y) \quad (4.7)$$

This continues similarly for higher order terms. Variances of the functions of the decomposition can be taken as:

$$V_i = V_{X_i}(E_{\mathbf{X}_{-i}}(Y | X_i)) \quad (4.8)$$

$$V_{ij} = V_{X_i X_j}(E_{\mathbf{X}_{-ij}}(Y | X_i, X_j)) - V_{X_i}(E_{\mathbf{X}_{-i}}(Y | X_i)) - V_{X_j}(E_{\mathbf{X}_{-j}}(Y | X_j)) \quad (4.9)$$

Thus, the variance of the response Y to function f may be decomposed into a set of partial-variances:

$$V(Y) = \sum_i V_i + \sum_i \sum_{j>i} V_{ij} + \dots + V_{12\dots d} \quad (4.10)$$

4.3.2. Sobol Indices

Normalising Eq. (4.10) with respect to the unconditional variance $V(Y)$ results in the Sobol sensitivity indices:

$$\sum_i S_i + \sum_i \sum_{j>i} S_{ij} + \dots + S_{12\dots d} = 1 \quad (4.11)$$

This presents a fractional contribution to the total, unconditional variance. The significance of Sobol's work is that it allows a direct, quantifiable measure of global sensitivity only using values of $f(X)$, achievable through Monte Carlo simulation [53].

First-Order Effects

The first-order index, S_i , represents the main contribution to the variance of the output of each input. It quantifies the effect of varying X_i alone [50, 52].

$$S_i = \frac{V_i}{V(Y)} = \frac{V_{X_i}(E_{\mathbf{X}_{-i}}(Y | X_i))}{V(Y)} \quad (4.12)$$

Taking the fuelburn example of Section 4.2, the first-order effects of the drag multiplier and CO₂ EI can be straight forwardly calculated from the expectations presented in Fig. 4.3. For the drag multiplier, the variance

³ i and j are on the interval $[1, d]$

of these expectations, $V_{X_i}(E_{\mathbf{X}_{-i}}(Y | X_i))$, is $4.95e + 20$, while for CO₂ EI, this term equals zero. The unconditional variance of fuelburn $V(Y)$ is $8.39e + 20$.

$$\text{Drag Multiplier : } S_i = \frac{4.25e + 20}{8.39e + 20} = 0.5066 \quad (4.13)$$

$$\text{CO}_2\text{EI : } S_i = \frac{0}{8.39e + 20} = 0 \quad (4.14)$$

Thus it is readily apparent that the drag multiplier contributes significantly to the variance in fuelburn, while CO₂ EI is a non-influential factor. Moreover, this estimate of sensitivity is quantified.

Interaction Effects

A useful property of Sobol's decomposition of variance is that it allows the quantification of interaction effects between factors. These are denoted higher order terms in Eq. (4.11) [50, 51]. For instance, the second-order index, S_{ij} measures the joint effect of two input factors, $(X_i X_j)$, on Y :

$$S_{ij} = \frac{V_{ij}}{V(Y)} = \frac{V_{X_i X_j}(E_{\mathbf{X}_{-ij}}(Y | X_i, X_j)) - V_{X_i}(E_{\mathbf{X}_{-i}}(Y | X_i)) - V_{X_j}(E_{\mathbf{X}_{-j}}(Y | X_j))}{V(Y)} \quad (4.15)$$

This continues for all higher-order indices, up to $S_{12\dots d}$, fully capturing interaction effects.

Total-Order Effects

The variance terms required to compute interaction effects increase exponentially with the number of input factors. Calculating interaction effects of increasingly higher dimension can quickly become computationally expensive when Monte Carlo simulations are required to assess each term (especially when the number of input factors is large). The total-order index, S_{T_i} , provides a measure for the total contribution of X_i to Y , however in practice it is used to identify any interactions [54]. It is the sum of the first-order index, S_i , and all higher order interactions indices: ie. $S_{ij} + S_{ijk} + S_{ijk\dots d}$ [51]. It can be calculated by computing all terms in the decomposition of Eq. (4.11). However, the total-order index can be calculated at the same expense as first-order index, using the identity (derived in Appendix A):

$$V(Y) = V_{X_i}(E_{\mathbf{X}_{-i}}(Y | X_i)) + E_{\mathbf{X}_{-i}}(V_{X_i}(Y | X_i)) \quad (4.16)$$

This decomposes the variance of output Y into two terms: the first-order effect, and the residual. The residual variance, $E(V(Y | \mathbf{X}_i))$, is the discrepancy between the variance of Y and the variance of Y estimated using the model, effectively representing the contribution of all higher-order terms in the variance decomposition (Eq. (4.10)) [52]. Considering the variance decomposed into the first effect and residual, conditioning with respect to all factors *but* X_i :

$$V(Y) = V_{X_i}(E_{\mathbf{X}_{-i}}(Y | \mathbf{X}_{-i})) + E_{\mathbf{X}_{-i}}(V_{X_i}(Y | \mathbf{X}_{-i})) \quad (4.17)$$

The term $V_{X_i}(E_{\mathbf{X}_{-i}}(Y | \mathbf{X}_{-i}))$ can be considered as the first order effect of all terms excluding X_i . The residual $E_{\mathbf{X}_{-i}}(V_{X_i}(Y | \mathbf{X}_{-i}))$ can thus be interpreted as the contribution of all terms in the variance decomposition that do include X_i [52, 55]. Thus, the total effect index of X_i can be calculated as:

$$S_{T_i} = \frac{E_{\mathbf{X}_{-i}}(V_{X_i}(Y | \mathbf{X}_{-i}))}{V(Y)} = 1 - \frac{V_{X_i}(E_{\mathbf{X}_{-i}}(Y | \mathbf{X}_{-i}))}{V(Y)} \quad (4.18)$$

5

Uncertainty Propagation

As per the second step in the uncertainty quantification framework presented in Section 4.1, this chapter deals with the propagation of uncertainty through AEIC's global, full-flight fuelburn and emissions modelling, and represents the first set of results of this thesis. The application of the Monte Carlo method to AEIC is explained, and the results of the uncertainty propagation are presented.

5.1. Methodology

As mentioned, AEIC can be run in the nominal case, using fixed, nominal input values, as well as the probabilistic case, where inputs are described stochastically around these nominal values. Here, both cases are run. The nominal case serves as a point of comparison, from which the effects of uncertainty propagation can be inferred. The probabilistic case is used in conjunction with the Monte Carlo method to propagate uncertainties.

The Monte Carlo method is an established approach to propagating uncertainties. It is based on repeated random sampling of the input variables, according to their respective distribution. For each state in the input space, the model is run, generating a range of outputs which demonstrates the distribution of the solution. This is done for a sufficiently high number of samples, typically in the thousands, to give a full representation of the outputs [25, 47].

In AEIC, the uncertainty in each input variable is described with a triangular distribution (as explained in Chapter 3). Random values from these distributions are generated using a function which is based on an inverse transform of uniformly distributed random values, $X \sim U(0, 1)$. Thus to generate the full input space, a random variable matrix of random values in $X \sim U(0, 1)$, of size $N \times d$ is generated. Here, N is the number of Monte Carlo simulations, and d is the number of dimensions, or input variables. In the case of AEIC, $N=1,000$ simulations is considered sufficient, and $d=49$ [5, 34, 56]. Each row of this random variable matrix represents a state in the input space; each value is mapped onto the distribution of its corresponding variable resulting in a stochastically generated input value for that variable. Each state is run through AEIC, each time generating an output for each emissions species. This process is outlined in Fig. 5.1.

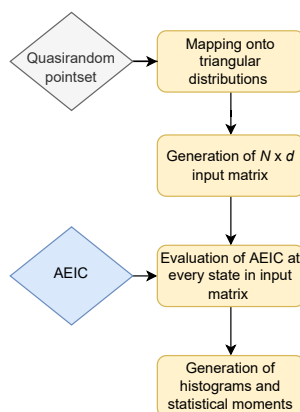


Figure 5.1: Flowchart of Monte Carlo process

The values $X \sim U(0, 1)$ are generated using a Sobol quasirandom point set¹, which offers a low-discrepancy sequence. A low-discrepancy sequence fills the input space more evenly than a random or pseudorandom sequence: thus leaving no clusters or gaps in the space [51]. This is this a quasi-Monte Carlo method.

Here, AEIC is run with baseline settings which produce estimates for global civil aviation, for the year 2005, similar to the research of Simone et al. (2013). The species of interest are fuelburn, NO_x, CO and HC (as per Simone et al. (2013)). The Monte Carlo results for each species are presented in histogram form, and statistical moments are derived.

5.1.1. Computational expense

One of the major drawback to Monte Carlo method is the computational expense due to the high number of repeated simulations required. This is the case for AEIC, where a single global simulation takes an hour, a Monte Carlo simulation of 1,000 runs takes 1,000 hours. Thus, the code is parallelised, to spread computations over multiple processors of Cartesius, the Dutch national supercomputer. One ‘fat’ compute node on Cartesius is made up of 32 cores, each with 8 GB of RAM². Parallelising the code over 20 cores allows for a 1,000 run Monte Carlo simulation of AEIC to be completed in 50 hours.

5.2. Results

A summary of the nominal and probabilistic AEIC estimates of global, annual fuelburn, NO_x, CO and HC are presented in Table 5.1. Here, the results of the nominal simulation are presented in the first column. The results of the probabilistic case are summarised by statistical moments: Mean, Median, Standard Deviation, Coefficient of Variation and the 5th-95th percentile uncertainty range. These values can be directly compared to those from Simone et al. (2013) in Table 3.7, thus validating the correct application of the AEIC model.

Table 5.1: Summary of global civil aviation fuelburn and emissions estimated by AEIC

Emissions	Nominal (Tg)	Mean (Tg)	Median (Tg)	Standard Deviation (Tg)	Coefficient of Variation (%)	5 th -95 th percentile uncertainty range (Tg)
Fuelburn	180.4	182.1	180.6	29.0	15.9	134.4-229.7
NO _x	2.681	2.654	2.583	0.592	22.3	1.681-3.628
CO	0.756	0.774	0.748	0.233	30.1	0.391-1.158
HC	0.191	0.203	0.194	0.092	45.2	0.052-0.354

It is interesting to note that for each species, the median values of the probabilistic case, rather than the mean values, are more closely aligned to the results of the nominal simulation. The coefficient of variation is the ratio of the standard deviation to the mean, effectively presenting a measure of relative uncertainty. HC presents the largest relative uncertainty, while that for fuelburn is the lowest. Histograms depicting the full distributions of fuelburn and emissions estimates are presented in Fig. 5.2, which demonstrate the propagated uncertainty.

¹<https://uk.mathworks.com/help/stats/sobolset.html>

²<https://userinfo.surfsara.nl/systems/cartesius/description>

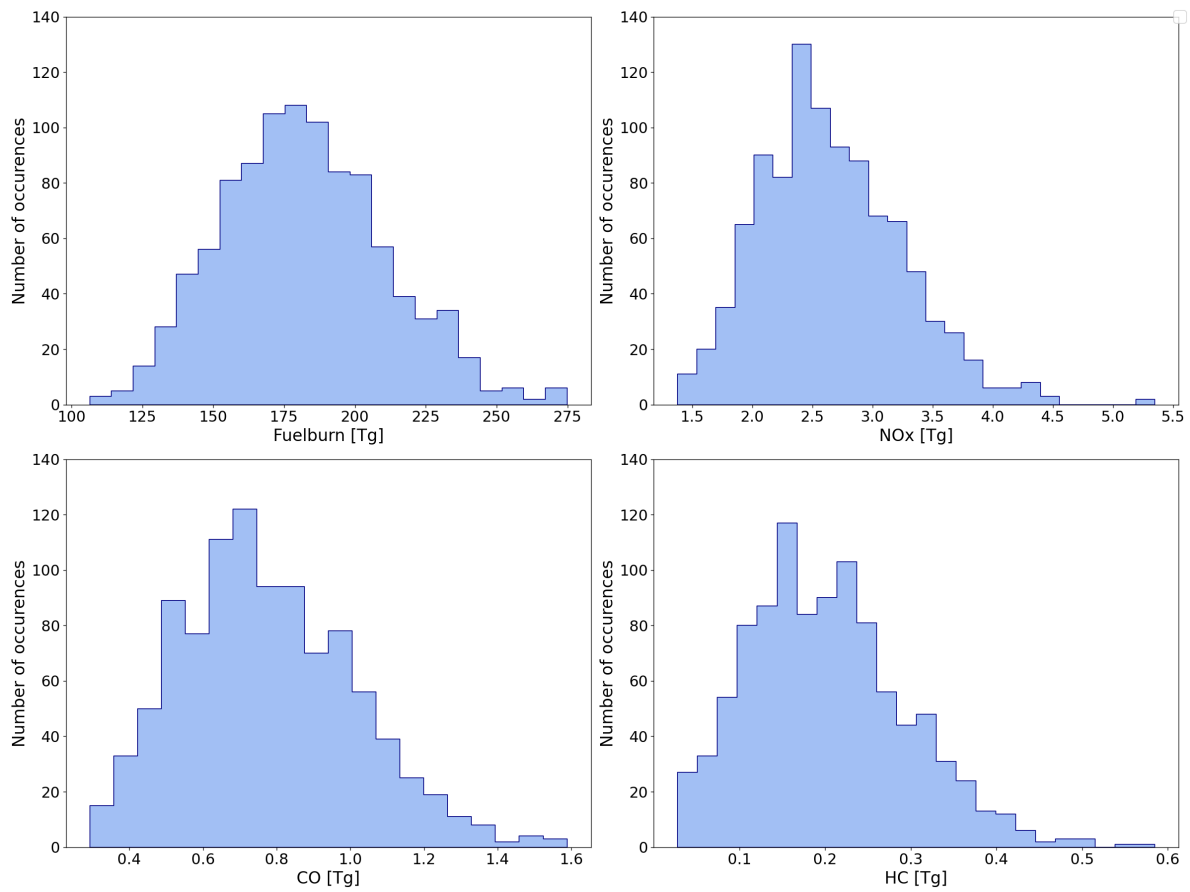


Figure 5.2: Results of Monte Carlo uncertainty propagation

6

Sobol Analysis

This chapter addresses the third step of the uncertainty quantification framework: sensitivity analysis. This is done by way of a Sobol analysis to identify key contributors to the uncertainties quantified in Chapter 5. The methodology of applying the Sobol analysis to AEIC is discussed, followed by a validation of this method. Finally, the results of the Sobol analysis are presented, where the inputs with significant contributions to uncertainty in global fuelburn and emissions estimates are identified.

6.1. Methodology

The methodology behind Sobol's method of sensitivity analysis is outlined in Section 4.3: based on variation of input variables, the variance in model response is measured. The significance of this method is that it can be achieved through (quasi-)Monte Carlo simulations, thus making it suitable for application to AEIC. Very generally, a Sobol analysis of AEIC requires the generation of a specific quasi-Monte Carlo input space, running AEIC for each state in the input space, and evaluating outputs to calculate the Sobol indices.

The quasi-Monte Carlo sampling sequence employed here is the Saltelli sampling sequence, which allows for the computation of both first-order indices, S_i , and total-order indices, S_{T_i} , using a single input space [52]. To construct the input space, two $N \times d$ sample matrices are constructed; \mathbf{A} and \mathbf{B} . Then for every dimension, d , a $N \times d$ matrix $\mathbf{A}_B^{(i)}$ is constructed. The columns of this $\mathbf{A}_B^{(i)}$ matrix are from \mathbf{A} , but every i -th column is substituted with the i -th column of \mathbf{B} (here, i runs from 1 through to d). Each row of the matrices \mathbf{A} , \mathbf{B} and \mathbf{A}_B are run through AEIC, which results in a total of $N \times (d + 2)$ model evaluations. To compute the Sobol indices S_i , and S_{T_i} , the terms in Eqs. (4.12) and (4.18) are found using Eqs. (6.1) and (6.2), respectively [52].

$$V_{X_i}(E_{\mathbf{X}_{-i}}(Y | X_i)) = \frac{1}{N} \sum_{j=1}^N f(\mathbf{B})_j (f(\mathbf{A}_B^{(i)})_j - f(\mathbf{A})_j)^2 \quad (6.1)$$

$$E_{\mathbf{X}_{-i}}(V_{X_i}(Y | \mathbf{X}_{-i})) = \frac{1}{2N} \sum_{j=1}^N (f(\mathbf{A})_j - f(\mathbf{A}_B^{(i)})_j)^2 \quad (6.2)$$

To compute second-order indices, the matrix \mathbf{A}_B is $2N \times d$, which results in a total of $N \times (2d + 2)$ model evaluations. The construction of the input space and calculation of Sobol indices is handled by the SALib library in Python¹. The process can be summarised by the flowchart in Fig. 6.1.

In general conclusions are drawn from first-order indices, as these values are most significant to variance in the output. Total-order indices are used to reveal any interaction effects, while second-order indices are used to identify specific interaction pairs [54]. When discussing the contribution of an input variable, it is the uncertainty with which this variable is modelled, which is being referred to.

¹<https://salib.readthedocs.io/en/latest/basics.html>

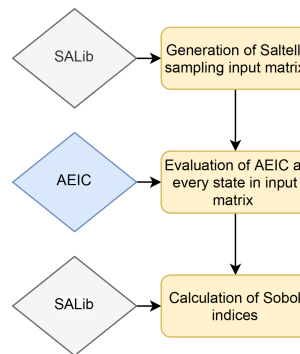


Figure 6.1: Flowchart of Sobol analysis process

6.1.1. Computational Expense

The required $N \times (2d + 2)$ model evaluations can become extremely computationally expensive, for a model with many inputs dimensions, d . As AEIC has 49 input variables, running 1,000 Monte Carlo simulations, as per Chapter 5 would result in 100,000 hour-long evaluations of AEIC required. Parallelising computations across 3 separate nodes², with 20 cores each, this analysis would still take over three months to complete. Thus, to keep within the timeline of this project, a considerably lower N had to be selected, while still maintaining stable Monte Carlo results.

This was done by analysing the convergence of the fuelburn estimates from the $N = 1,000$ Monte Carlo simulation of Chapter 5. For each successive model execution, the cumulative relative error to the total mean was calculated. It was found that Monte Carlo simulations with over 200 executions maintained a relative error within 1% of the mean. This is shown in Fig. 6.2. Thus, N of 240 was deemed sufficient, and selected, resulting in 24,000 required model evaluations. Parallelising across 3 nodes with 20 cores each allows the Sobol analysis of AEIC to be run in just over 2 weeks.

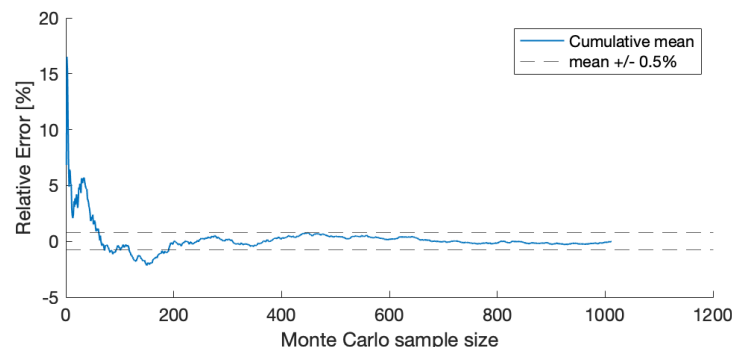


Figure 6.2: Flowchart of Sobol analysis process

6.2. Comparison With Existing Literature

To assess this Sobol analysis methodology, the results of the sensitivity analysis of Stettler et al. (2011) were emulated and compared. The Stettler et al. (2011) study concerns an earlier version of AEIC, when it was first developed as an aviation emissions inventory for LTO activities at UK airports [1, 48]. The sensitivity analysis undertaken by Stettler et al. (2011) was also a Sobol analysis, and computed both the first-order indices, S_i , and total-order indices, S_{T_i} of each input factor on the sensitivity of $\text{CO}_2\text{-eq}$ and $\text{PM}_{2.5}$ emissions. The results of their Sobol analysis are presented in Figs. 6.3 to 6.6.

²3 nodes is the maximum number of nodes usable with a single Matlab license on Cartesius

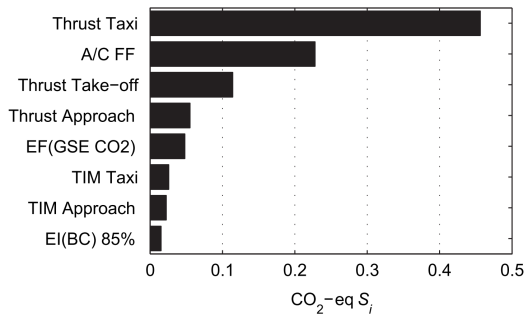


Figure 6.3: First-order Sobol indices for CO₂-equivalent from Stettler et al. (2011) [1]

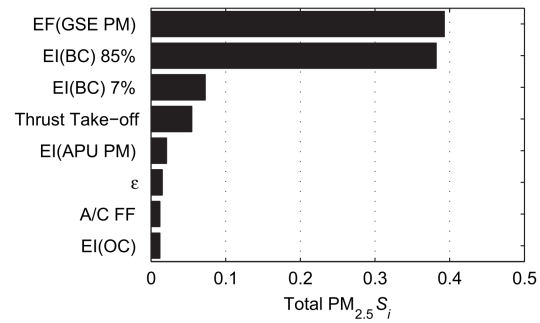


Figure 6.4: First-order Sobol indices for total PM_{2.5} from Stettler et al. (2011) [1]

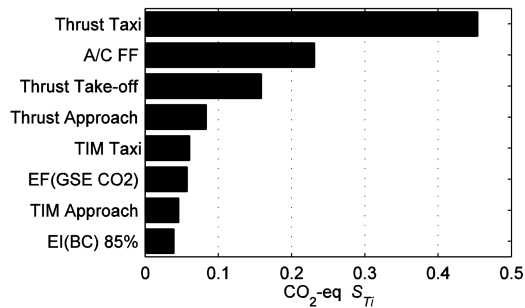


Figure 6.5: Total-order Sobol indices for CO₂-equivalent from Stettler et al. (2011) [2]

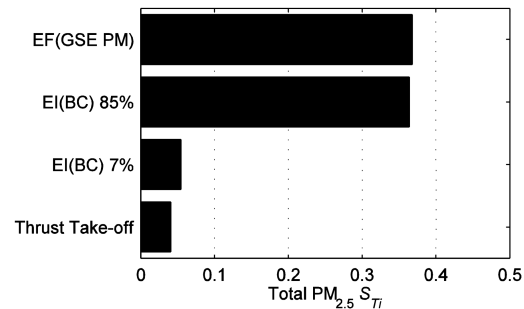


Figure 6.6: Total-order Sobol indices for total PM_{2.5} from Stettler et al. (2011) [2]

The current version of AEIC used in this study is a very different model to that used by Stettler et al. (2011), as it has been expanded from UK LTO emissions index to the global, full flight emissions index of Simone et al. (2013) [48]. As such, various calculation methods and input parameters have since been changed, such as the PM estimation methods [57]. Nevertheless, it is still possible to run AEIC for UK airports, and derive LTO emissions for CO₂-eq and non-volatile PM. Running a Sobol analysis of AEIC with these settings produces the results of Figs. 6.7 and 6.8. Here, the total-order and first-order indices are plotted on the same axes.

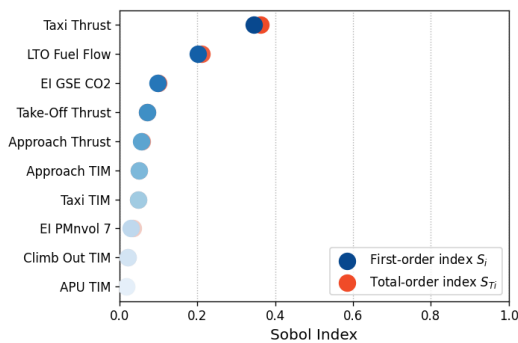


Figure 6.7: First- and total-order Sobol indices for CO₂-eq

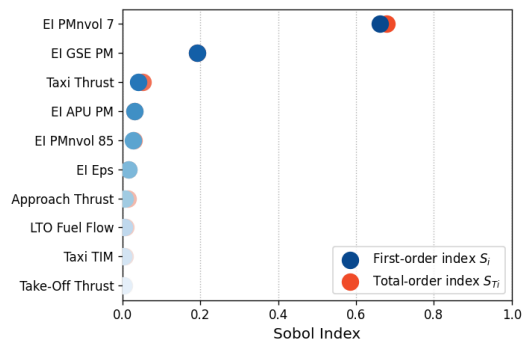


Figure 6.8: First- and total-order Sobol indices for non-volatile PM

In both this study and that of Stettler et al. (2011), the Taxi Thrust and Fuel Flow parameters are the greatest contributors to uncertainty in CO₂-eq estimates. In fact, the results of both studies' Sobol analyses identify the same top 8 contributors to uncertainty in CO₂-eq, with the exception of EI BC 85%³ being replaced by EI non-volatile PM 7%. This may be a result of the updated PM estimation methods [57]. Despite this, and different ordering of EI GSE CO₂ and Taxi and Approach TIMs, the results of this Sobol analysis are highly comparable to those of Stettler et al. (2011).

³The percentage refers to the thrust level to which the emission index applies

In terms of non-volatile PM, the Sobol analysis results of the two studies are less comparable with respect to their ranking. EI non-volatile PM 7% dominates this Sobol analysis ($S_i = 0.66$), which again is likely due to the different PM estimation method employed. Despite this, the same top 8 contributors to uncertainty in non-volatile PM estimates are identified in this study, with the exception of EI OC.

In terms of validation, it is first good to note that no variables related to CCD are identified in the Sobol analyses of LTO emissions. Following from this, it should be noted that the values of the Sobol indices in this study are in general slightly lower than those of Stettler et al. (2011) as the variance of the output is decomposed across more input variables (LTO and CCD variables) of this newer version of AEIC. As per decomposition of variance (Eq. (4.10)), the first-order Sobol indices in both cases sum to unity. Furthermore, total-order Sobol indices are slightly higher (and never lower) than first-order indices for some parameters, indicating higher-order effects, and proving the need for a second-order sensitivity analysis despite higher computational costs. For the purposes of this study, which are focused on the estimates of fuelburn, NO_x , CO and HC (as per Simone et al. (2013)), the application of the Sobol analysis methodology is considered validated.

6.3. Results

Having compared the Sobol analysis of LTO emissions at UK airports against existing literature, this section presents the Sobol analysis of global, full-flight fuelburn and emissions estimates. The top 10 first-order Sobol indices for fuelburn, NO_x , CO and HC are considered here, and summarised in Table 6.1. Results have been ranked according to first-order Sobol index, where $S_i > 0.1$ is considered significant [1, 21].

Table 6.1: Summary of first-order indices for fuelburn, NO_x CO and HC

Fuel Burn		NO_x		CO		HC	
Input Parameter	S_i	Input Parameter	S_i	Input Parameter	S_i	Input Parameter	S_i
BADA Drag	0.532	BADA Drag	0.308	EI CO	0.681	EI HC	0.692
BADA Fuel Flow	0.284	EI NOx	0.292	Taxi Thrust	0.126	Taxi Thrust	0.128
TOW	0.122	TOW	0.194	BADA Drag	0.055	BADA Drag	0.030
Enroute Inefficiency	0.005	BADA Fuel Flow	0.157	BADA Fuel Flow	0.040	BADA Fuel Flow	0.023
Arrival Inefficiency	0.004	Enroute Inefficiency	0.006	Arrival Inefficiency	0.031	Arrival Inefficiency	0.023
Cruise Altitude	0.002	Fuel Flow	0.004	Fuel Flow	0.011	Taxi TIM	0.014
Taxi Thrust	0.002	Take-Off Thrust	0.003	Cruise Altitude	0.006	Fuel Flow	0.002
Departure Inefficiency	0.001	Cruise Altitude	0.001	Taxi Thrust	0.003	Cruise Altitude	0.002
Take-Off Thrust	0.001	Climb Out TIM	0.001	Enroute Inefficiency	0.003	Enroute Inefficiency	0.000
Approach Thrust	0.001	Departure Inefficiency	0.001	TOW	0.001	TOW	0.000

From these results it is apparent that there are few key inputs that contribute significantly to uncertainty in fuelburn and emissions estimates. BADA Drag and Fuel Flow multipliers are significant contributors to uncertainty in fuelburn and NO_x , and are ranked in the top four across each species. For the emitted species, their respective EI is a significant contributor to uncertainty. The TOW multiplier is another significant contributor in fuelburn and NO_x , while Taxi Thrust is the only other factor considered significant in the estimates of CO and HC.

The output-specific results are discussed further in detail in each respective section below. Total-order indices are also presented alongside first-order indices to reveal interactions (if any) with other inputs. Second-order indices, from which interacting input pairs can be identified, are calculated and presented in Appendix B for completeness.

6.3.1. Fuelburn

The results of the Sobol analysis for fuelburn estimates are presented in Fig. 6.9. Uncertainty is attributed largely to the corrective multipliers on the BADA performance calculations for CCD: BADA Drag ($S_i = 0.532$), BADA Fuel Flow ($S_i = 0.284$). The third most significant significant contributors to uncertainty is TOW ($S_i = 0.122$), which is used as an input into the BADA performance calculations. Note, the Sobol index for the BADA Drag multiplier is the same as calculated in the example of Section 4.2. These three parameters are modelled with relatively high variation, as per Section 3.6, with uncertainties of $\pm 31.5\%$, $\pm 24.75\%$ and $\pm 29.25\%$, respectively. The identification of these variables is significant, as their uncertainty ranges are consistent with (if not taken directly from) the values used in System for Assessing Aviation's Global Emissions (SAGE)⁴ [5, 41].

⁴SAGE is the global emissions estimation module of AEDT

Though not as significant as the aforementioned variables ($S_i < 0.1$), all three Inefficiency (Departure, Enroute and Arrival) factors are contributors to fuelburn uncertainty, as they also act as direct multipliers on fuelburn. The Cruise Altitude is the 6th largest contributor to uncertainty here, however it has the 4th largest contribution in terms of total-order effects.

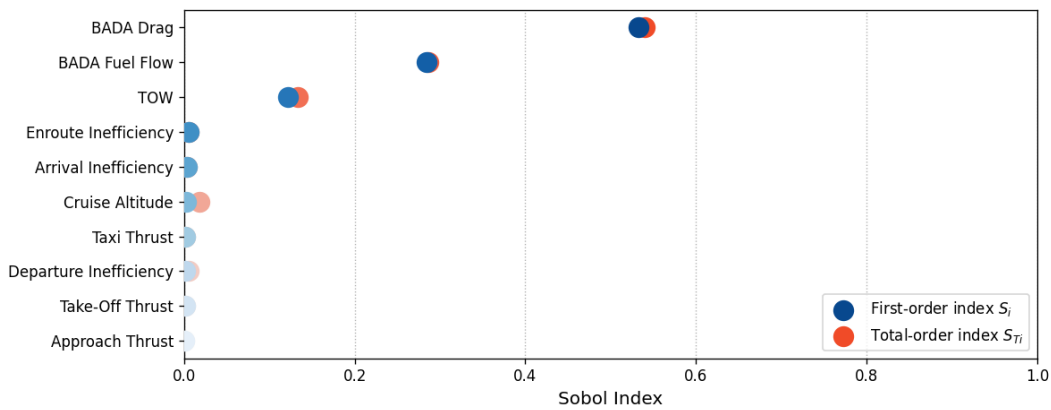


Figure 6.9: First and total-order Sobol indices for Fuelburn

In general, the total-order indices for BADA Drag ($S_{T_i} = 0.540$), TOW ($S_{T_i} = 0.133$) and Cruise Altitude ($S_{T_i} = 0.018$) adjustment factors indicate interactions, albeit of insignificant consequence. Interaction pairs can be identified in Fig. B.1. Both inputs into the BADA performance calculations, the TOW and Cruise Altitude adjustment factors, are seen to interact with the corrective fuelburn multipliers; BADA Drag and lateral inefficiencies. The largest interaction is the TOW-Departure Inefficiency combination ($S_{ij} = 0.053$). However on the whole, second-order sensitivities are low, with all $S_{ij} < 0.1$.

6.3.2. NO_x

For NO_x emissions, Fig. 6.10 demonstrates a similar pattern to that of fuelburn, demonstrating high sensitivity to factors surrounding the BADA performance calculations. Again multipliers on BADA Drag ($S_i = 0.308$), TOW ($S_i = 0.194$), and BADA Fuel Flow ($S_i = 0.157$) inputs are identified as significant contributors to uncertainty, with the addition of EI NO_x ($S_i = 0.292$), as this is modelled with a $\pm 30\%$ uncertainty.

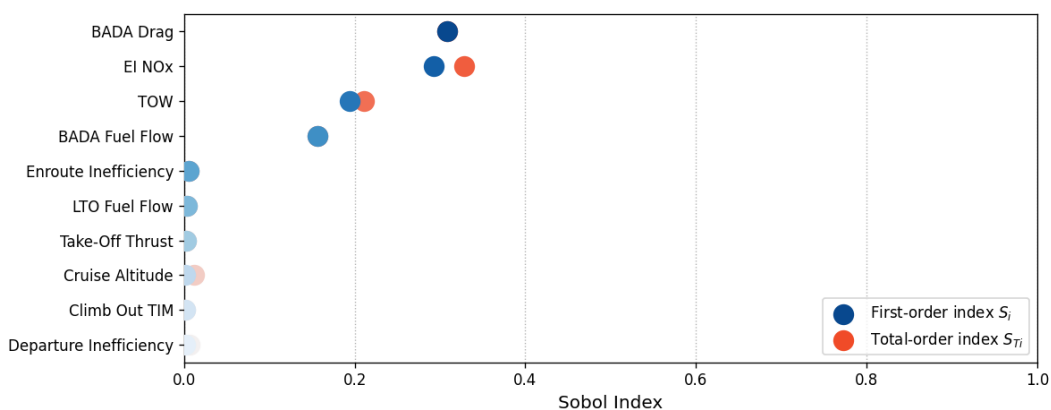


Figure 6.10: First and total-order Sobol indices for NO_x

Variation in NO_x emissions are driven by first-order effects, however total total-order sensitivities demonstrate some interaction between variables. This is largely due to interaction between EI NO_x and TOW ($S_{ij} = 0.039$), which can be identified in Fig. B.2. This is because EI NO_x itself is dependent on the ambient pressure and temperature which are derived from the BADA flight performance calculations, where TOW is a direct input with significant uncertainty bounds. Again, in general, interaction effects are very low.

6.3.3. CO

The uncertainty in CO estimates is dominated by EI CO ($S_i = 0.681$), as is evident in Fig. 6.11. This is due to the large uncertainty in EI CO ($\pm 60\%$), and its sensitivity to thrust level: its EI decreases with increasing thrust level [5, 21]. Apart from BADA Drag ($S_i = 0.055$), and BADA Fuel Flow ($S_i = 0.040$) multipliers, many of the top contributors to uncertainty are factors concerning low-thrust modes: Taxi Thrust ($S_i = 0.126$), Arrival Inefficiency ($S_i = 0.031$) and Taxi TIM ($S_i = 0.003$). Compared to fuelburn and NO_x , CO demonstrates higher sensitivity to inputs in the LTO regime.

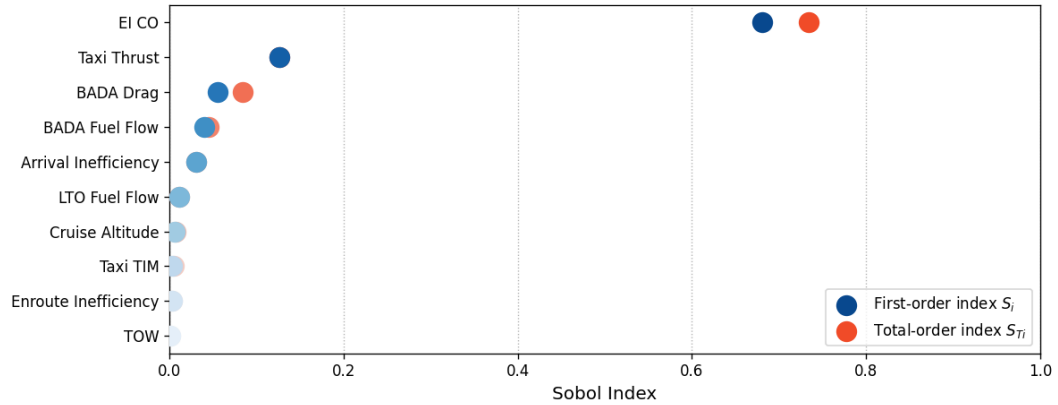


Figure 6.11: First and total-order Sobol indices for CO

The largest interaction effect between the EI CO and BADA Drag ($S_{ij} = 0.107$) multipliers, as both are modelled with high uncertainty. Furthermore, drag directly affects thrust level, upon which CO emissions are dependent. This also represents the greatest second-order sensitivity of all estimates discussed in this chapter.

6.3.4. HC

First-order sensitivities for HC reflect those of CO, as their calculation methods similar. As described in Section 5.2, HC estimates demonstrated the largest degree of relative uncertainty, with a coefficient of variation 45.2%. This uncertainty is dominated by the EI HC ($S_i = 0.691$), as is evident in Fig. 6.12. Again this is due to the large uncertainty in EI HC ($\pm 90\%$), and its sensitivity to low thrust levels, as evidenced by sensitivity to Taxi Thrust ($S_i = 0.128$), Arrival Inefficiency ($S_i = 0.023$) and Taxi TIM ($S_i = 0.014$).

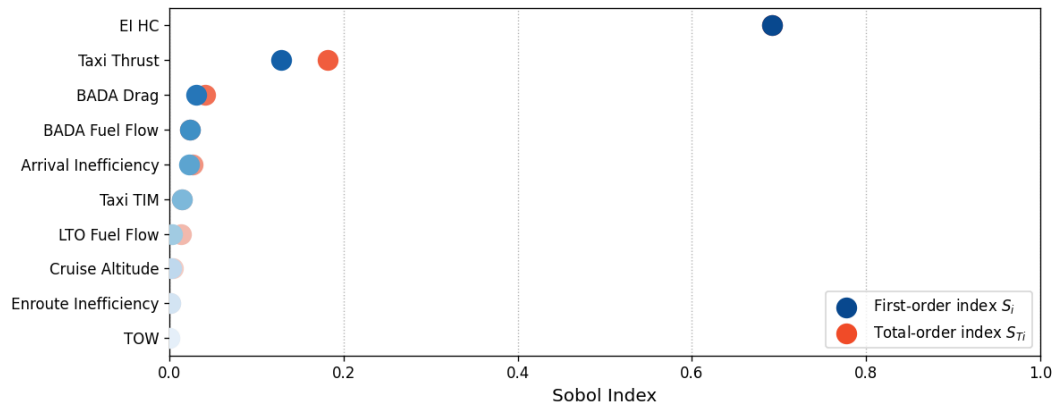


Figure 6.12: First and total-order Sobol indices for HC

For HC emissions, largest interaction effect is demonstrated by the combination of EI HC and Taxi Thrust ($S_{ij} = 0.069$). As detailed in Section 3.4.1, Taxi Thrust is the mode with the lowest thrust level, and its uncertainty is uniformly distributed, leading to equal probability of thrust at the lowest bound. Ultimately however, interaction effects are again low.

Improving Sources of Uncertainty

This chapter will detail the fourth step of the uncertainty quantification in global aviation emissions; improving sources of uncertainty. Variables with large contributions to uncertainty present an opportunity for revision. To identify a suitable option for improvement, the results of the Sobol analysis of the previous chapter will be briefly discussed. This will be followed by an in-depth exploration of the background behind the original input distribution, from which a method for updating the input distributions is developed. The resulting updated distributions are then generated and discussed. Finally, the implementation of the new input distribution into AEIC will be demonstrated.

7.1. Improvement Opportunities

Looking at the results of Chapter 6, multiple opportunities for improvement are presented, however to keep within the bounds of this research, only one can be selected as the focus of revision. Firstly, the selected input to be improved should most preferably have a broad influence; this selection will only concern variables which apply to more than one output. Thus even though the EIs of NO_x , CO and HC are key contributors to variation in their respective emissions, they will not be considered.

The BADA Drag and Fuel Flow multipliers are significant contributors, appearing in the top four key inputs of analysis. The TOW multiplier is another significant contributor to variance in fuelburn and NO_x . It has been shown in Chapter 3 that the conservative uncertainty estimates bounding these three variables are consistent with current state-of-the-art inventories, and are based on comparisons which use input from aircraft manufacturers and Flight Data Recorder (FDR) data from airlines [41]. Thus, these do not present much opportunity for updating with publicly available resources.

When considering the rest of the input variables, the Inefficiency family of variables (especially Arrival and Enroute) are consistently listed just below the aforementioned options, across all emissions species. With the recent publications of archived aircraft flight track data by EUROCONTROL¹, producing more up-to-date insights into operational inefficiencies are possible. Thus, the opportunity presents itself to improve AEIC's modelling of lateral inefficiencies using a more data-driven approach. Furthermore, lateral inefficiency adjustments are used in similar reduced-order aviation emissions models, such as Fuel Estimation in Air Transportation (FEAT), which models flights along a Great Circle route, and applies a similar corrective lateral flight inefficiency [58]. Thus, the results of this revision have potential for application outside of AEIC.

7.2. Lateral Flight Inefficiencies

The role of lateral inefficiency factors in AEIC has been explained in Section 3.6. As mentioned, AEIC makes use of lateral inefficiencies determined in Reynolds (2008), which analyses several sets of flight data to determine the average ground track extension of intracontinental flights in Europe and the US [3]. This section will detail the methodology used in Reynolds (2008) study, and its interpretation in AEIC.

Lateral flight inefficiency is divided across departure, enroute and arrival. Here, the departure and arrival phases are defined as all activity within a 50 NM Terminal Area (TA) radius of the origin or destination airport, with the enroute phase being the portion of flight between the two TA radii, as illustrated in Fig. 7.1. Departure and arrival inefficiencies are characterised in terms of the XD flown when compared to leaving the TA in a straight line (R_{TA} in Fig. 7.1). Enroute inefficiency is the extra distance flown with respect to the Great circle path ($D_{Enroute_GC}$ in Fig. 7.1) [3, 5]. Extra distances are expressed in NM.

¹<https://www.eurocontrol.int/dashboard/rnd-data-archive>

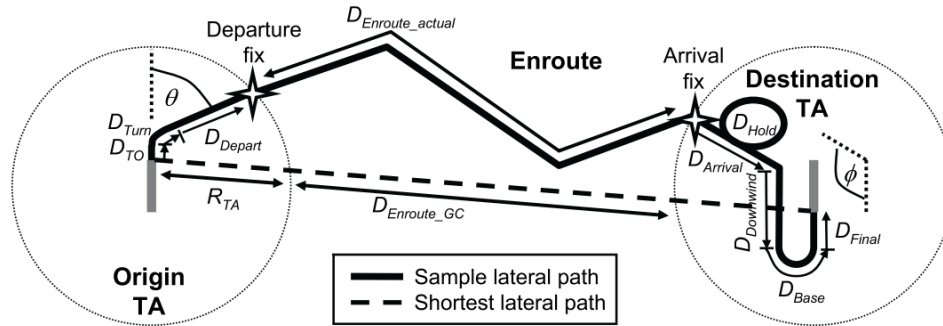


Figure 7.1: Departure, enroute and arrival inefficiencies compared to the great circle path [3]

As thousands of flights are analysed, inefficiencies for departure and arrival are presented in histogram form, as per Fig. 7.3. Enroute inefficiencies are plotted against the enroute Great Circle distance (GCD), as in Fig. 7.12. The nominal results of these analyses have already been presented in Section 3.6, but are repeated here for clarity (Table 7.1 shows nominal departure and arrival inefficiencies, and Eqs. (7.1) and (7.2) are expressions for nominal enroute inefficiency).

Table 7.1: Overview of lateral inefficiency uncertainty distributions, per region

Inefficiency	Nominal Inefficiency		Uncertainty Distributions	
	EU	US	EU	US
Departure [NM]	9.0	7.8	$\sim Tri(0, 5, 25)$	$\sim Tri(0, 3, 23)$
Enroute [-]	1.0	1.0	$\sim Tri(0.25, 1.0, 2.5)$	$\sim Tri(0.25, 1.0, 2.0)$
Arrival [NM]	26.9	27.7	$\sim Tri(0, 22, 57)$	$\sim Tri(0, 2, 75)$

$$XD_{Enroute_EU} = 0.020 \cdot GCD_{Enroute} + 12 \quad (7.1)$$

$$XD_{Enroute_US} = 0.029 \cdot GCD_{Enroute} + 22 \quad (7.2)$$

The uncertainty distributions for departure and arrival have simply been approximated from the histograms of Reynolds (2008) such that the mean of the triangular distribution matches the mean of the calculated inefficiency. Enroute uncertainty is modelled as a multiplier on the nominal enroute inefficiency. These bounds seem to be chosen arbitrarily. These may be unrepresentative of actual behaviour, as is apparent when comparing Figs. 7.2 and 7.3.

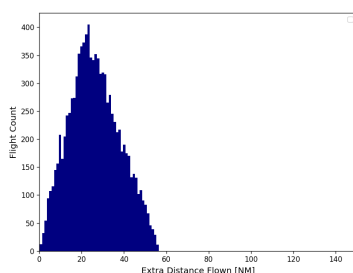


Figure 7.2: Distribution of EU arrival inefficiencies from AEIC, based on results of Reynolds (2008)

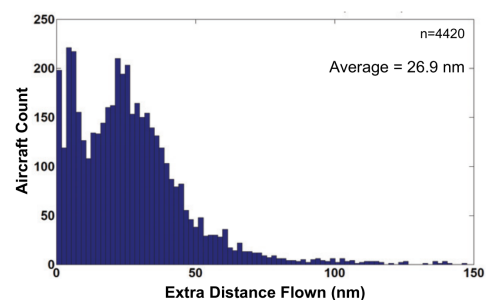


Figure 7.3: EU arrival inefficiencies from Reynolds (2008) [3]

In terms of implementing the inefficiencies from Reynolds (2008) into AEIC's flight, inefficiencies are applied to CCD using the same structure: departure inefficiencies are applied to the first 50 NM of climb, enroute inefficiencies are then applied to the flight distance up until the last 50 NM, and arrival inefficiencies are applied to the last 50 NM of descent [34]. In the departure and arrival phases of flight, AEIC makes use

of these inefficiencies as a multiplier, IM , on the first and last 50 NM portions of the flown flight, as per Eq. (7.3). The enroute extension is calculated using the enroute GCD, which is the total GCD minus 100 NM, and applying either Eq. (7.1) or Eq. (7.2), depending on the location of the flight track.

$$IM = \frac{XD + 50}{50} \tag{7.3}$$

To define regions in which to apply the appropriate inefficiency, AEIC arbitrarily defines a bounding box for Europe. For the purposes of this thesis, the area enclosed by this bounding box will be referred to as ‘EU’, and is unrelated to the European Union. For all departures, arrivals and enroute portions of the generated flight track within this box, AEIC applies EU inefficiencies. For all departures, arrivals and enroute flight portions which occur outside of this box, the US inefficiency values are assumed, due to a lack of data [48]. This bounding box is defined between the latitudes of 36° to 72°, and longitudes of -13° to 45°, and can be visualised in Fig. 7.4.

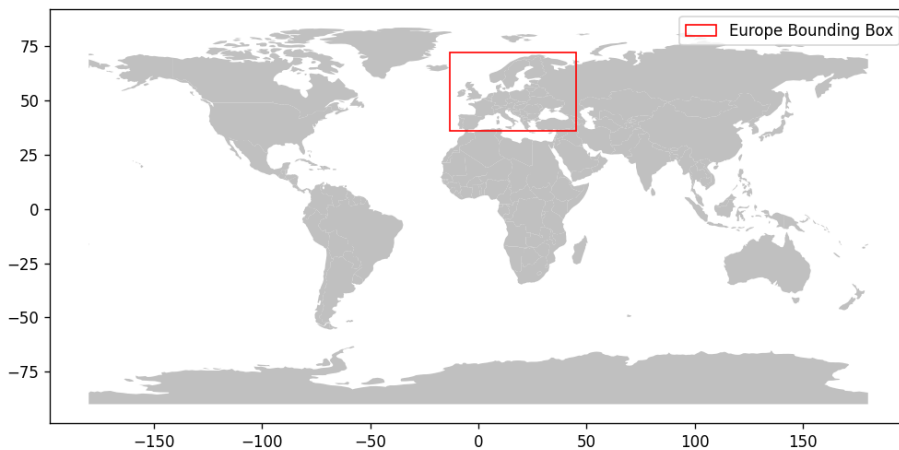


Figure 7.4: Region in which AEIC applies EU inefficiencies

The lateral inefficiency factors from the Reynolds (2008) study present an appropriate correction for AEIC’s Great Circle route assumption, as they are also calculated based on a GCD. However, a due to an admitted lack of data, values from the US analysis are applied to the rest of the world, which can be unrepresentative of actual flight inefficiencies in these regions [34]. Furthermore, the US inefficiencies are based on domestic flights, which may not accurately represent the intercontinental flights that they are applied to. Developing inefficiencies based specifically on AEIC’s EU definition may allow for a more appropriate representation of flight behaviour within this region and the rest of the world.

Finally, the results of the previous show inefficiencies as one variable; no region is specified. This is due to the respective variable being mapped onto the distributions of the two regions. This is demonstrated in Fig. 7.5, and is the same for departure, enroute and arrival. Inefficiencies are the only variables in AEIC divided in this way. The results of the re-propagation of improved uncertainties should also reveal which region the model is most sensitive to.

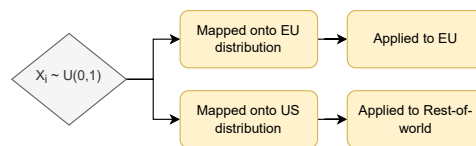


Figure 7.5: Flowchart of stochastic mapping of inefficiency across EU and US variables

7.3. Methodology

Since the publication of AEIC and the inefficiencies of Reynolds (2008), there have been various studies quantifying lateral flight inefficiencies using different methodologies [16, 59, 60]. Many of these studies quantify inefficiency in terms of different indicators such as fuel burn, or time. However, more importantly these studies consider inefficiency with respect to the nominal full-flight distance; not the direct Great Circle route. As AEIC employs lateral flight inefficiencies to extend the Great Circle route of each phase (departure, enroute, arrival), from which fuel burn is then calculated, the results of these studies are not applicable to the calculation process of AEIC. As such, the methodology of this study will be largely based on that of Reynolds (2008).

7.3.1. EUROCONTROL R&D data archive

The EUROCONTROL R&D data archive is a huge archive of real flight data, from Instrument flight rules (IFR) flight plans, which is then updated with live flight data. Flight plans are submitted by airlines and other aircraft operators to EUROCONTROL's Network Manager (NM). The planned flight profile through points in the airspace is then generated by NM's Air Traffic Flow Management (ATFM) systems. Once a flight plan is activated, more accurate data of the actual flown flight is then used to update flight points. This data is received by EUROCONTROL's Central Route Charges Office (CRCO), and comes from air navigation service providers around Europe, using sources such as flight data systems, radar and datalink communications. As all flights in IFR flights in the EUROCONTROL NM area are required to report their flight plans, the EUROCONTROL R&D data archive presents ATM-quality data of all commercial flights departing/arriving in, or flying over Europe [61].

EUROCONTROL makes data from 4 months (March, June, September, December) per year available, which contain roughly 3 million flights per year. Released with a 2-year delay, there is currently 5 years worth of these 4-month datasets, from March 2015 through to September 2019 (at the time of writing), represented across 19 separate files. The bulk of the available data is flight point data, spread across two files: Filed (flight plan) Flight Points, and Actual Flight Points. These two files contain sequential information (per unique flight) on flight level, latitude and longitude, and time at which the point was crossed for the entirety of the flight. For the purpose of this study, the Actual Flight Points file is of interest. Accompanying these flight point files is a Flights file, which gives an overview of a flight's origin and destination airports, off-block and arrival times (filed and actual), aircraft type, operator and registration, and actual flight distance flown.

Each unique flight is identified using a numeric EUROCONTROL ID in both the Flights and Flight Points file. Using the Flights file in conjunction with the Actual Flight Points file allows for identification of a flight of interest based on origin and departure airport information, and subsequent analysis of the flight's actual trajectory.

7.3.2. Calculating Lateral Inefficiencies

As outlined in the previous section, AEIC's methodology for modelling operational inefficiencies comes from Reynolds (2008), and is based on the average Great Circle route extension [56]. Thus, in order to have the results of this analysis be the most applicable to AEIC, the methodology will be consistent with that of Reynolds (2008), with some modifications to make it uniquely applicable to AEIC.

Using actual flight point data from EUROCONTROL, a flight from London Heathrow Airport (LHR) to Amsterdam Schiphol Airport (AMS) is plotted against the Great Circle route in Fig. 7.6 (which can be directly compared with Fig. 7.1). Here the 50 NM departure and arrival TA radii, $r_{TA_{dep}}$ and $r_{TA_{arr}}$, are clear. The portion of flight between the two radii is considered enroute. Knowing the total Great Circle distance between airports, GCD_{total} , the enroute Great Circle distance, $GCD_{enroute}$, is simply the total Great Circle distance minus 100 NM, as in Eq. (7.4). Thus, to measure enroute inefficiencies, a flight needs to be over 100 NM (direct, airport to airport).

$$GCD_{enroute} = GCD_{total} - (r_{TA_{dep}} + r_{TA_{arr}}) \quad (7.4)$$

Using the actual flight points, it is possible to calculate the distance of the flown flight by summing the GCD between each successive flight point [58]. This method of finding the actual distance flown (of the whole flight) is verified against the 'Actual Distance Flown' column of the Flights file.

This is done to calculate each of the departure, enroute and arrival distances, D_{dep} , $D_{enroute}$ and D_{arr} , respectively. Inefficiencies are calculated as the extra distance, XD , flown by the flight when compared to the direct, straight-line GCD. This is calculated separately, for each portion of the flight as per Eqs. (7.5) to (7.7).

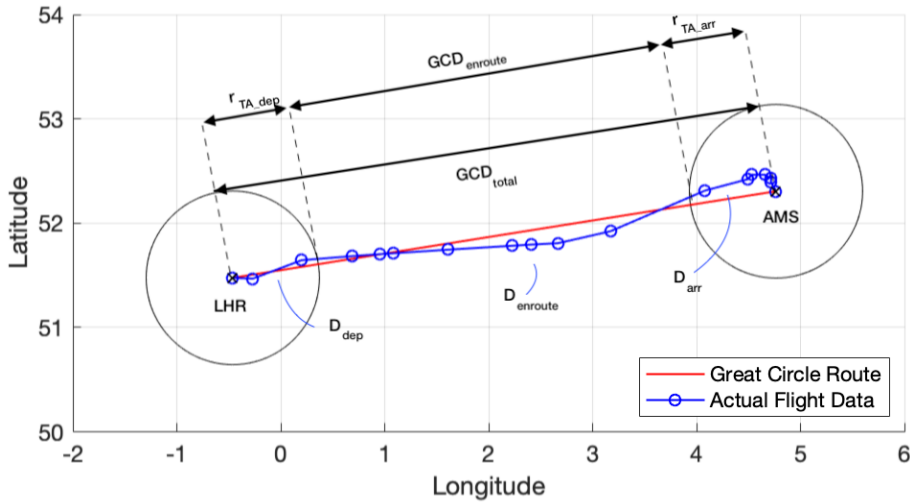


Figure 7.6: Comparison of flight point data and Great Circle route between Amsterdam Schiphol and London Heathrow

This process is done on a flight-by-flight basis, by grouping flight points in the Actual Flight Points file by their unique EUROCONTROL ID.

$$XD_{dep} = D_{dep} - r_{TA_{dep}} \tag{7.5}$$

$$XD_{enroute} = D_{enroute} - GCD_{enroute} \tag{7.6}$$

$$XD_{arr} = D_{arr} - r_{TA_{arr}} \tag{7.7}$$

7.3.3. Modifications

As is evident from Fig. 7.6, there may not always be a flight point on the 50 NM TA radius. As there is no interpolation between points, a TA radius may not be identified. Thus a slight modification to account for this is necessary; the TA radius is defined as a window around 50 NM, to try and capture a larger number of flights. This is visible in Fig. 7.7, where the radius window is set to 50 NM ± 10 NM.

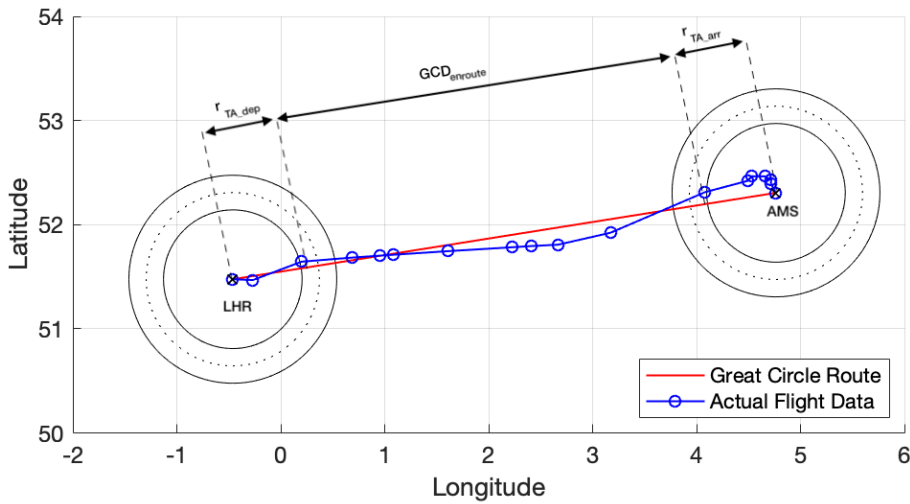


Figure 7.7: Illustration of TA radius range

Here, the TA radius used for inefficiency calculations (Eqs. (7.5) to (7.7)) is set by the first point within this window, closest to the departure or arrival point. For example, $r_{TA_{dep}}$ is equivalent to the GCD from LHR to the first point within this window (the third flight point in this flight). Similarly, $r_{TA_{arr}}$ is set as the GCD from the last flight point within the arrival TA radius window and AMS (in this case the 7th to last flight point). As

the TA radii change depending on the flight data points, as does $GCD_{enroute}$ according to Eq. (7.4). In this manner, XD s are calculated with respect to a relevant TA radius.

In terms of the flown flight, departure and arrival data consists of all flight points up to, and including, this identified r_{TA} . The enroute data is all flight points between the two r_{TAs} . If there is no flight point within the TA radius window, the inefficiency here is not calculated. For instance, if the third data point in Fig. 7.7 was further west, the XD_{dap} case would not be calculated. In this case, the enroute data then consists of all flight points between the first flight point outside the TA radius, up until r_{TAarr} . Thus, enroute and arrival inefficiencies are still calculated despite insufficient data at departure. Adjusting the bounds of this window closer to 50 NM ensures that inefficiencies more are closely comparable to Reynolds (and applicable to AEIC), however this means flights which do not have a flight point within this window are filtered out, resulting in less flights analysed. The sensitivity to this window is addressed in Section 7.6.

In terms of modifying the method to make the results of this analysis uniquely relevant to AEIC, the regions of interest are defined as per AEIC: namely, defining EU inefficiencies as per the bounding box of Fig. 7.4. As analysis is already coordinate based, results can be categorised based on location. Thus, depending on the location of the departure airport, enroute portion or arrival airport, the inefficiency calculated is added to one of two lists: EU or Rest-of-World, depending on where it occurred. This should correct for the assumption that US inefficiencies from Reynolds (2008) are applied to flights everywhere outside the EU bounding box. Furthermore, this ensures that the behaviour of both domestic and intercontinental flights are accounted for, not just domestic as per Reynolds (2008). For instance a flight departing Europe, but arriving in Asia will have its departure accounted for in the EU values. However, due to the nature the EUROCONTROL data set, one major limitation is noted: domestic flights outside of the EUROCONTROL NM area are not recorded, and thus cannot be included in this analysis.

7.4. Comparisons With Existing Literature

To compare the results of the described method, the inefficiency calculations of two other inefficiency studies are emulated. The first being the original Reynolds (2008) study that this analysis is based on. The second is the EUROCONTROL EFEI study performed in 2004, to further validate the method. This second study is chosen as it also calculates inefficiencies based on a direct Great Circle route, and uses a similar data type to the data used in this study, being sourced from EUROCONTROL [4, 62, 63]. It is also referenced by Reynolds (2008) [3]. Validation will be done using the month's worth of data of for March 2015 from the EUROCONTROL R&D data archive. A TA radius of $50 \text{ NM} \pm 5 \text{ NM}$ is used throughout.

7.4.1. Reynolds (2008)

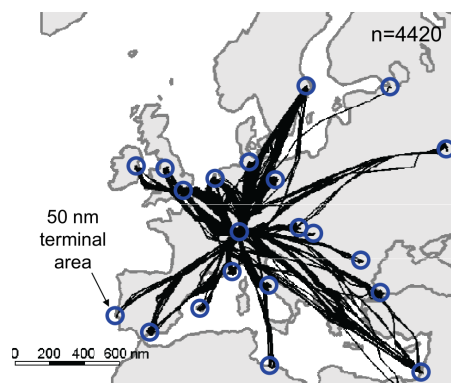


Figure 7.8: Ground tracks of Swiss A320-family flights analysed by Reynolds (2008) [3]

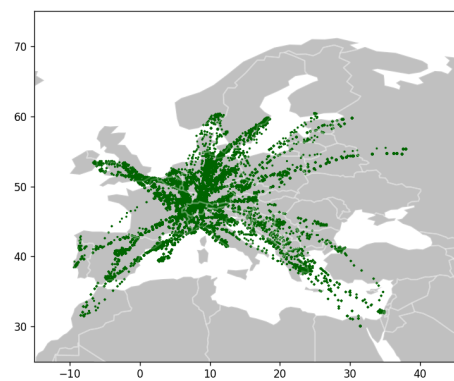


Figure 7.9: Ground tracks of Swiss A320-family flights from the EUROCONTROL R&D data archive

The analysis EU and US inefficiency studies from Reynolds (2008) will be replicated using similar input data, and compared. For the EU analysis of Reynolds (2008), the FDR archive data of a random selection of 4,400 Swiss Airlines A320-family flights, flown within Europe in 2008, were used [3, 64]. The ground tracks of these flights are shown in Fig. 7.8. Note the 50 NM radii of TAs. From the EUROCONTROL R&D data archive Flights file, it is possible to filter flights by aircraft type and operator; thus their unique IDs are obtainable. For the month of March in 2015, filtering flights by Swiss Airlines operated A319, A320 and A321 results in 5,600

individual EUROCONTROL ID's. Their associated flight points are then obtainable in the Actual Flight Points file. The flight tracks of these flights are shown in Fig. 7.9. This demonstrates largely the same route network with the addition some routes, for instance to Morocco, Norway and Finland. This is expected, given route expansions in the years between the two data sets.

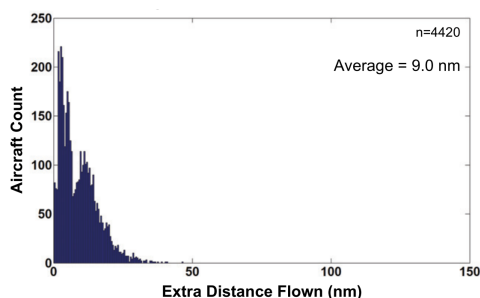


Figure 7.10: European departure inefficiencies from Reynolds (2008) [3]

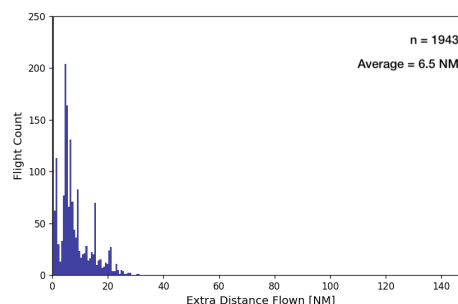


Figure 7.11: Swiss Airlines A320-family departure inefficiencies from March 2015

Plotting the results of the departure inefficiencies shows a similar trend to Reynolds (2008). Figs. 7.10 and 7.11 demonstrate two peaks: one near zero, and another before 20 NM. There are no instances of flights flying more than 50 NM extra in departure. The average departure inefficiency of 6.5 NM from this study is 28% lower than the 9 NM calculated in Reynolds (2008), and results demonstrate a strong bias towards zero. This may be due to the lower fidelity data of the EUROCONTROL archive data. In the TA radius, there is an average of 4 minutes between consecutive flight points, while the points in the Reynolds (2008) data set are characterised by update rates of at least 60 seconds [3]. This may result in a less detailed representation of the flown flight in these phases. This lower inefficiency may also be a product of improved ATFM systems, and general improvement in operations efficiency over the decade between these flights. Also important to note here is the effect of filtering due to lack of points in the TA radius. From the 5,600 flights identified, 1,943 departures have sufficient data to determine a TA radius, and are analysed.

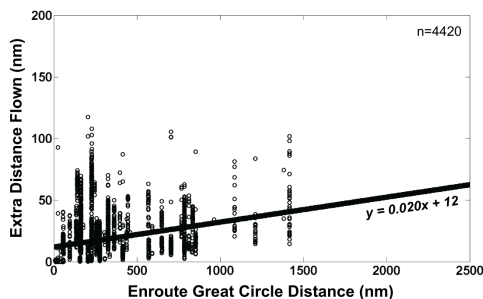


Figure 7.12: Intra-EU Enroute inefficiencies from Reynolds (2008) [3]

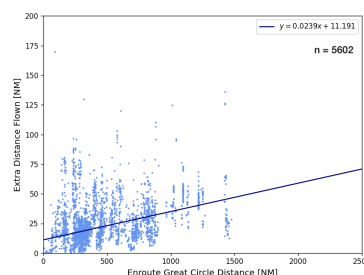


Figure 7.13: Swiss Airlines A320-family enroute inefficiencies from March 2015

Comparing enroute inefficiencies shows a high degree of similarity between this study and Reynolds (2008). The average enroute extra distance calculated in this study is 21.6 NM which is consistent with the 21.2 NM inefficiency from Reynolds (2008). This is reflected in the almost equivalent equations of nominal extra distance (which express extra distance in terms of enroute GCD) demonstrated in Figs. 7.12 and 7.13. Here, the vertical columns of points clearly illustrate the variance in extra distance for unique routes.

As with departure inefficiency, the arrival inefficiency of this study clearly shares the same two-peak trend as Reynolds (2008), but are more heavily skewed towards the right, as per Figs. 7.14 and 7.15. This study presents a much stronger peak at approximately 10NM, while a significant portion of the flights in the Reynolds (2008) study are distributed around 25 NM. Furthermore, Reynolds (2008) demonstrates inefficiencies up to 150 NM, however in this study, no arrival flies more than 90 NM extra. A calculated average arrival inefficiency of 14.42 NM represents a 46% decrease from the 26.9 NM inefficiency of Reynolds (2008).

When considering the relative contribution of each phase to the total flight inefficiency, the departure/enroute/arrival contributions are 15%/51%/34%, compared to 16%/37%/47% from Reynolds (2008).

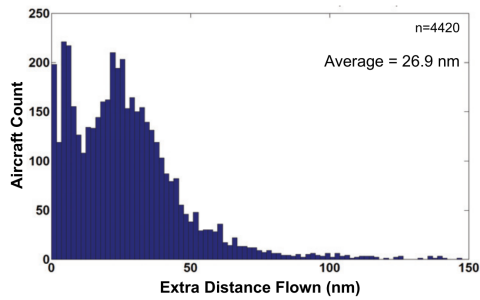


Figure 7.14: European arrival inefficiencies from Reynolds (2008) [3]

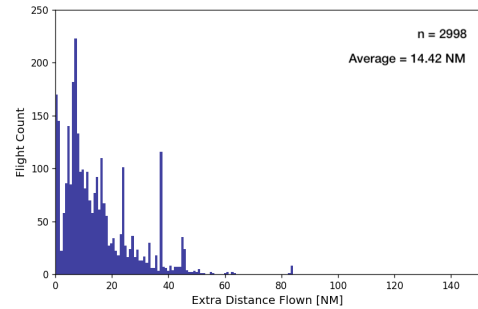


Figure 7.15: Swiss Airlines A320-family arrival inefficiencies from March 2015

The most significant difference is from the much greater arrival inefficiency of Reynolds (2008), which reduces the contribution of the enroute phase. However, taking into account the lower fidelity data sets, and improvements in ATFM systems, the model can be considered validated when replicating European inefficiency trends.

For the US, the Reynolds study analyses the Enhanced Traffic Management System (ETMS) flight track data of 3,000 domestic flights originating from 9 major airports² which took place on the 25 January 2005. From the EUROCONTROL R&D data archive, for the month of March in 2015, filtering flights arriving or departing from these airports identifies 14,000 flights. Due to the nature of the EUROCONTROL data source, these flights all have a portion of their flight track over the EUROCONTROL NM area. As such, none are domestic, and flight tracks are immediately incomparable when looking at Figs. 7.16 and 7.17.

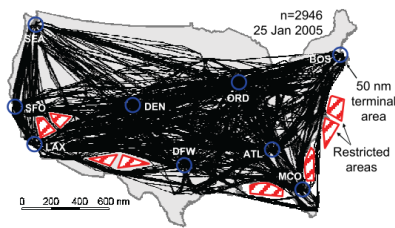


Figure 7.16: Ground tracks of domestic flights originating from 9 major US airports [3]

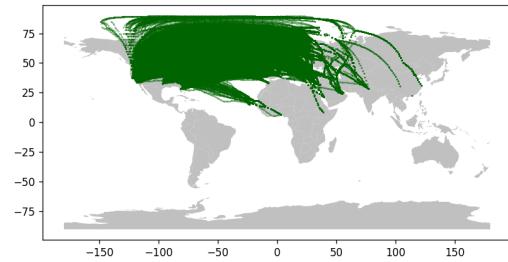


Figure 7.17: Ground tracks of flights originating or arriving at the 9 major US airports

With the aim to analyse US departures and arrivals, it was discovered that there is insufficient data to analyse TA inefficiencies, possibly due to security reasons. Looking at the first flight points departing a US airport, and last flight points arriving at a US airport, this is clearly demonstrated. Figs. 7.18 and 7.19 show the first flight point is typically further than 50 NM away from the departure airport, and is over FL150. Similarly, Figs. 7.20 and 7.21 show the last flight point is typically further than 50 NM away from the destination airport, and is over FL100. For flights with a first or last point within the TA radius window, the distance flown in the TA is the same as the TA radius. Thus, inefficiencies here are calculated as zero according to Eqs. (7.5) and (7.7). Ultimately, the model used for this study is not validated for US inefficiencies on the basis of insufficient data.

²Boston (BOS), Atlanta (ATL), Orlando (MCO), Dallas (DFW), Chicago (ORD), Denver (DEN), Seattle (SEA), San Francisco (SFO) and Los Angeles (LAX)

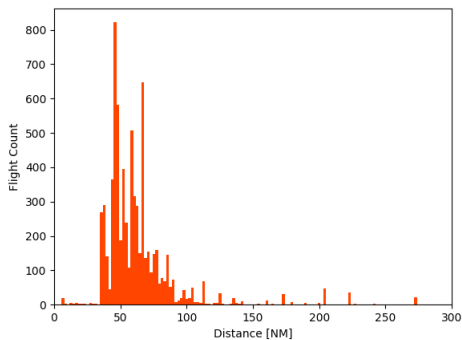


Figure 7.18: Distance from departure airport to first flight point in the US

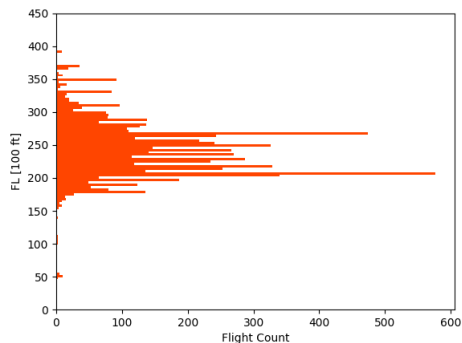


Figure 7.19: Flight level of the first flight point after departure in the US

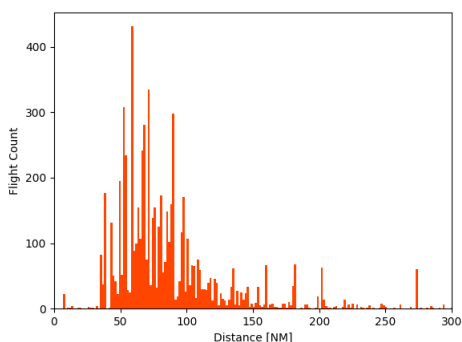


Figure 7.20: Distance from last flight point to destination airport in the US

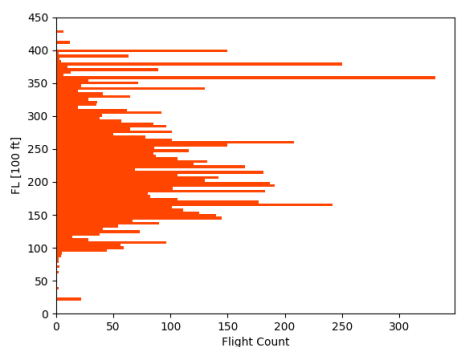


Figure 7.21: Flight level of the last flight point before arrival in the US

Interestingly, when looking at all flights with departure or arrival outside the EU bounding box, it seems most flights with sufficient data (more than one flight point in the TA radius) are clustered around Europe. This is visible in Fig. 7.22. This is unsurprising, considering the nature of the EUROCONTROL dataset. However, for the purposes of this validation, using these departures and arrivals outside of the bounding box do not provide a good description of US flight behaviours.

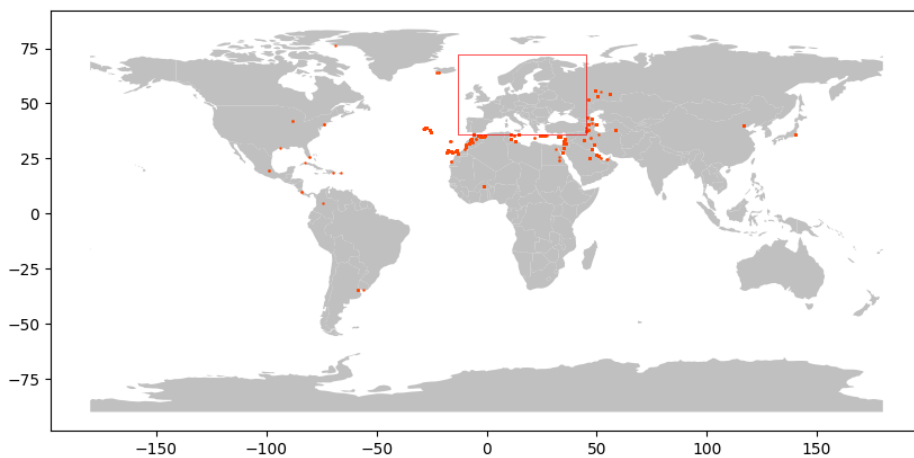


Figure 7.22: Flights with sufficient TA data outside of the European bounding box

7.4.2. EUROCONTROL (2004)

To further compare the results of this method for EU inefficiencies, the inefficiencies developed by the EUROCONTROL Enhanced Flight Efficiency Indicators (EFEI) study are emulated. The EFEI (2004) study is an earlier study, however shares many similarities with Reynolds (2008), and is often referenced by Reynolds (2008). It compares actual trajectories to an optimum trajectory, which is considered the GCD between airport pairs. Similarly, the TA is defined as a radius of 50 NM, with the portion of flight between the rings considered enroute [4, 63]. On top of employing a similar method, the EFEI (2004) study also makes use of data from EUROCONTROL. The main difference is that it presents inefficiencies in terms only two phases: TA (combining both departure and arrival), and enroute. In this study, three airport pairs are analysed: London Heathrow Airport (LHR)-Geneva Airport (GEN), Paris Orly Airport (ORY) - Nice Cote d'Azur Airport (NCE) and Birmingham Airport (BHX)-Copenhagen Airport (CPH).

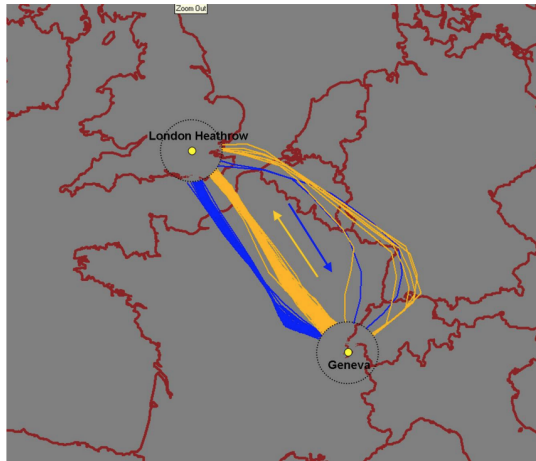


Figure 7.23: Actual trajectories between LHR-GEN from EFEI (2004) [4]

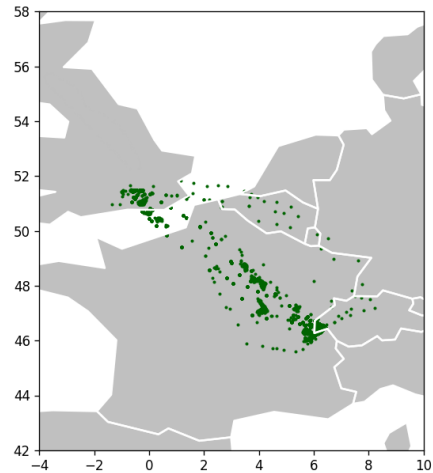


Figure 7.24: Actual trajectories between LHR-GEN from March 2015

For the LHR-GEN route, actual flight tracks from the Enhanced Flight Efficiency Indicators (EFEI) study and this study can be compared in Figs. 7.23 and 7.24. Do note the EFEI (2004) images do not show trajectories within the TA radii. Nonetheless, the same airways are present in this study. The relative share of total extra distance flown in TA/enroute is calculated as 75%/25% in the EFEI (2004) study and 71%/29% in this study, demonstrating a strong correspondence. Furthermore, the EFEI (2004) study reports an average total extra distance flown of 42.1 NM, compared to 44.2 NM in this study, implying TA inefficiencies and enroute inefficiencies are similar.

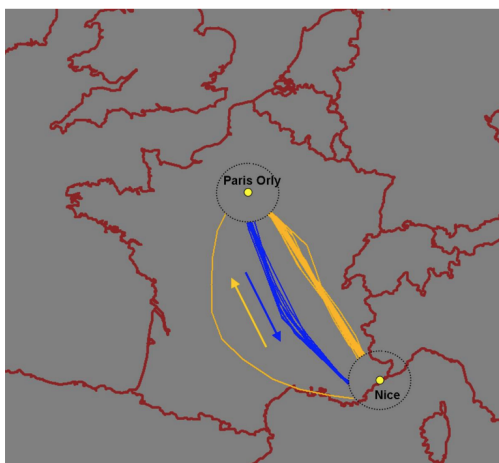


Figure 7.25: Actual trajectories between ORY-NCE from EFEI (2004) [4]

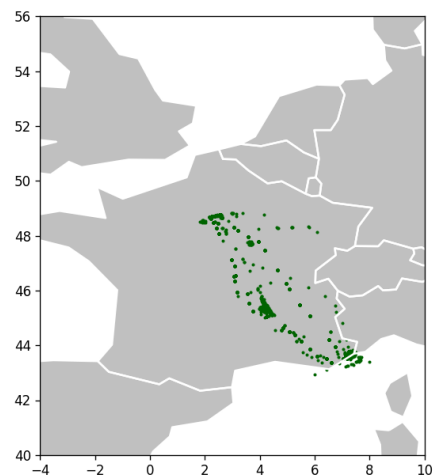


Figure 7.26: Actual trajectories between ORY-NCE from March 2015

The ground tracks for the ORY - NCE routes present significant variation between the two studies, as is apparent in Figs. 7.25 and 7.26. This difference is reflected in the enroute extra distances calculated: 4.6 NM from EFEI (2004) and 23.3 NM from this study. This is explained by the rather direct, and thus efficient routes of the EFEI (2004) data, compared to the more spread out routes taken in the data of this study. Despite this, total extra distances are similar: from 39.7 NM EFEI (2004) and 43.3 NM for this study. The TA to enroute share of inefficiencies are 88%/12% and 47%/53%, respectively.

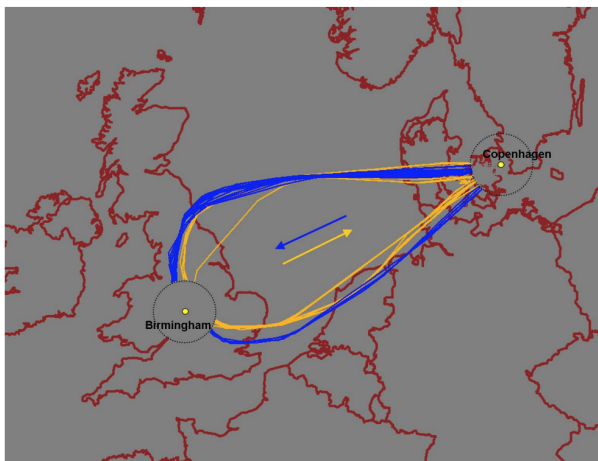


Figure 7.27: Actual trajectories between BHX-CPH from EFEI (2004) [4]

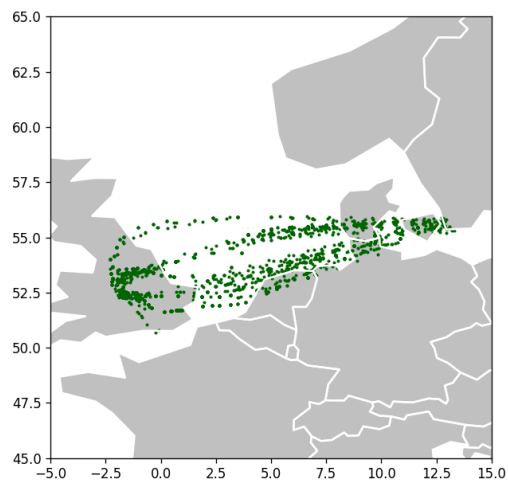


Figure 7.28: Actual trajectories between BHX-CPH from March 2015

Finally, the BHX-CPH route presents an interesting view of flight track efficiency improvements, which are clearly visible in the more less direct flights of Fig. 7.27 versus those presented in Fig. 7.28. The total average extra distance for this route was 97.2 NM in the EFEI (2004) study, and 71.2 NM in this study; an almost 30 NM improvement in efficiency from 2003 to 2015. Despite this, the share of inefficiency is split similarly: 36%/64% from EFEI (2004) and 32%/68% from this study. This is due to the larger total extra distance which is flown.

The results of this comparison justify the method described for intra-EU flights. The comparison between calculated values from the EFEI (2004) study and this study are present in Table 7.2.

Table 7.2: Comparison between values calculated in the EFEI (2004) study and this study

	LHR-GEN		ORY-NCE		BHX-CPH	
	EFEI	This Study	EFEI	This Study	EFEI	This Study
TA XD [NM]	31.59	31.24	34.83	20.18	35.09	22.74
Enroute XD [NM]	10.53	12.90	4.86	23.13	62.10	48.44
Total XD [NM]	42.12	44.15	39.69	43.31	97.19	71.18
TA/Enroute Share	75%/25%	71%/29%	88%/12%	47%/53%	36%/64%	32%/68%

7.5. Results

Both validation studies have proved that the prescribed method is reliable in terms of calculating the inefficiencies of EU flights. Thus, the analysis is run for all 19 sets of data from March 2015 through September 2019. This represents 30 GB worth of the actual flight point data of 15,670,824 flights departing, arriving or flying through the EUROCONTROL NM area. Do note that the actual number of flights analysed is lower due to data availability in the TA radius. Processing each of the 19 Actual Flight Points file takes between 11 to 16 hours on a single core of a 'fat' compute node from the Dutch national supercomputer Snellius. Each of the 128 cores on a fat node has 64 GB of memory.

To extend this method to make full use of the EUROCONTROL archive data, enroute inefficiencies in the rest of the world will still be calculated, as the enroute portion does not suffer from data insufficiency overseas. However, due to the nature of the EUROCONTROL data, this will largely mean that these flights are

intercontinental (ie. no international domestic flights are captured as they do not overfly the NM area). These will thus be referred to as intercontinental enroutes.

7.5.1. Departure

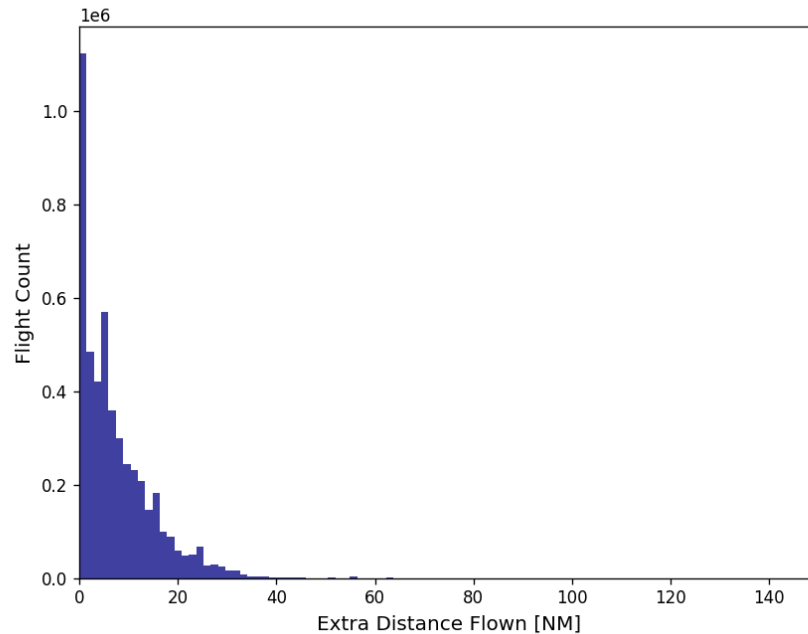


Figure 7.29: Distribution of extra distance flown during EU departures

The results for EU departure inefficiencies for the whole data set are presented in Fig. 7.29. The average extra distance flown in EU departures is 7.61 NM, roughly 15% lower than the value from Reynolds (2008). This is measured across 4.8 million analysed flights. The average value for the departure radius point is 50.05 NM, and inefficiencies are calculated using an average of 5 flight points. These results demonstrate a strong bias towards zero, with a significant peak in the first bin. Unlike the results of the Swiss Airlines flights of the validation study, the two peak pattern is not as apparent, however there is a second spike in inefficiencies between 5-6.5 NM.

7.5.2. Enroute

Intra-EU enroute inefficiencies are presented in Fig. 7.30, as a function of enroute GCD. This result is measured across 11.6 million flights. Approximately 2 million flights are filtered out of the total number of intra-EU flights as they are under 100 NM in length (no enroute portion by definition of TA radii). Despite this, there is still a significant number of enroutes analysed, and significant scattering. There is however a general trend, reflected in the line of best fit, suggesting an average inefficiency of 3.3% of the flight's enroute GCD, plus 7.2 NM. Compared to the original function (shown in Fig. 7.12), this line is steeper but is shifted down by 5 NM. The lines of the updated and original functions intercept at around 370 NM, thus suggesting that flights with enroute distances below 370 NM fly less extra distance, and past this point, enroute inefficiencies are greater than the results of the Reynolds (2008) study. As the enroutes analysed here are up to 2,500 NM, this represents a greater enroute inefficiency for a significant portion of flights.

The intercontinental enroute inefficiencies of 3.6 million flights, with both departure and arrival airports outside of the EU bounding box, are shown in Fig. 7.31. The average inefficiency is 2.2% of the GCD, plus 37.4 NM. As mentioned in Section 7.2, the domestic US enroute inefficiency of Reynolds (2008) is used in AEIC is assumed to describe all enroute behaviour outside of the EU bounding box. Comparing to the US enroute inefficiency (Eq. (7.2)), the updated intercontinental enroute inefficiency demonstrates a shallower slope. As a result of this, the updated intercontinental enroute inefficiency is lower for enroute distances greater than 2,200 NM. This is a significant result, as the Reynolds (2008) study of domestic US flights only considered

enroute distances up to 2,500 NM, whereas this study analyses flights covering over 8,000 NM.

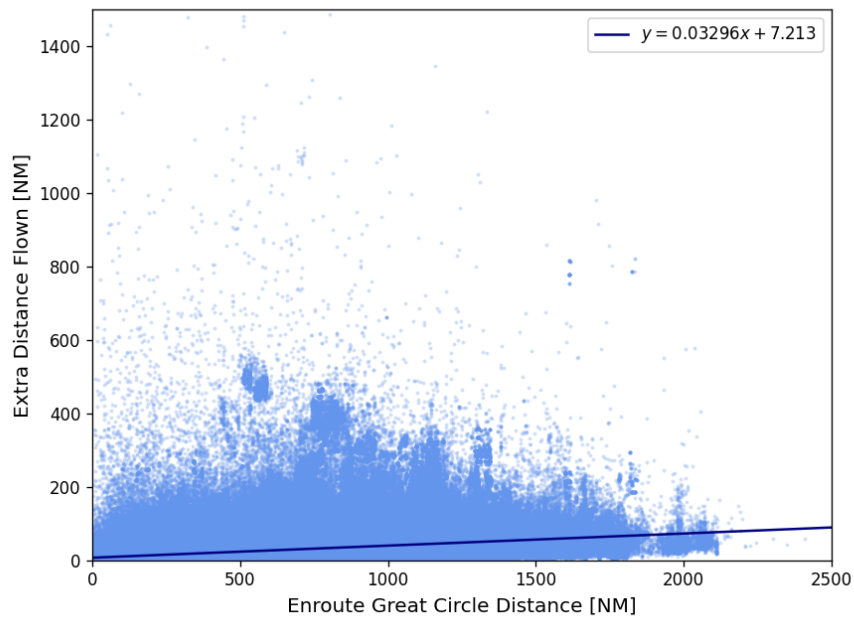


Figure 7.30: Extra distance flown enroute against great circle routes for intra-EU flights

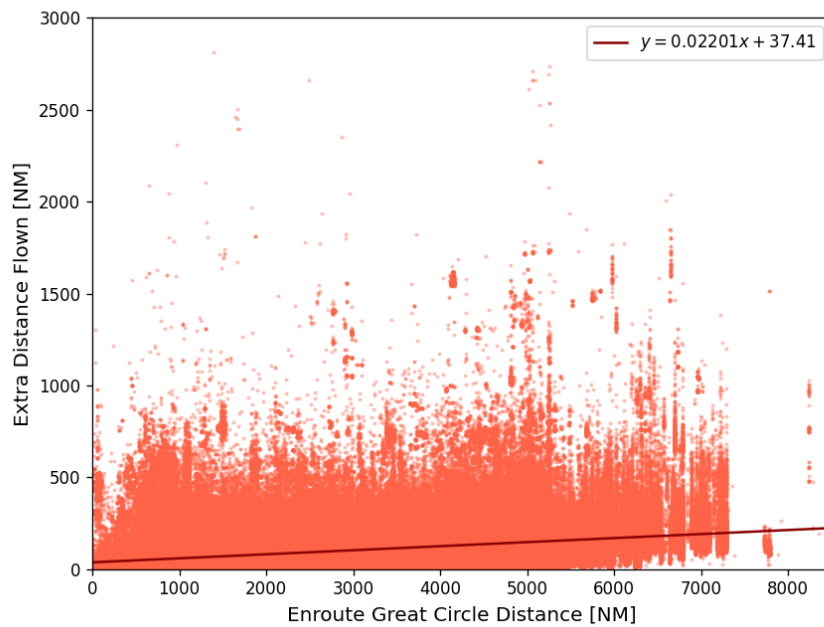


Figure 7.31: Extra distance flown against great circle routes for intercontinental flights

As is evident from Fig. 7.31, the variation of extra distance for specific flights is much clearer than in the intra-EU enroutes, as there are less flights analysed. Specific flights appear as vertical columns of data at specific points along the horizontal axis, which demonstrates some interesting flights. The most-right column of

data points represents the longest flight in the world at the time, with a GCD of 8,285 NM: Singapore Changi Airport (SIN)-Newark Liberty International Airport (EWR) flight flown by Singapore Airlines (SQ21/SQ22). The flight typically covers 9,000 NM, and is flown by the Airbus A350-900ULR which has an extended range of 9,700 NM, explaining the often high extra distance flown compared to the GCD³.

The cluster of data points just to the left of the SIN-EWR flights, and below the line of best fit, are the Perth Airport (PER)-LHR flights flown by Qantas (QF9/QF10) with a GCD of 7,830 NM. Here, the extra distance flown is very limited, as the route actually exceeds the standard 7,565 NM range of the Boeing 787-9 aircraft used for this flight⁴, however Qantas likely flies these aircraft with a lower load factor to exceed the design range.

Finally, most of the longest flown flights in the dataset are actually those between Indira Gandhi International Airport (DEL)-San Francisco International Airport (SFO), which has a GCD of 6,700 NM. Though this route is not the longest in terms of GCD, the flown flights consistently exceed 8,000 NM, which can be seen in the large vertical dispersion of points at the 6,700 NM mark on the horizontal axis. This flight is flown by Air India's Boeing 777-200LRs, where they are flown near the limit of their 8,555 NM design range⁵. This longer route is may flown to take advantage of winds. This highlights a potential limitation of measuring inefficiencies as extra distance with respect to the Great Circle route: a longer route does not necessarily imply a more fuel-intensive flight.

7.5.3. Arrival

The inefficiencies of 6.3 million EU arrivals are presented in Fig. 7.32. As is expected, arrival inefficiencies are over twice as large as those in the departure phase, however again do not demonstrate the two-peak distribution, with a strong bias towards zero. The average extra distance flown is 15.74 NM, approximately 40% lower than the inefficiency currently used by AEIC. The average arrival radius is 50.35 NM, and inefficiency is calculated using 5.3 flight points on average.

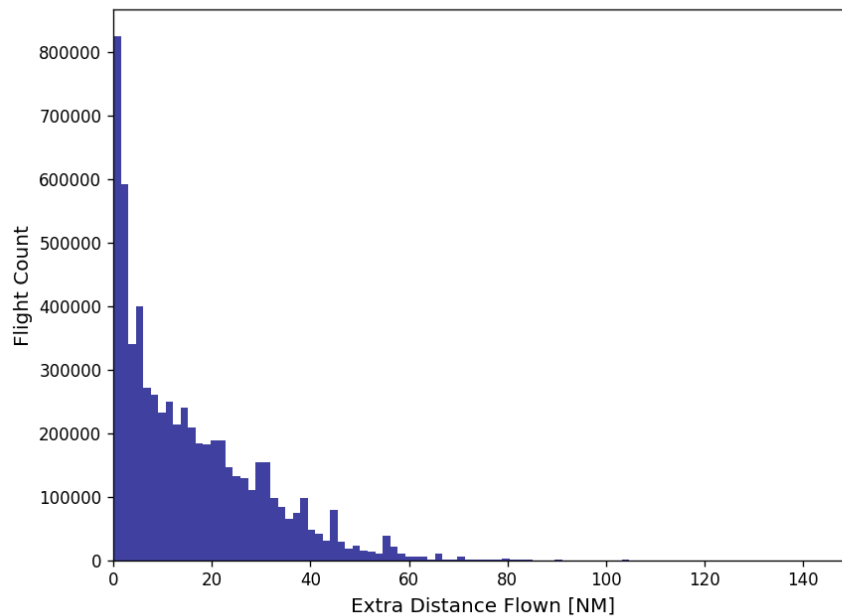


Figure 7.32: Distribution of extra distance flown during EU arrivals

³<https://aircraft.airbus.com/en/aircraft/a350/a350-900>

⁴<https://www.boeing.com/commercial/787/#/technical-specs>

⁵<https://www.boeing.com/commercial/777/#/technical-specs>

7.6. Sensitivity Analysis

As the only variable subject to change in this analysis is the TA radius window, the sensitivity of results to the size of this window is investigated. The idea behind implementing this range is to allow for the analysis of flights which do not have a flight points at the 50 NM benchmark radius. Thus, it effectively acts as a filter for flights with insufficient TA data. Thus, an appropriate range must be selected such that it captures a sufficient number of flights to analyse, without skewing inefficiency results.

To investigate this, the full analysis is run for the following different TA radius ranges. To investigate the effect of changing the size of the window, the following windows are used: 50 NM ± 5 NM, 50 NM ± 10 NM. These represent a TA radius window centered on 50 NM, of 45 to 55 NM and 40 to 60 NM, respectively. The placement of a 10 NM-wide window is then tested using the following windows: 50 NM – 10 NM, 50 NM + 10 NM. These represent a TA radius window offset from the 50 NM benchmark, of 40 to 50 NM and 50 to 60 NM, respectively.

These different ranges result in different TA radius fixes, and thus effect the calculation of the flown flight distance inside TAs and enroute. Thus, sensitivity of the TA model to these ranges is presented by comparing the average flown distance to the average TA radius, as inefficiency is a function of these values. Sensitivity of the enroute model is presented in the comparison of the extra distance flown to the enroute GCD.

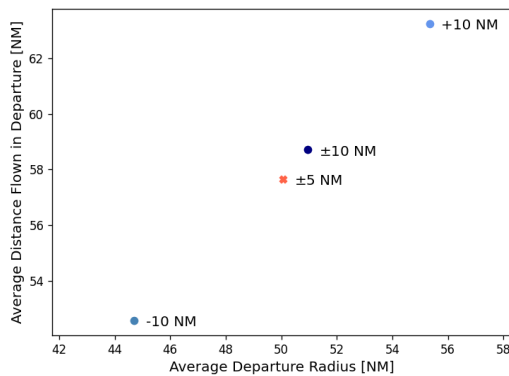


Figure 7.33: Sensitivity of departure inefficiencies to TA radius window

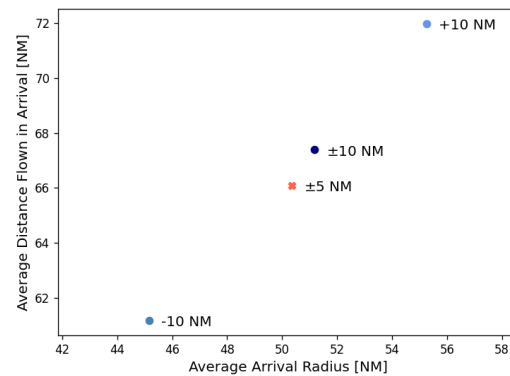


Figure 7.34: Sensitivity of arrival inefficiencies to TA radius window

Figs. 7.33 and 7.34 show very clearly that the changing bounds directly affects the flight point taken as the departure radius. This in turn dictates the flight points considered for TA analyses. Having the 10 NM window before or after the 50 NM benchmark unexpectedly serve to decrease or increase the average TA radius. In turn, the average flown distance in the TA respond linearly. Centring the window on 50 NM and changing the size from 5 NM to 10 NM seems to increase the average departure radius, and the average flown distance responds accordingly.

The effective filtering of flights due to the size and placement of this window are presented in Table 7.3. Doubling the size of the window significantly increases the number of flights analysed in both departure and arrival. Shifting the 10 NM window does not appreciably affect the number of flights analysed. However in departures, there seem to be more flights with flight points in these windows, than a window of equal size (10 NM) centred on 50 NM. However, because the 50 NM ± 5 NM case results in average departure and arrival radii closest to 50 NM, this window is selected as results are more applicable to AEIC.

Table 7.3: Number of departures and arrivals analysed in each case

TA radius range	EU Departures	EU Arrivals
50 NM ± 5 NM	4,842,554	6,274,707
50 NM ± 10 NM	8,917,584	9,784,748
40 NM - 50 NM	5,554,924	6,585,413
50 NM - 60 NM	5,234,556	5,751,267

The little variation in enroute inefficiencies in Figs. 7.35 and 7.36 suggest little sensitivity of the enroute inefficiencies to changes in the TA radius window. The relationship between TA radius and enroute GCD is

apparent in the proportional (~ 5 NM) changes between the average enroute distance. Between the four tests, calculated inefficiencies differ by 1.2 NM in the intra-EU case, and 0.6 NM in the intercontinental case. With increasing enroute distance (intra-EU versus intercontinental), changing the TA radius proves insignificant with respect to enroute inefficiencies.

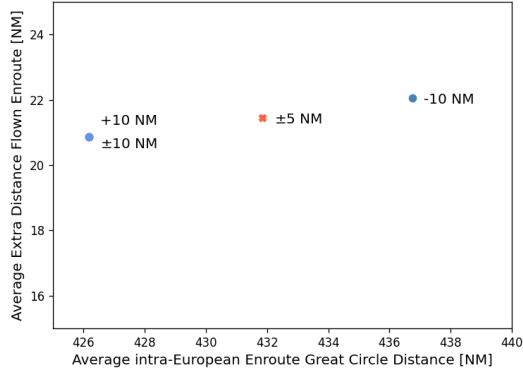


Figure 7.35: Sensitivity of intra-EU enroute inefficiencies

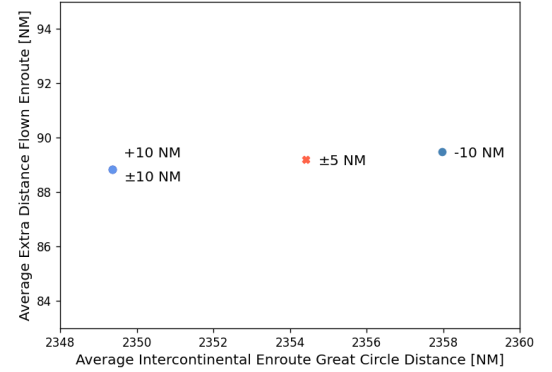


Figure 7.36: Sensitivity of intercontinental enroute inefficiencies

This insensitivity is also reflected in the numbers of enroute flight portions analysed of Table 7.4. There is relatively little variation in the enroute flights analysed across the different tests.

Table 7.4: Number of enroute flight portions analysed in each case

TA radius range	Intra-EU Enroutes	Intercontinental Enroutes
50 NM \pm 5 NM	11,643,524	3,545,289
50 NM \pm 10 NM	11,564,686	3,543,123
50 NM - 10 NM	11,732,492	3,549,898
50 NM + 10 NM	11,564,686	3,543,123

7.7. Implementation

To update inefficiencies in AEIC, it is straightforward to change the nominal values of the average departure and arrival inefficiency, as well as the relationship between enroute inefficiency and enroute GCD. A summary of these changes is shown in Table 7.5.

Table 7.5: Comparison of original and updated nominal values for inefficiency variables

Inefficiency	Original [NM]	Updated [NM]
EU Departure	9.0	7.61
EU Arrival	26.9	15.74
Intra-EU Enroute	0.020(GCD) + 12.000	0.033(GCD) + 7.213
Intercontinental Enroute	0.029(GCD) + 22.000	0.022(GCD) + 37.410

However, for the probabilistic case, a probability distribution must first be fitted to the data in order to describe the results stochastically. This is done using a maximum likelihood estimation (MLE) method, where the parameters of an assumed probability distribution are determined. This method serves to identify the parameters under which the observed data is most likely [65]. Goodness of fit is determined by the Akaike information criterion (AIC), which is itself based on MLE. The process of fitting the new distributions is explained below. The variables are then updated from the current triangular distributions to these new distributions in Aviation Emissions Inventory Code (AEIC). A summary of these changes is shown in Table 7.6.

Table 7.6: Comparison of original and updated distributions of inefficiency variables

Inefficiency	Original Distribution	Updated Distribution
EU Departure	$\sim Tri(0, 5, 25)$	$\sim Gam(0.61, 12.49)$
EU Arrival	$\sim Tri(0, 22, 57)$	$\sim Gam(0.75, 20.87)$
Intra-EU Enroute	$\sim Tri(0.25, 1.00, 2.50)$	$\sim Logn(-0.54, 1.10^2)$
Intercontinental Enroute	$\sim Tri(0.25, 1.00, 2.00)$	$\sim Logn(-0.63, 0.99^2)$

7.7.1. Departure and Arrival Inefficiencies

As both the departure and arrival demonstrate positive skew, the following distributions are tested: Exponential, Lognormal, Weibull and Gamma. These fitted distributions are plotted in Figs. 7.37 and 7.38, overlaying the (normalised) data. In both cases, the Gamma distributions (plotted in orange), proved to fit the data best. The new distributions can be visualised with respect to the original triangular distributions of AEIC in Figs. 7.39 and 7.40.

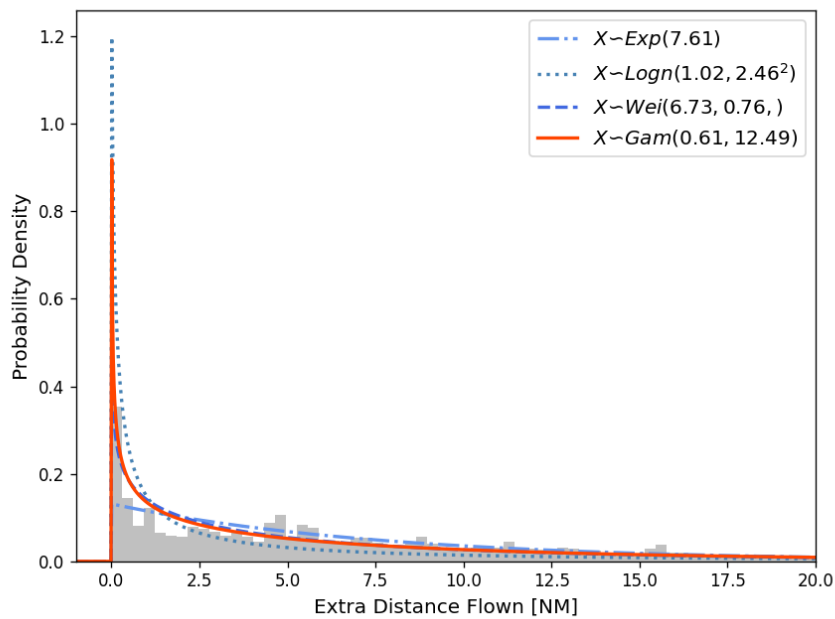


Figure 7.37: Probability distribution fitting to departure inefficiencies

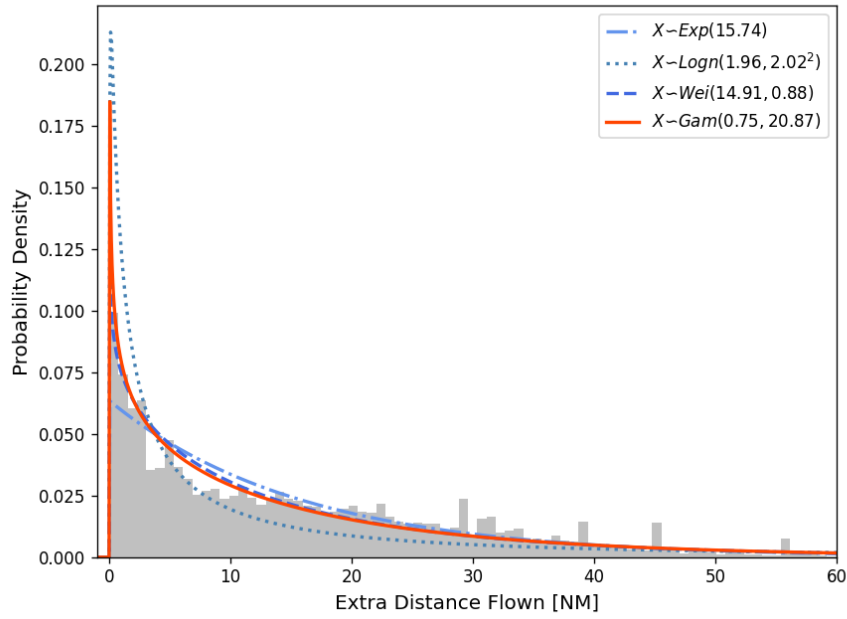


Figure 7.38: Probability distribution fitting to arrival inefficiencies

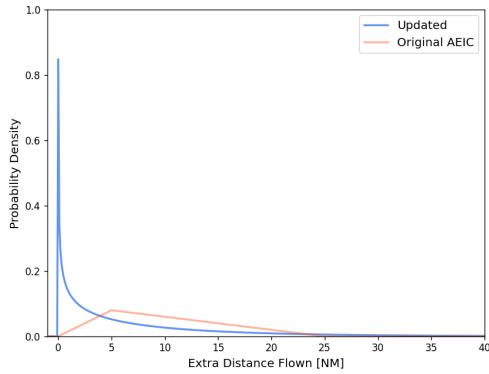


Figure 7.39: Comparison of updated and original departure inefficiency distributions

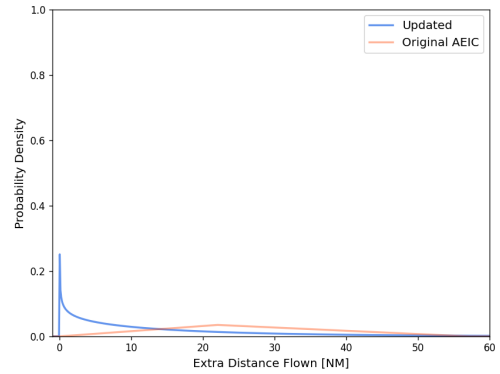


Figure 7.40: Comparison of updated and original arrival inefficiency distributions

7.7.2. Enroute Inefficiencies

Uncertainty around enroute inefficiency, $IM_{enrt, uncertainty}$ in AEIC is expressed as a multiplier on the nominal enroute inefficiency [5]. It is calculated in terms of enroute inefficiency multipliers, IM_{enrt} :

$$IM_{enrt, uncertainty} = \frac{IM_{enrt}}{IM_{enrt, avg}} \quad (7.8)$$

where

$$IM_{enrt} = \frac{XD_{enrt} + GCD_{enrt}}{GCD_{enrt}} \quad (7.9)$$

$IM_{enrt, avg}$ is simply IM_{enrt} with average XD_{enrt} and GCD_{enrt} . The average Great Circle distances for intra-EU and intercontinental enroutes are 218 NM and 788 NM, respectively. Using these values with the expressions for nominal enroute inefficiency results in the following values for average enroute inefficiency multipliers: 1.0662 and 1.0695 for intra-EU and intercontinental, respectively. Thus, IM_{enrt} is calculated for each flight, normalised by $IM_{enrt, avg}$, and plotted before distributions are fitted.

As these distributions are again positively skewed, the same distributions are tested: Exponential, Log-normal Weibull and Gamma. The results of the distribution fitting are plotted in Figs. 7.41 and 7.42. In both cases, the Lognormal distributions proved to fit the data best. Updated distributions can be visualised with respect to the original triangular distributions of AEIC in Figs. 7.43 and 7.44.

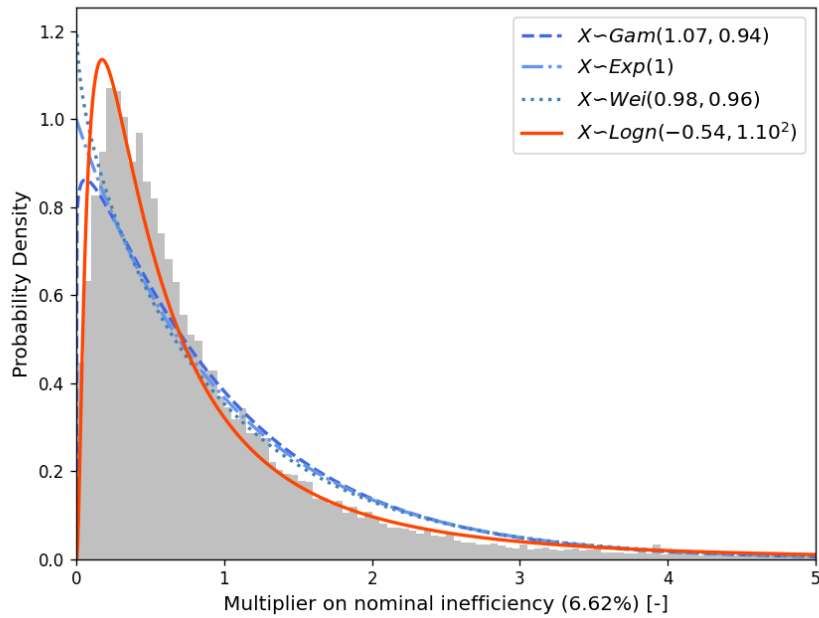


Figure 7.41: Probability distribution fitting to Intra-EU Enroute inefficiencies

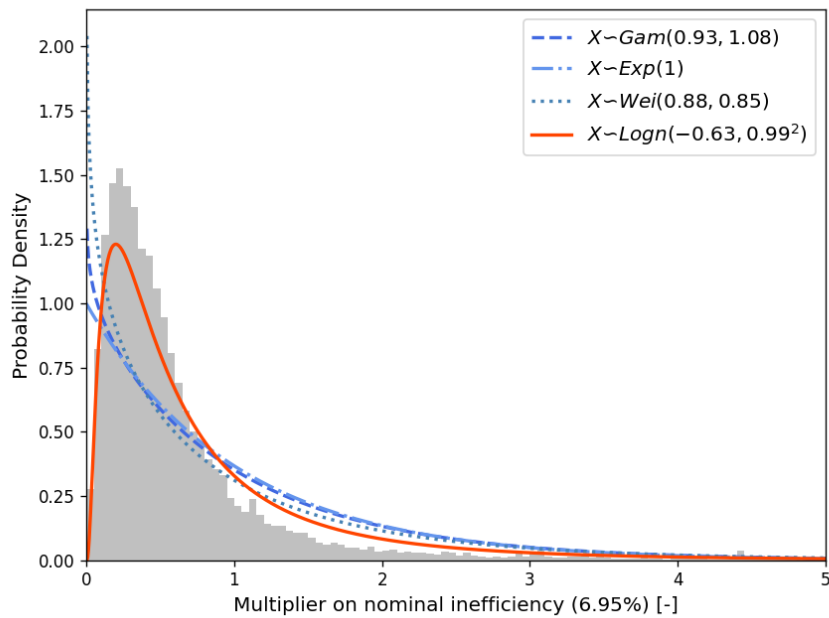


Figure 7.42: Probability distribution fitting to intercontinental enroute inefficiencies

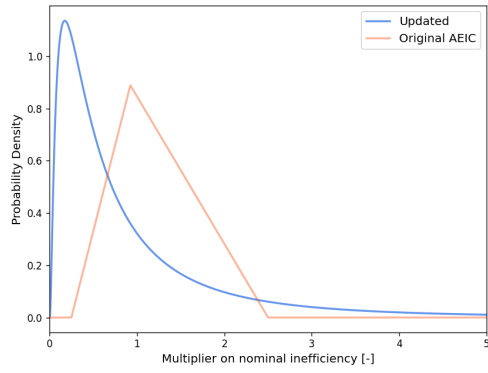


Figure 7.43: Comparison of updated and original Intra-EU Enroute inefficiency distributions

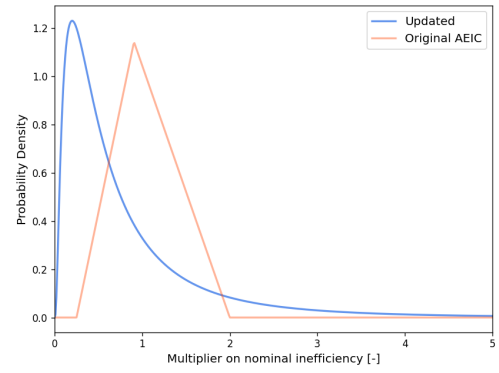


Figure 7.44: Comparison of updated and original intercontinental enroute inefficiency distributions



Re-propagation of Updated Inputs

This chapter presents the results of the first iteration of propagation in the uncertainty quantification framework presented in Section 4.1. Following the development of the updated, data-derived distributions of Chapter 7 and their implementation into AEIC, the effect of these improved input distributions on AEIC's outputs is investigated.

8.1. Methodology

As mentioned, AEIC has six separate variables to describe lateral inefficiencies; these are the arrival, enroute and departure inefficiencies, for both the EU and the rest of the world (as defined by the EU bounding box). Having implemented updated distributions for four of these input variables (summarised in Table 7.6), the effect of each variable is tested by running AEIC for six different cases. Here, the relevant variable is updated, while all other variables maintain their original distribution. This is summarised in Table 8.1, in comparison to the baseline case of Chapter 5.

Table 8.1: Overview of inefficiencies used per simulation case

Simulation	EU			Rest of World		
	Departure	Enroute	Arrival	Departure	Enroute	Arrival
Baseline	Reynolds (2008) EU	Reynolds (2008) EU	Reynolds (2008) EU	Reynolds (2008) US	Reynolds (2008) US	Reynolds (2008) US
EU Departure	Updated EU	Reynolds (2008) EU	Reynolds (2008) EU	Reynolds (2008) US	Reynolds (2008) US	Reynolds (2008) US
Intra-EU Enroute	Reynolds (2008) EU	Updated intra-EU	Reynolds (2008) EU	Reynolds (2008) US	Reynolds (2008) US	Reynolds (2008) US
EU Arrival	Reynolds (2008) EU	Reynolds (2008) EU	Updated EU	Reynolds (2008) US	Reynolds (2008) US	Reynolds (2008) US
All EU	Updated EU	Updated intra-EU	Updated EU	Reynolds (2008) US	Reynolds (2008) US	Reynolds (2008) US
Intercontinental Enroute	Reynolds (2008) EU	Reynolds (2008) EU	Reynolds (2008) EU	Reynolds (2008) US	Updated intercontinental	Reynolds (2008) US
Total	Updated EU	Updated intra-EU	Updated EU	Reynolds (2008) US	Updated intercontinental	Reynolds (2008) US

These six studies are run for both for the nominal and the probabilistic case. The nominal case investigates the effects of the updated nominal values, and results are presented as a single, nominal value. The probabilistic case investigates the propagation of uncertainty as a result of the new uncertainty distributions, done using the same methodology of Chapter 5, with a Monte Carlo simulation of $N = 1,000$, for each case. The results of the probabilistic case are summarised by statistical moments: Mean, Median, Standard Deviation, Coefficient of Variation and the 5th-95th percentile uncertainty range.

Furthermore, the gridded output of AEIC spatially resolves fuelburn and emissions into latitude and longitude. The coordinates of the EU bounding box are used to effectively isolate the fuelburn and emissions sums from either EU or the Rest-of-world. Thus the effects of each input can be expressed with respect to its area of application ie. when testing EU variables, fuelburn and emissions within the EU bounding-box are obtained and compared.

The obvious limitation here is that inefficiency behaviour of flights flown between 2015 and 2019 is applied to the 2005 schedule. However, the goal of this re-propagation is to assess the effects of updating inputs which are key sources of uncertainty.

8.2. Results

The resulting distributions of AEIC's global fuelburn, NO_x, CO and HC estimates with all updated variables implemented (as per the 'Total' case in Table 8.1) are presented in Fig. 8.1. Here, the results can be directly compared to the baseline case, as the distributions are overlaid. A kernel density estimation (KDE) of each distribution is generated simply to compare the changes in shape of the resulting distributions. In general,

the distributions in the ‘Total’ case demonstrate a slight shift to the left – a decrease in emissions across each output due to all updated variables.

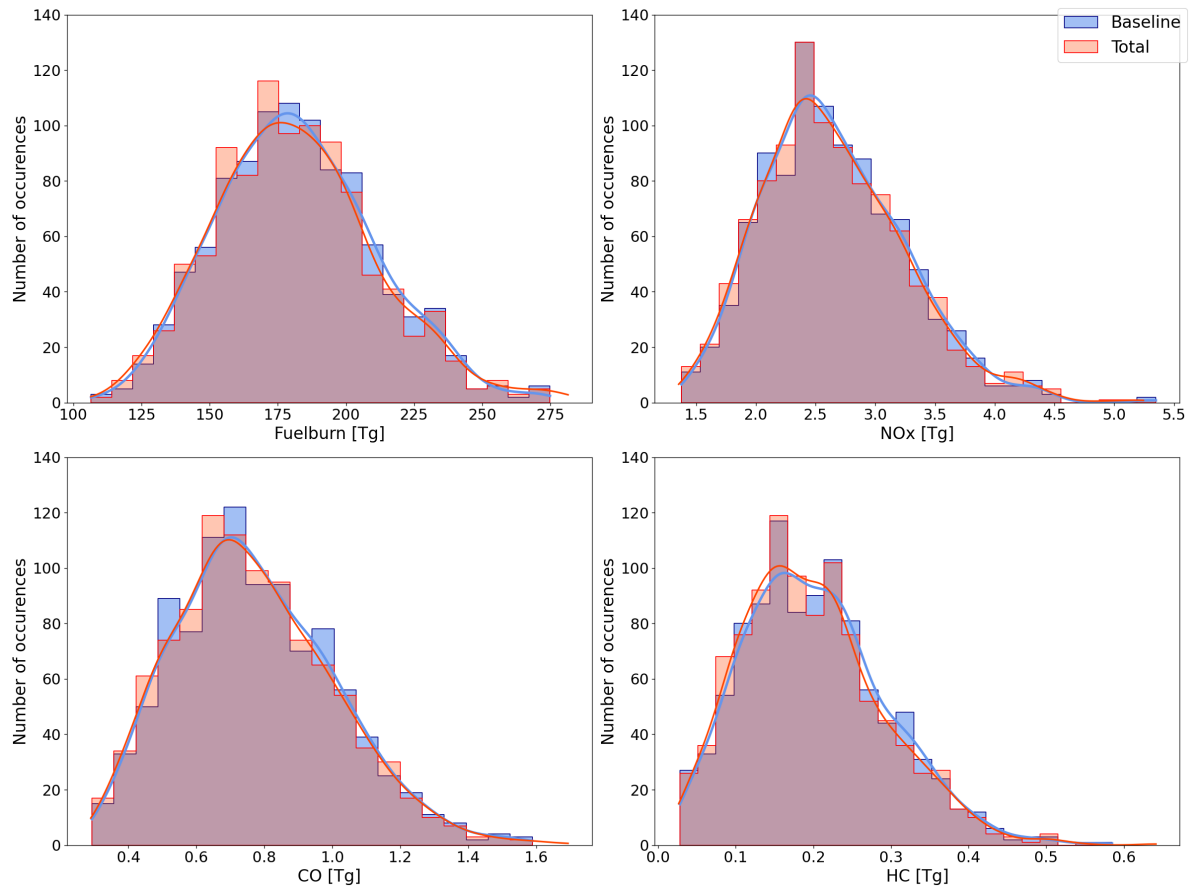


Figure 8.1: Distribution comparing the Baseline and Total estimates of global fuelburn, NO_x, CO and HC

The changes in fuelburn and emissions are attributed to the change in extra distance flown (all emissions logically decrease with decreasing distance flown), coupled with the fuel flow rate of the CCD phase at which the inefficiency is applied to. The driving factors behind these changes can be attributed to certain inefficiencies, which can be identified from specific simulations, and are addressed in the following sections. Here, the effect of each inefficiency is presented with respect to its area of application (EU or Rest-of-world) while effects on global fuelburn and emissions are presented in Appendix C, for completeness. Results are discussed in terms of the nominal and probabilistic effects, separately.

8.2.1. Fuelburn

Table 8.2 presents the relative difference in fuelburn response of each EU simulation, with respect to the EU portion of the baseline case. Table 8.3 demonstrates the effects of the intercontinental enroute inefficiency on fuelburn in the Rest-of-world. From these tables, the relative effect of each variable on the baseline is identifiable.

Table 8.2: Relative difference to EU fuelburn estimates due to updated EU inefficiencies

Simulation	Nominal (Tg)	Mean (Tg)	Median (Tg)	Standard Deviation (Tg)	Coefficient of Variation (%)	5 th -95 th percentile uncertainty range (Tg)
Baseline (EU)	34.00	34.51	34.18	5.39	15.91	25.643-43.383
EU Departure	-0.44%	-0.77%	-1.11%	-0.01%	+0.76%	25.380-43.118
Intra-EU Enroute	+0.38%	+0.07%	-0.82%	+2.03%	+1.96%	25.486-43.586
EU Arrival	-0.53%	-0.50%	-0.71%	-0.41%	+0.09%	25.508-43.175
EU All	-0.62%	-1.20%	-2.63%	1.60%	+2.83%	25.088-43.112
EU All (values)	33.79	34.10	33.29	5.48	16.07	—"——"

Table 8.3: Relative difference to rest-of-world fuelburn estimates due to updated intercontinental enroute inefficiency

Simulation	Nominal (Tg)	Mean (Tg)	Median (Tg)	Standard Deviation (Tg)	Coefficient of Variation (%)	5 th -95 th percentile uncertainty range (Tg)
Baseline (Rest-of-world)	146.43	147.57	146.39	23.58	0.16	108.774-186.363
Intercontinental Enroute	+0.60%	-0.14%	-0.61%	+3.72%	+3.86%	107.130-187.603
Intercontinental Enroute (values)	147.32	147.37	145.50	24.46	0.17	—"——"

Nominal Case

The results from nominal simulations of AEIC with updated variables present some expected results: the lower departure and arrival inefficiencies logically result in lower fuelburn. However, the increases due to enroute inefficiencies, in both areas, produce interesting insights.

As explained in Section 7.5.2, the updated intra-EU enroute inefficiency function results in longer extra distance flown for flights longer than 370 NM. As the fuelburn has increased due to this update, it is evident that a significant portion of intra-EU flights are longer than 370 NM. Conversely, the updated, shallower, intercontinental enroute inefficiency function results in longer extra distance flown for flights shorter than 2,200 NM. As fuelburn also increases due to this update, it can be concluded that a significant portion of the flights to which this inefficiency is applied are shorter than 2,200 NM. This suggests that intercontinental flight behaviour is being applied to domestic flights outside of the EU bounding box. This is largely a result of the nature of the EUROCONTROL flight data, where external domestic flights are not captured. This is significant, as it demonstrates the largest relative change in nominal fuelburn.

Probabilistic Case

In terms of the mean value of fuelburn from the stochastic simulations, the same pattern is demonstrated in all cases except in intercontinental enroutes. Here, it serves to decrease fuelburn relative to the baseline. This can be attributed to the positive skew of the updated distribution, which would result in a concentration of multipliers lower than one. In fact, the more positive skews of all distributions ultimately serve to decrease the total fuelburn estimates (relative to nominal results), except in the EU arrivals. Departures, now contribute a larger decrease in the stochastic case. The intra-EU enroute contributes less increase to fuelburn, and intercontinental enroute now contributes to a decrease in fuelburn. In the case of intercontinental enroutes, the skew of the distribution has a significant impact on the fuelburn relative to the nominal case.

The effect of the skew on the distribution of fuelburn can again be seen when assessing median values. In the baseline cases, the median and mean values are similar, indicating the distribution of fuelburn has very little skew. When incorporating the improved distributions, there is a significant decrease in median fuelburn values, compared to the mean. A property of positive skewed distributions is the mean being greater than the median. This demonstrates the non-trivial effect of input uncertainty distributions on output distributions.

In terms of uncertainty, the introduction of all updated inefficiencies increase the coefficient of variation. However, both simulations testing the updated enroute inefficiencies demonstrate the largest increases here, due the tail of the updated distributions increasing the spread of possible values. Intercontinental enroute inefficiency results in the largest increase in coefficient of variation, as it is applied to a significant portion

of flights. The results of the EU departure and arrival inefficiency simulations both demonstrate very slight decreases in standard deviation, which could be due to their tighter distributions.

8.2.2. NO_x

The relative difference of each simulation's NO_x emission estimates on their respective area of application are tabulated in Tables 8.4 and 8.5. Though the emission of NO_x is not directly proportional to fuelburn, it does still increase somewhat linearly with fuelburn. Thus, the results of each simulation again demonstrate a similar pattern to those of fuelburn.

Table 8.4: Relative difference to EU NO_x estimates due to updated EU inefficiencies

Simulation	Nominal (Tg)	Mean (Tg)	Median (Tg)	Standard Deviation (Tg)	Coefficient of Variation (%)	5 th -95 th percentile uncertainty range (Tg)
Baseline	0.509	0.506	0.492	0.111	21.90	0.324-0.689
EU Departure	-0.66%	-1.10%	-0.71%	-0.26%	+0.84%	0.319-0.682
Intra-EU enroute	+0.40%	+0.14%	+1.10%	+1.58%	+1.44%	0.322-0.692
EU Arrival	-0.25%	-0.22%	-0.36%	-0.23%	-0.02%	0.323-0.687
EU All	-0.51%	-1.18%	-0.40%	+1.08%	+2.28%	0.316-0.685
EU All (values)	0.507	0.500	0.490	0.112	22.40	——"———

Table 8.5: Relative difference to rest-of-world NO_x estimates due to updated intercontinental enroute inefficiency

Simulation	Nominal (Tg)	Mean (Tg)	Median (Tg)	Standard Deviation (Tg)	Coefficient of Variation (%)	5 th -95 th percentile uncertainty range (Tg)
Baseline (Rest-of-world)	2.171	2.148	2.090	0.481	0.22	1.357-2.939
Intercontinental Enroute	+0.48%	-0.15%	+0.12%	+2.11%	+2.27%	1.337-2.953
Intercontinental Enroute (values)	2.182	2.145	2.093	0.491	0.229	——"———

Nominal Case

In the nominal case, the lower EU departure and arrival inefficiencies decrease NO_x emissions. The overall NO_x emission increase in the nominal case is due to the steeper slope of intra-EU enroute inefficiency affecting European flights longer than 370 NM, and intercontinental enroute inefficiency affecting sub-2,200 NM flights in the rest of the world.

Probabilistic Case

In the stochastic case, the positive skew of the updated inefficiencies again shift the relative impact of each inefficiency further negative. Intercontinental enroute inefficiencies now lead to a decrease in NO_x emissions, again highlighting the impact of the distribution shape of the input variable. The overall effect of applying all EU updates is a decrease in NO_x emissions from the baseline. Interestingly, the median and mean values of the EU All simulation are closer together than in the baseline case, suggesting a reduction in skew.

Considering the coefficient of variation, all inefficiencies increase this, except for EU arrivals. This is due to both a decrease in standard deviation coupled with a relatively slight decrease in mean. Enroute inefficiencies demonstrate large increases to uncertainty: their improved distributions are much wider than the original. The results of the EU departure and arrival inefficiency simulations both demonstrate very slight decreases in standard deviation, which could be due to their tighter distributions.

8.2.3. CO

CO emissions do not scale linearly with fuelburn, rather it decreases with increasing power. As such the results for each simulation, shown in Tables 8.6 and 8.7, do not follow the same pattern as the results of fuelburn and NO_x.

Table 8.6: Relative difference to EU CO estimates due to updated EU inefficiencies

Simulation	Nominal (Tg)	Mean (Tg)	Median (Tg)	Standard Deviation (Tg)	Coefficient of Variation (%)	5 th -95 th percentile uncertainty range (Tg)
Baseline (EU)	0.178	0.182	0.176	0.053	29.47	0.094-0.270
EU Departure	-0.10%	-0.16%	-0.07%	-0.19%	-0.03%	0.093-0.269
Intra-EU enroute	+0.12%	-0.08%	+0.44%	+0.60%	+0.68%	0.093-0.270
EU Arrival	-3.92%	-3.42%	-4.17%	-1.40%	+2.08%	0.089-0.262
EU All	-3.90%	-3.65%	-3.83%	-0.99%	+2.76%	0.088-0.262
EU All (values)	0.171	0.175	0.169	0.053	30.285	——"———

Table 8.7: Relative difference to rest-of-world CO estimates due to updated intercontinental enroute inefficiency

Simulation	Nominal (Tg)	Mean (Tg)	Median (Tg)	Standard Deviation (Tg)	Coefficient of Variation (%)	5 th -95 th percentile uncertainty range (Tg)
Baseline (Rest-of-world)	0.578	0.593	0.572	0.180	0.30	0.297-0.888
Intercontinental Enroute	+0.63%	+0.19%	+0.60%	+1.30%	+1.11%	0.294-0.893
Intercontinental Enroute (values)	0.582	0.594	0.575	0.182	0.307	——"———

Nominal Case

In the nominal results, the updated EU arrival inefficiencies result in a significant decrease in CO. This is because the descent phase, as a naturally low power phase, is responsible for the majority of CO emissions. Arrival inefficiencies are applied to the last 50 NM of descent, thus lower arrival inefficiencies result in a decrease in CO emissions.

Intercontinental enroute inefficiencies demonstrate the next largest effect. As per the results of fuelburn and NO_x, both updated enroute inefficiencies serve to increase the length of the enroute portion of flights. The enroute inefficiencies are applied to the cruise phase, which exhibits relatively low fuel flow rates. Thus, with longer enroute inefficiencies, CO emissions increase. However this increase is much more evident in the intercontinental case, potentially due to the longer intercontinental flights reaching cruise altitude, where fuel flow is optimised.

Probabilistic Case

Again in the stochastic cases, the positive skew of the updated distributions result in a net decrease in across CO emissions, except for EU arrival. EU arrival inefficiencies decrease standard deviation of CO, however the significant relative decrease in mean value results in an increase in coefficient of variation.

8.2.4. HC

The HC emission results per simulation share the same pattern as those for CO, and are presented in Tables 8.8 and 8.9. Here however, the sensitivity to arrival inefficiencies is even more apparent.

Table 8.8: Relative difference to EU HC estimates due to updated EU inefficiencies

Simulation	Nominal (Tg)	Mean (Tg)	Median (Tg)	Standard Deviation (Tg)	Coefficient of Variation (%)	5 th -95 th percentile uncertainty range (Tg)
Baseline (EU)	0.080	0.082	0.079	0.036	43.53	0.023-0.141
EU Departure	-0.04%	-0.06%	-0.11%	-0.03%	+0.03%	0.023-0.141
Intra-EU enroute	+0.09%	-0.07%	-0.13%	+0.06%	+0.13%	0.023-0.141
EU Arrival	-7.51%	-6.31%	-6.73%	-1.56%	+5.06%	0.019-0.135
EU All	-7.46%	-6.43%	-7.23%	-1.56%	+5.20%	0.019-0.135
EU All (values)	0.074	0.077	0.073	0.035	45.795	——"———

Table 8.9: Relative difference to rest-of-world HC estimates due to updated intercontinental enroute inefficiency

Simulation	Nominal (Tg)	Mean (Tg)	Median (Tg)	Standard Deviation (Tg)	Coefficient of Variation (%)	5 th -95 th percentile uncertainty range (Tg)
Baseline (Rest-of-world)	0.111	0.121	0.115	0.056	0.463	0.029-0.213
Intercontinental Enroute	0.49%	0.06%	0.15%	0.23%	0.17%	0.029-0.213
Intercontinental Enroute (values)	0.112	0.121	0.115	0.056	0.464	————

Nominal Case

HC emissions are evidently very sensitive to the arrival phase, and less sensitive to the cruise phase compared to CO. The total change in HC emissions due to the improved EU arrival exceeds 7%, the largest relative change of all outputs discussed in this chapter.

Probabilistic Case

The relative changes due to the input distributions demonstrate the same trends that have been seen in this chapter: the mean of each simulation demonstrates a net decrease compared to the nominal case, except for EU arrivals.

The increases in coefficient of variation are also dominated by EU arrival inefficiencies. The decrease in standard deviation due to EU arrival inefficiencies, another recurring theme throughout this chapter, is amplified due to insensitivity to other variables. Thus, HC is the only emission in this chapter to demonstrate a narrower 5th-95th percentile uncertainty range after updating all EU inefficiencies.

Conclusions and Recommendations

This report has followed the various steps of a full iteration of uncertainty quantification for a full-flight, global aviation emissions inventory. Ultimately the results of this research have led to an answer to the original research question: “*How do sources of uncertainty contribute to the uncertainty in global aviation fuelburn and emissions estimates, and how can they be improved?*”. This chapter will present the significant findings of this research, in the context of the research sub-questions outlined in Chapter 2. Recommendations for future work are then discussed.

9.1. Conclusions

The results of this research effectively build upon the uncertainty quantification results of Simone et al. (2013). Following the uncertainty quantification framework outlined in Chapter 4, systematic analysis of the uncertainty and sensitivities of a full-flight aviation emissions inventory has been achieved, using AEIC. Each of the Chapters 5 to 8 concerns a single step, and outlines the methodology employed and the results obtained. Each successive chapter is built upon the results of the preceding chapter.

First, forward uncertainty propagation has been investigated to build a baseline case which can be compared to the original results of Simone et al. (2013), and serves as a point of comparison for the final uncertainty re-propagation. A global sensitivity analysis was then performed, to gain insight into the parameters that contribute significantly to the uncertainty in global fuelburn and emissions. Isolating key sources of uncertainty allowed for a focused improvement of their associated uncertainty ranges – this was done for lateral flight inefficiencies using a data-driven approach. Finally, uncertainty in fuelburn and emissions has been re-propagated with improved input uncertainty, and compared to the baseline case, representing the ultimate results of this study. Conclusions in the context of each research subquestion are detailed below:

Subquestion:

- (a) Which input(s) lead to the greatest source of uncertainty in global fuelburn and emissions estimates?

The results of the Sobol analysis of Chapter 6 demonstrate the sensitivities of fuelburn, NO_x , CO and HC estimates. Ranking inputs by their first-order index, S_i leads to the identification of considerable sources of uncertainty. In general, significant contributors to uncertainty across all outputs are the BADA Drag and Fuel Flow corrective multipliers. These consistently appear in the top four parameters of all outputs analysed here.

In terms of fuelburn and NO_x , the TOW multiplier represents the third largest contributor to uncertainty. In the case of CO and HC, their sensitivities to low thrust modes make them susceptible to the uncertainties in Taxi Thrust and Arrival Inefficiency. Across the emitted species, variance is driven by their respective EI uncertainty.

Subquestion:

- (b) To what extent do these input(s) effect the overall uncertainty in global fuelburn and emissions estimates?

The value of the first-order index, S_i , effectively quantifies the extent of the input’s effect on output uncertainty. These are summarised in Table 9.1, where $S_i > 1$ indicates a significant contributor. As can be seen from this table, there are typically between two and four input parameters which demonstrate significant contributions to the variance per output. These results demonstrate the inputs which should be the focus of re-calibration or a more accurate analysis.

Table 9.1: Summary of first-order indices for fuelburn, NO_x, CO and HC

Fuel Burn		NO _x		CO		HC	
Input Parameter	S_i	Input Parameter	S_i	Input Parameter	S_i	Input Parameter	S_i
BADA Drag	0.532	BADA Drag	0.308	EI CO	0.681	EI HC	0.692
BADA Fuel Flow	0.284	EI NO _x	0.292	Taxi Thrust	0.126	Taxi Thrust	0.128
TOW	0.122	TOW	0.194	BADA Drag	0.055	BADA Drag	0.030
Enroute Inefficiency	0.005	BADA Fuel Flow	0.157	BADA Fuel Flow	0.040	BADA Fuel Flow	0.023
Arrival Inefficiency	0.004	Enroute Inefficiency	0.006	Arrival Inefficiency	0.031	Arrival Inefficiency	0.023
Cruise Altitude	0.002	Fuel Flow	0.004	Fuel Flow	0.011	Taxi TIM	0.014
Taxi Thrust	0.002	Take-Off Thrust	0.003	Cruise Altitude	0.006	Fuel Flow	0.002
Departure Inefficiency	0.001	Cruise Altitude	0.001	Taxi Thrust	0.003	Cruise Altitude	0.002
Take-Off Thrust	0.001	Climb Out TIM	0.001	Enroute Inefficiency	0.003	Enroute Inefficiency	0.000
Approach Thrust	0.001	Departure Inefficiency	0.001	TOW	0.001	TOW	0.000

Subquestion:

(c) How can a data-driven approach be used to update input uncertainty distributions?

In terms of making improvements to sources of uncertainty, the lateral flight inefficiencies present the most suitable opportunity, due to available flight track data. Despite not being top contributors to uncertainty, they are consistently ranked in the top five parameters. Furthermore, the triangular distributions which model variation in inefficiencies are especially unrepresentative of the research off of which they are approximated. The original assumption that US values for inefficiency apply to the rest of the world can also be addressed.

The publication of the EUROCONTROL R&D data archive allows for a reproduction of the Reynolds (2008) study. This includes a re-definition of regions according to the definitions used in AEIC: analysis was divided across EU and the rest of the world. The resulting distributions of inefficiency can be appropriately fitted, and implemented in AEIC to better model the variance in lateral flight inefficiencies.

The revised lateral inefficiency inputs are summarised in Table 9.2. In general, the revised nominal departure and arrival inefficiencies are shorter, and their distributions are more positively skewed. The revised intra-EU enroute inefficiency demonstrates a steeper relationship between GCD and inefficiency. This suggests lower inefficiencies for enroutes shorter than 370 NM, and higher inefficiencies for longer enroutes. The intercontinental enroute study suggests an average inefficiency of 2.2% of the flight's enroute Great Circle distance, plus 37.41 NM. When compared to the domestic US enroute inefficiency, this results in a higher inefficiency for enroutes shorter than 2,200, while the opposite is true for longer enroutes.

Table 9.2: Summary of revised lateral flight inefficiency variables

Inefficiency	Nominal inefficiency [NM]	Uncertainty Distribution
EU Departure	7.61	$\sim \text{Gam}(0.61, 12.49)$
EU Arrival	15.74	$\sim \text{Gam}(0.75, 20.87)$
Intra-EU Enroute	$0.033(\text{GCD}) + 7.213$	$\sim \text{Logn}(-0.54, 1.10^2)$
Intercontinental Enroute	$0.022(\text{GCD}) + 37.410$	$\sim \text{Logn}(-0.63, 0.99^2)$

Subquestion:

(d) How do these updated input parameters affect fuelburn and emissions estimates?

For each of the updated inefficiencies, AEIC was run in both the nominal and probabilistic case to isolate the effect of the updated input on each of the estimates of fuelburn, NO_x, CO and HC, as well as to investigate the re-propagation of uncertainty. The results of these simulations are compared to the baseline case to investigate relative change per input. In general, the updated departure and arrival inefficiencies reduced the fuelburn and emissions estimates, while both the updated intra-EU and intercontinental enroute inefficiencies served to increase fuelburn and emissions estimates. Despite lateral flight inefficiencies not ranking at the top of the global sensitivity analysis, the propagation of their revised parameters has a non-negligible effect on outputs.

The lower values of the departure and arrival inefficiencies serve to reduce the distance shown, logically reducing fuelburn and emissions. This is especially apparent in the case of CO and HC, where their sensitivity to arrival inefficiency sees reductions in nominal EU emissions of 3.92% and 7.51%, respectively. The

increased fuelburn and emissions due to enroute inefficiencies results suggest that a significant portion of intra-EU enroute flights are longer than 370 NM, while a significant portion of enroute flights in the rest of the world are shorter than 2,200 NM.

In the stochastic case, the positive skew of the updated uncertainty distributions served to decrease fuelburn and emissions from the baseline. In some cases, the enroute inefficiencies which nominally results in an increase in fuelburn and emissions, demonstrated a net decrease in emissions. This skew is an aspect of the original Reynolds (2008) results that could not be captured fully by triangular distributions. In general, histograms of outputs with improved variables display a slight shift left with respect to the baseline case, indicating that the original triangular distributions may lead to an overestimation of fuelburn and emissions.

Finally, the coefficient of variation, a measure for relative uncertainty, increases across almost all outputs. This is due to the 'tail' of the updated distributions which allow for inputs to take larger values compared to triangular distributions. Despite each revised variable increasing relative uncertainty, the more accurately described distributions benefit AEIC: rapid calculations are maintained, while increasing the reliability of estimates.

9.2. Recommendations for Future Work

The key sources of uncertainty identified in the global sensitivity analysis of Chapter 6 naturally lead to recommendations for further research. As the inputs and methods which AEIC uses are common across other full-flight aviation emissions inventories, these results demonstrate potential for application outside of AEIC. The re-propagation of improved lateral flight inefficiency uncertainties demonstrates non-trivial effects on estimated fuelburn and emission, despite not being top contributors to uncertainty. Furthermore, the results of the inefficiency study have direct relevance to the development of other emissions models of reduced complexity, which make use of schedule data to generate Great Circle routes, and apply corrective lateral adjustments.

Uncertainty quantification is an iterative process which aims to highlight sources of uncertainty which would benefit from further research and improvement. Ultimately, in light of robust model development, it is recommended to repeat the processes of Chapters 7 and 8 with the following inputs:

BADA Drag and Fuel Flow, and TOW

Compared to lateral flight inefficiencies, the multipliers on BADA Drag and Fuel Flow, and TOW have been identified to contribute considerably more to uncertainty in this study. They have also been identified as significant sources of uncertainty in other studies [20, 24]. These parameters present opportunity for revision, which would result in significant improvements to reliability in AEIC's output.

Emission Indices

The emissions index of each species present source of significant uncertainty in AEIC. This is consistent with uncertainty analyses of other aviation emissions inventories which use emissions values the ICAO EDB with BFFM2 [20, 21, 24]. As many traditional aviation emissions inventories make use of ICAO EDB values, efforts to measure the variation in emissions indices at altitude would be valuable [30, 40, 66–68].

Vertical Flight Inefficiencies

On top of lateral flight inefficiencies, vertical flight inefficiencies should be considered for revision. The current assumption that cruise altitude is 7,000 ft below an aircraft's maximum cruise height, may not be truly representative of real operations. As the EUROCONTROL data provides flight level information as well as aircraft type information, this assumption can be tested. A preliminary analysis of the distribution of inter-continental cruise flight level was conducted using one month the EUROCONTROL data, shown in Fig. 9.1. This demonstrated an apparent average cruise height with variation in the order 2,300 ft for a 1σ uncertainty level, compared to 3,000 ft, used in AEIC. Analysis of cruise behaviour is straightforward using the EUROCONTROL data, and revisions to the modelling of cruise altitude will be beneficial to the reliability of AEIC estimates.

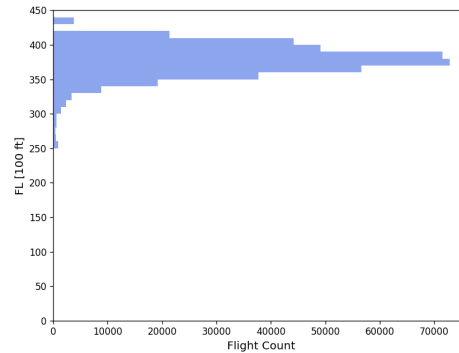


Figure 9.1: Distribution of intercontinental FL cruise using 1 month of EUROCONTROL flight data

Lateral Flight Inefficiencies

In terms of the lateral flight inefficiency analysis, two refinements can be made to the modelling of enroute inefficiencies. The first concerns better suiting the analysis of enroutes to fit AEIC's use of the enroute inefficiency. Currently, the revision in this study is based on the method of Reynolds (2008) and analyses the full-flight enroute within the AEIC-defined EU. Thus only capturing (domestic) intra-EU enroutes ie. flights departing and arriving within the EU area. However, in AEIC's application of enroute inefficiencies, the EU inefficiency is applied to the portion of any flight which takes place over this bounding box, including flights departing EU and arriving elsewhere, and vice versa, and flights overflying EU. Using the EUROCONTROL data, the enroute portion of any flight overflying this bounding box can be analysed and used to describe a complete EU enroute inefficiency.

The second improvement regards the modelling of inefficiencies in the rest of the world. A limitation the EUROCONTROL dataset only includes data on flights flying in or over the EUROCONTROL NM area. Naturally, the behaviour of flights in the rest of the world cannot be fully approximated using this data. This limitation has been addressed in Chapter 7, as there was insufficient TA data to analyse departure and arrival in the US, effectively invalidating the dataset for TA analyses. Despite this, intercontinental enroute inefficiencies were still analysed to make full use of the data sets (and enroute flight does not suffer from the same data insufficiency). The results of the re-propagation of intercontinental enroute inefficiency demonstrate that a significant portion of flights are shorter than 2,200 NM, implying that intercontinental flight behaviour is applied to a significant number of domestic flights. Due to these limitations, their implementation as a representation of flight behaviour outside of the AEIC-defined EU bounding box is inappropriate.

The intercontinental enroute inefficiency demonstrate a large influence on fuelburn and emissions, compared to the intra-EU enroute inefficiency. This is effectively due to their area of application; the Rest-of-world, which may account for approximately 3 times more flights than the intra-EU area [69]. Thus, re-evaluation of the extra-EU lateral flight inefficiencies using a more appropriate data set would complement the revised EU lateral flight inefficiencies presented in this study.

Fixed Variables and Scenarios

One final recommendation would be to use the process described throughout this thesis to investigate the effects of uncertainty in other, fixed variables. AEIC's open source nature leads to various research applications, as variables can be straightforwardly manipulated to investigate its effects on emissions estimates. Despite the 49 variables already described with uncertainty ranges, there are still some fixed variables which would benefit from uncertainty representation. One of these fixed variables is aircraft-engine assignments; engine models are assumed constant for each aircraft type, however this is untrue in reality. An investigation into engine distributions across the fleet can be conducted and implemented into AEIC's modelling of aircraft performance to determine the impact of engine-assignments on fuelburn and emissions estimates.



Variance Identity

This is proof of the identity $V(Y) = E(V(Y | X)) + V(E(Y | X))$. It makes use of the following definitions and identities.

Definitions for variance and conditional variance:

$$V(Y) = E(Y^2) - E(Y)^2 \quad (\text{A.1})$$

$$V(Y | X) = E(Y^2 | X) - E(Y | X)^2 \quad (\text{A.2})$$

$$(\text{A.3})$$

The law of iterated expectation:

$$E(Y) = E(E(Y | X)) \quad (\text{A.4})$$

The property of linearity of expectations:

$$E(a + b) = E(a) + E(b) \quad (\text{A.5})$$

Thus, starting with the definition of variance:

$$V(Y) = E(Y^2) - E(Y)^2 \quad (\text{A.6})$$

$$= E(E(Y^2 | X)) - E(E(Y | X))^2 \quad (\text{A.7})$$

$$= E(V(Y | X) + E(Y | X)^2) - E(E(Y | X))^2 \quad (\text{A.8})$$

$$= E(V(Y | X)) + E(E(Y | X)^2) - E(E(Y | X))^2 \quad (\text{A.9})$$

$$= E(V(Y | X)) + V(E(Y | X)) \quad (\text{A.10})$$

Equation A.7 is the substitution of the law of iterated expectation into the definition of variance. Equation A.8 follows from the definition of conditional variance. Equation A.9 follows logically from the property of linearity of expectations. Finally, Equation A.10 uses the original definition of variance.

B

Second-order Sobol Indices

B.1. Fuelburn

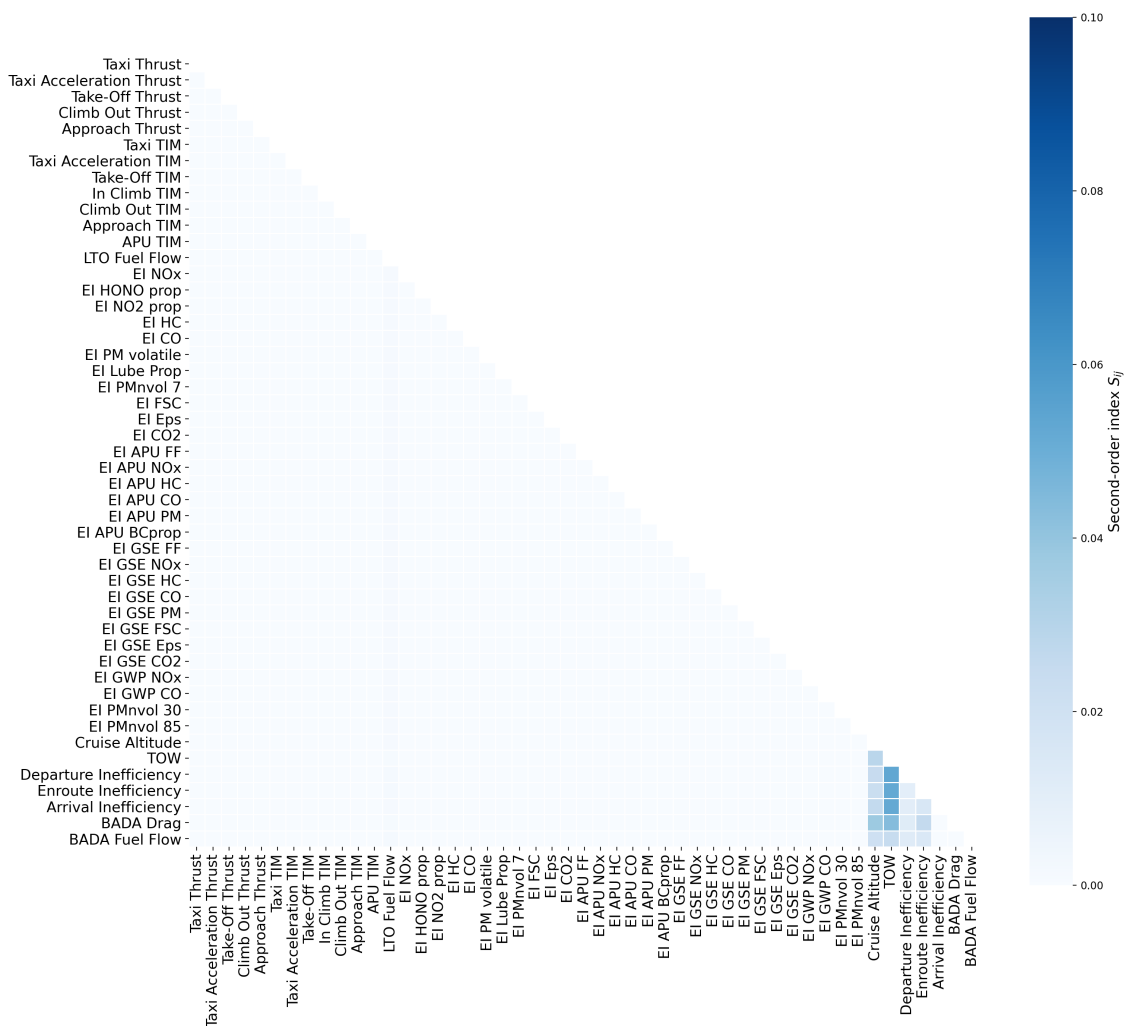


Figure B.1: Second-order Sobol indices for Fuelburn

B.2. NO_x

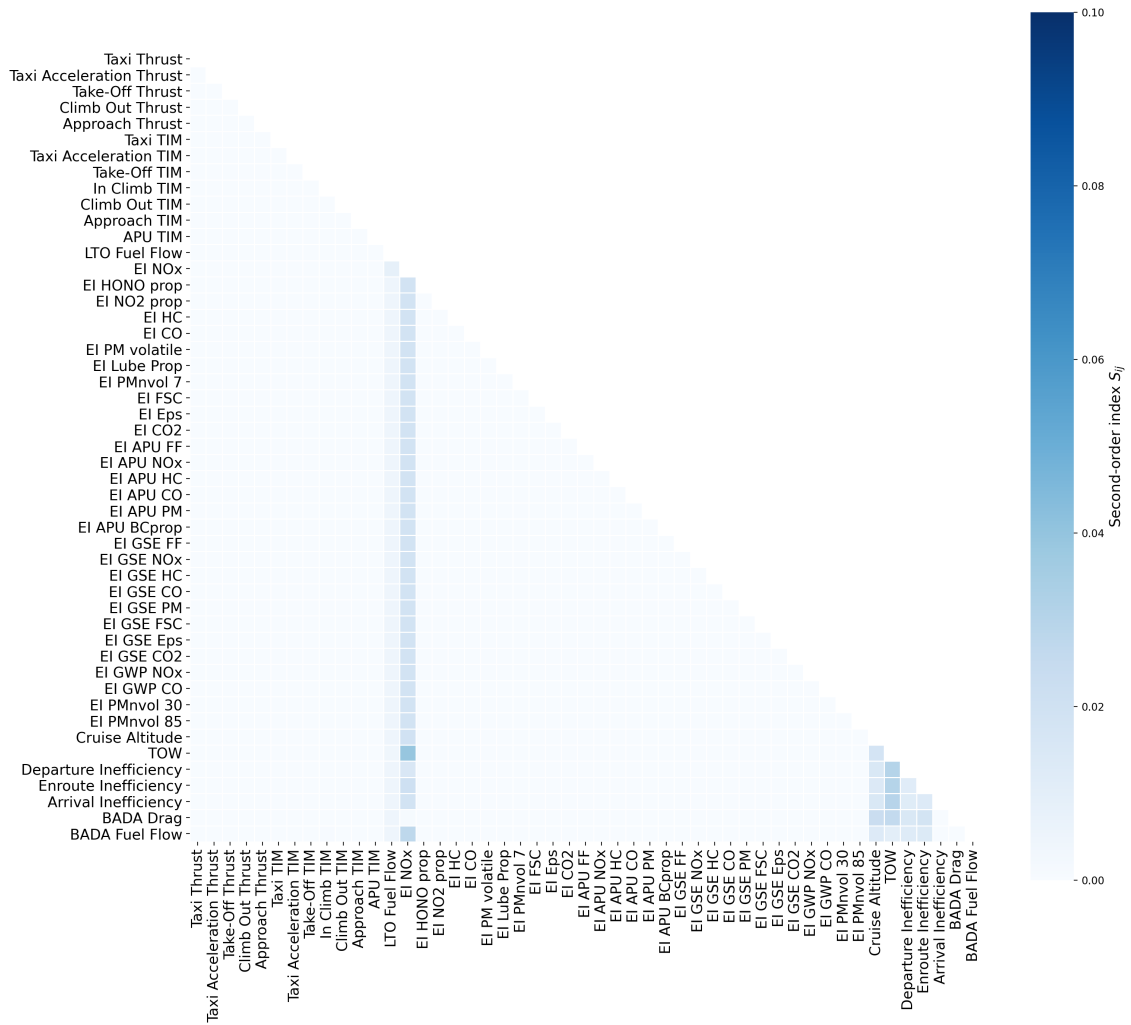


Figure B.2: Second-order Sobol indices for NO_x

B.3. CO

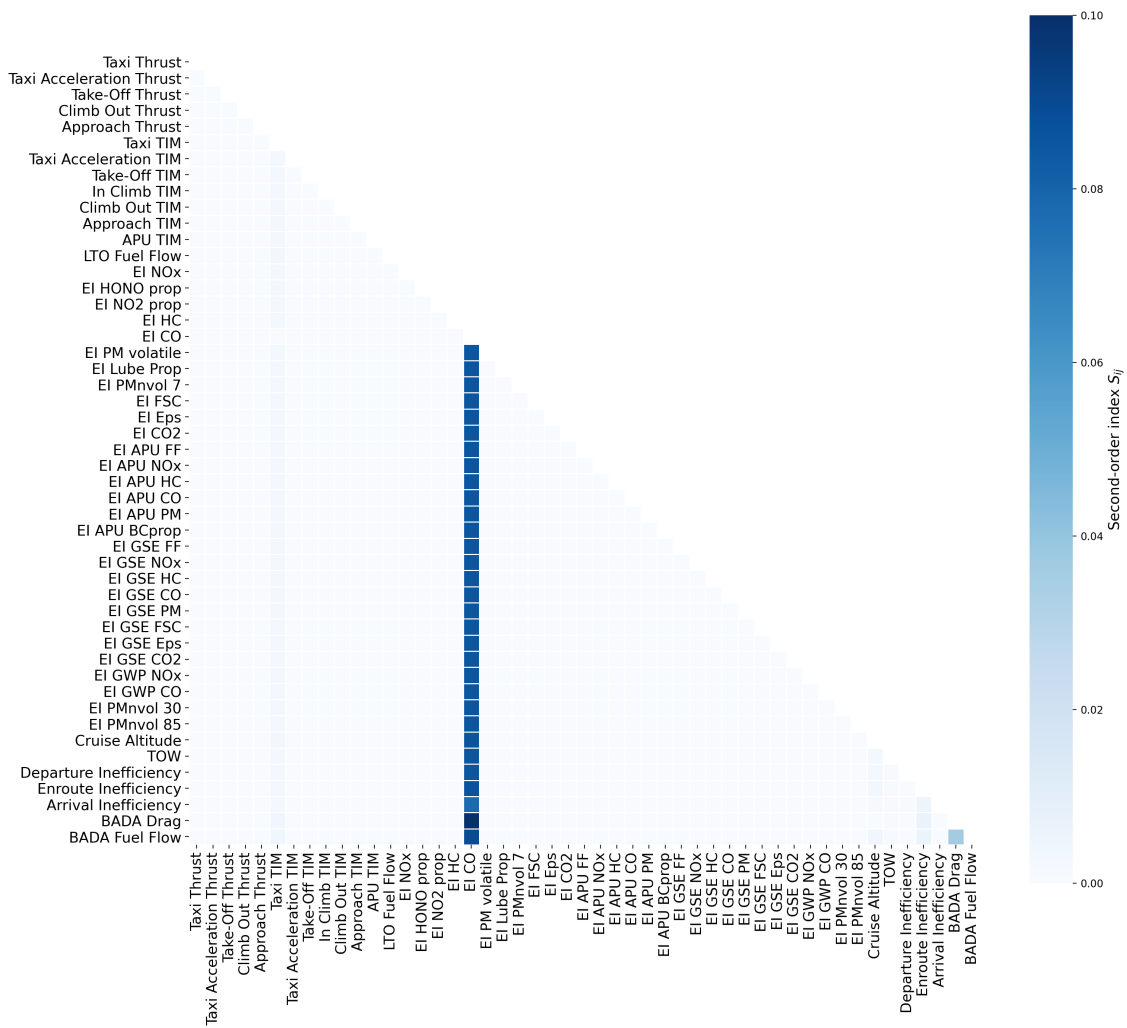


Figure B.3: Second-order Sobol indices for CO

B.4. HC

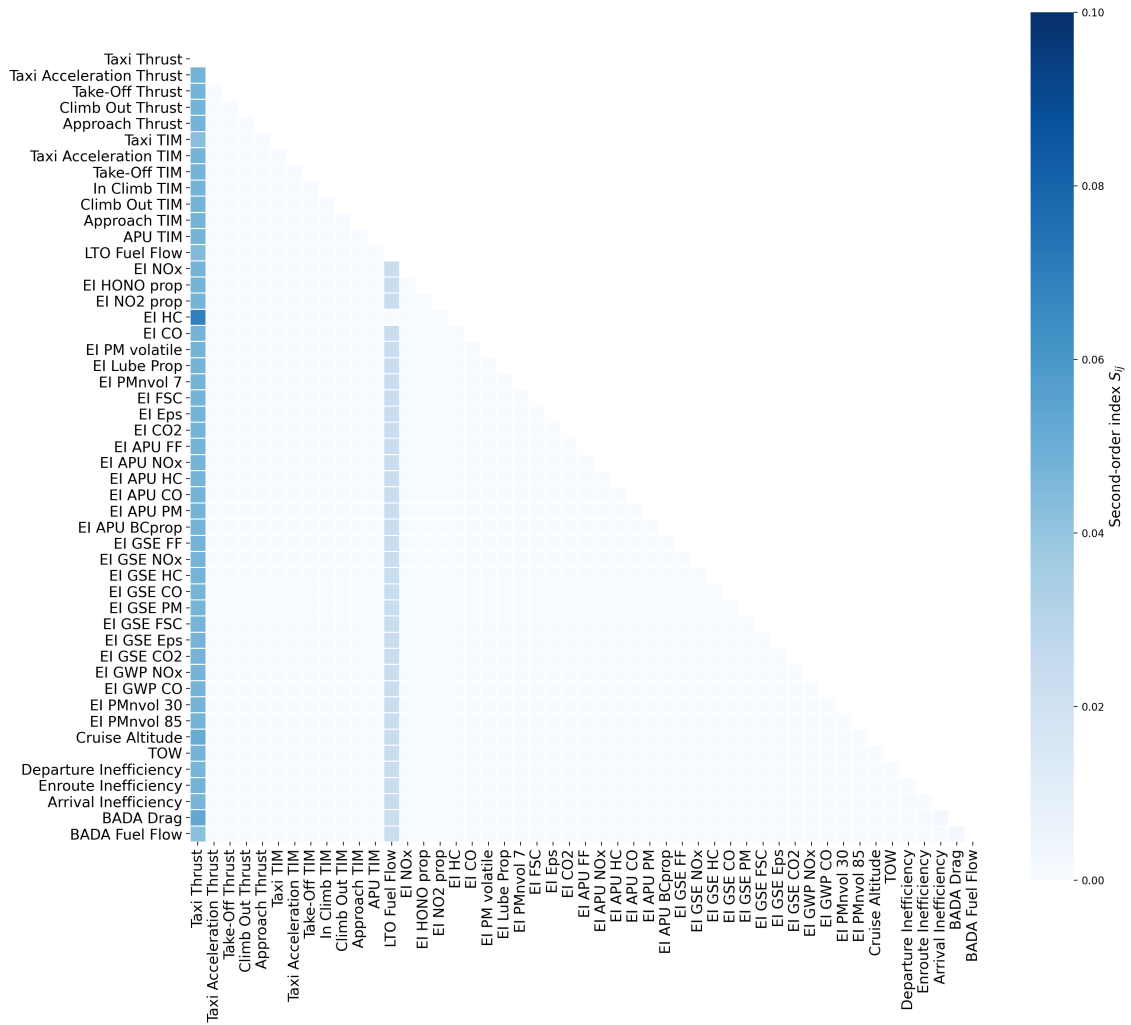


Figure B.4: Second-order Sobol indices for HC



Re-propagation Results for Global Fuelburn and Emissions Estimates

C.1. Fuelburn

Table C.1: Relative difference to global fuelburn estimates due to all updated inefficiencies

Simulation	Nominal (Tg)	Mean (Tg)	Median (Tg)	Standard Deviation (Tg)	Coefficient of Variation (%)	5 th -95 th percentile uncertainty range (Tg)
Baseline (Global)	180.44	182.08	180.58	28.98	15.91	134.42-229.75
EU Departure	-0.08%	-0.15%	-0.21%	0.00 %	+0.14%	134.15-229.48
Intra-EU Enroute	+0.07%	+0.01%	-0.16%	+0.38%	+0.37%	134.26-229.95
EU Arrival	-0.10%	-0.09%	-0.13%	-0.08%	+0.02%	134.28-229.54
Intercontinental Enroute	+0.49 %	-0.11%	-0.49%	+3.03%	+3.14%	132.77-230.99
Total	+0.37%	-0.34%	-0.70%	+4.01%	+4.36%	131.89-231.04
Total (values)	181.11	181.47	179.30	30.14	16.61	——"——

C.2. NO_x

Table C.2: Relative difference to global NO_x estimates for updated inefficiencies

Simulation	Nominal (Tg)	Mean (Tg)	Median (Tg)	Standard Deviation (Tg)	Coefficient of Variation (%)	5 th -95 th percentile uncertainty range (Tg)
Baseline	2.681	2.654	2.583	0.592	22.30	1.681-3.628
EU Departure	-0.12%	-0.21%	-0.13%	-0.05%	+0.16%	1.681-3.628
Intra-EU Enroute	+0.08%	+0.03%	+0.21%	+0.30%	+0.27%	1.676-3.622
EU Arrival	-0.05%	-0.04%	-0.07%	-0.04%	0.00%	1.679-3.631
Intercontinental Enroute	+0.39%	-0.12%	+0.09%	+1.72%	+1.84%	1.673-3.624
Total	+0.29%	-0.35%	-0.08%	+2.24%	+2.59%	1.661-3.641
Total (values)	2.688	2.645	2.580	0.605	22.88	——"——

C.3. CO

Table C.3: Relative difference to global CO estimates for updated inefficiencies

Simulation	Nominal (Tg)	Mean (Tg)	Median (Tg)	Standard Deviation (Tg)	Coefficient of Variation (%)	5 th -95 th percentile uncertainty range (Tg)
Baseline	0.756	0.774	0.748	0.233	30.12	0.391-1.158
EU Departure	-0.02%	-0.04%	-0.02%	-0.04%	0.00%	0.391-1.157
Intra-EU Enroute	+0.03%	-0.02%	+0.10%	+0.14%	+0.16%	0.390-1.158
EU Arrival	-0.92%	-0.80%	-0.98%	-0.32%	+0.48%	0.386-1.151
Intercontinental Enroute	+0.48%	+0.14%	+0.46%	+1.00%	+0.86%	0.388-1.163
Total	-0.44%	-0.71%	-0.54%	+0.89%	+1.61%	0.382-1.156
Total (values)	0.753	0.769	0.744	0.235	30.60	——"——

C.4. HC

Table C.4: Relative difference to global HC estimates for updated inefficiencies

Simulation	Nominal (Tg)	Mean (Tg)	Median (Tg)	Standard Deviation (Tg)	Coefficient of Variation (%)	5 th -95 th percentile uncertainty range (Tg)
Baseline	0.191	0.203	0.194	0.092	45.20	0.052-0.354
EU Departure	-0.01%	-0.02%	-0.05%	-0.01%	+0.01%	0.052-0.354
Intra-EU Enroute	+0.04%	-0.03%	-0.05%	+0.02%	+0.04%	0.052-0.354
EU Arrival	-3.13%	-2.56%	-2.75%	-0.61%	+2.00%	0.048-0.348
Intercontinental Enroute	+0.29%	+0.03%	+0.09%	+0.14%	+0.10%	0.052-0.354
Total	-2.82%	-2.57%	-2.98%	-0.45%	+2.18%	0.048-0.348
Total (values)	0.185	0.198	0.188	0.091	46.18	——"———

Bibliography

- [1] M. Stettler, S. Eastham, and S. Barrett. Air quality and public health impacts of UK airports. Part I: Emissions. *Atmospheric Environment*, 45(31):5415–5424, Oct 2011.
- [2] M. Stettler, S. Eastham, and S. Barrett. Air quality and public health impacts of UK airports. Part I: Emissions. Supporting Information. *Atmospheric Environment*, 45(31), Oct 2011.
- [3] T. Reynolds. Analysis of lateral flight inefficiency in global air traffic management. *8th AIAA Aviation Technology, Integration and Operations (ATIO) Conference*, (September):14–19, 2008.
- [4] I. Fuller, J.C. Hustache, and T. Kettunen. Enhanced Flight Efficiency Indicators. 2004.
- [5] N. Simone, M. Stettler, and S. Barrett. Rapid estimation of global civil aviation emissions with uncertainty quantification. *Transportation Research Part D: Transport and Environment*, 25:33–41, 2013.
- [6] Airbus. Global Market Forecast 2021-2040. In *Commercial Aircraft*. 2021.
- [7] Boeing. Global Environment Report 2020. In *Environment*. 2020.
- [8] International Energy Agency. Aviation – Analysis Report, 2020.
- [9] European Environment Agency. EMEP/EEA air pollutant emission inventory guidebook 2013: Technical guidance to prepare national emission inventories. *EEA Technical report*, (July):23, 2013.
- [10] Intergovernmental Panel on Climate Change. Long-term Climate Change: Projections, Commitments and Irreversibility. In *Climate Change 2013*. 2013.
- [11] C. Grobler, P. Wolfe, K. Dasadhikari, I. Dedoussi, F. Allroggen, R. Speth, S. Eastham, A. Agarwal, M. Staples, J. Sabnis, and S. Barrett. Marginal climate and air quality costs of aviation emissions. *Environmental Research Letters*, 14(11), 2019.
- [12] Air Transport Action Group. Fact Sheet #2: Aviation and Climate Change, 2020.
- [13] Intergovernmental Panel on Climate Change. Climate Change 2021: The Physical Science Basis. In *Contribution of Working Group I to the Sixth Assessment Report of the Intergovernmental Panel on Climate Change*. 2021.
- [14] UNFCCC. Article 2. *Kyoto Protocol to the United Nations Framework Convention on Climate Change*, 1998.
- [15] A. Bows, K. Anderson, and P. Peeters. Technology, Scenarios and Uncertainty. 2007.
- [16] International Civil Aviation Organization. ICAO 2019 Environment Report. *2019 Aviation and the Environment Report*, 2019.
- [17] Intergovernmental Panel on Climate Change. Summary for Policymakers. In *Aviation and the Global Atmosphere*. 1999.
- [18] Air Transport Action Group. The Right Flightpath to Reduce Aviation Emissions. *UNFCCC COP17*, (November):1–6, 2011.
- [19] International Civil Aviation Organization. ICAO Council adopts new CO2 emissions standard for aircraft, 2017.
- [20] Federal Aviation Administration. Aviation Environmental Design Tool (AEDT) 2a: Uncertainty Quantification Report. Technical Report February, FAA, 2014.

- [21] C. Zhu, R. Hu, B. Liu, and J. Zhang. Uncertainty and its driving factors of airport aircraft pollutant emissions assessment. *Transportation Research Part D: Transport and Environment*, 94(April), 2021.
- [22] D. Loucks and E. Beek. Water resource systems planning and management : An introduction to methods, models, and applications, 2017.
- [23] J. Lee. *Modeling aviation's global emissions, uncertainty analysis, and applications to policy*. PhD thesis, Massachusetts Institute of Technology, 2005.
- [24] D. Lim, Y. Li, M. Levine, M. Kirby, and D. Mavris. Parametric Uncertainty Quantification of Aviation Environmental Design Tool. 2018.
- [25] R. Smith. *Uncertainty Quantification: Theory, Implementation, and Applications*. Society for Industrial and Applied Mathematics, USA, 2013.
- [26] C. Lataniotis, S. Marelli, and B. Sudret. UQLab user manual – The Model module. Technical report, Chair of Risk, Safety and Uncertainty Quantification, ETH Zurich, Switzerland, 2021. Report # UQLab-V1.4-103.
- [27] International Civil Aviation Organization. Models and Databases, 2019.
- [28] M. Winther and K. Rypdal. EMEP/EEA air pollutant emission inventory guidebook 2019. Technical report, European Environment Agency, 2019.
- [29] C. Roof, A. Hansen, G. Fleming, T. Thrasher, A. Nguyen, C. Hall, E. Dinges, R. Bea, F. Grandi, B. Kim, S. Usdrowski, and P. Hollingsworth. Aviation Environmental Design Tool (AEDT) system architecture. 2007.
- [30] EUROCONTROL. Method for estimating aviation fuel burnt and emissions in the framework of the EMEP/EEA air pollutant emission inventory guidebook 2016. (July), 2016.
- [31] S. Olsen, D. Wuebbles, and B. Owen. Comparison of global 3-D aviation emissions datasets. *Atmospheric Chemistry and Physics*, 13(1):429–441, 2013.
- [32] B. Owen, D. Lee, and L. Lim. Flying into the future: Aviation emissions scenarios to 2050. *Environmental Science and Technology*, 44(7):2255–2260, 2010.
- [33] Federal Aviation Administration. Aviation Environmental Design Tool (AEDT) Version 3d, 2021.
- [34] N. Simone. Development of a Rapid Global Aircraft Emissions Estimation Tool with Uncertainty Quantification. Technical report, 2013.
- [35] J. Watterson, C. Walker, and S. Eggleston. Revision to the Method of Estimating Emissions from Aircraft in the UK Greenhouse Gas Inventory. Technical report, 2004.
- [36] B. Underwood, C. Walker, and M. Peirce. Heathrow Emissions Inventory 2002: Part 1. 2004.
- [37] APPENDIX Air quality and public health impacts of UK airports. (X):1–18, 2004.
- [38] European Union Aviation Safety Agency. ICAO Aircraft Engine Emissions Databank, 2018.
- [39] C. Wey, B. Anderson, C. Hudgins, X. Li-Jones, E. Winstead, L. Thornhill, P. Lobo, D. Hagen, and P. Whitefield. NASA.
- [40] C. Eyers, P. Norman, J. Middel, M. Plohr, S. Michot, K. Atkinson, and R. Christou. AERO2k Global Aviation Emissions Inventories for 2002 and 2025. 2004.
- [41] J. Lee, I. Waitz, B. Kim, G. Fleming, L. Maurice, and C. Holsclaw. System for assessing Aviation's Global Emissions (SAGE), Part 2: Uncertainty assessment. *Transportation Research Part D: Transport and Environment*, 12(6):381–395, 2007.
- [42] S. Baughcum, T. Tritz, S. Henderson, and D. Pickett. Scheduled Civil Aircraft Emission Inventories for 1992: Database Development and Analysis,. *NASA Contractor Report 4700*, 1996.

- [43] D. DuBois and G. Paynter. "Fuel Flow Method2" for Estimating Aircraft Emissions. *SAE Transactions*, 115:1–14, 2006.
- [44] M. Timko, S. Herndon, E. Wood, T. Onasch, M. Northway, J. Jayne, M. Canagaratna, R. Miake-Lye, and W. Knighton. Gas turbine engine emissions Part I: volatile organic compounds and nitrogen oxides. *Journal of Engineering for Gas Turbines and Power*, 132, 2010.
- [45] J. Hileman, R. Stratton, and P. Donohoo. Energy content and alternative jet fuel viability. *Journal of Propulsion and Power*, 26(6):1184–1195, 2010.
- [46] E. Wood, S. Herndon, M. Timko, P. Yelvington, and R. Miake-Lye. Speciation and chemical evolution of nitrogen oxides in aircraft exhausts near airports. *Environmental Science and Technology*, 42, 2008.
- [47] R. McClarren. Uncertainty quantification and predictive computational science : A foundation for physical scientists and engineers, 2018.
- [48] N. Simone, M. Stettler, S. Eastham, and S. Barrett. An open global civil aviation emissions dataset for 2005 (R1). Technical report, 2012.
- [49] E. de Cursi and R. Sampaio. Uncertainty Quantification and Stochastic Modeling with Matlab, 2015.
- [50] S. Marelli, C. Lamas, K. Konakli, C. Mylonas, P. Wiederkehr, and B. Sudret. UQLab user manual – Sensitivity analysis. Technical report, Chair of Risk, Safety and Uncertainty Quantification, ETH Zurich, Switzerland, 2021. Report # UQLab-V1.4-106.
- [51] A. Saltelli, M. Ratto, T. Andres, F. Campolongo, J. Cariboni, D. Gatelli, Saisana M., and Tarantola S. *Global Sensitivity Analysis: The Primer*. 2008.
- [52] A. Saltelli, P. Annoni, I. Azzini, F. Campolongo, M. Ratto, and S. Tarantola. Variance based sensitivity analysis of model output. Design and estimator for the total sensitivity index. *Computer Physics Communications*, 181(2):259–270, 2010.
- [53] I. Sobol'. Global sensitivity indices for nonlinear mathematical models and their Monte Carlo estimates. *Mathematics and Computers in Simulation*, 55:271–280, 2001.
- [54] D. Shao, G. Jiang, C. Zong, Y. Xing, Z. Zheng, and S. Lv. Global sensitivity analysis of behavior of energy pile under thermo-mechanical loads. *Soils and Foundations*, 61, 2021.
- [55] M. Jansen. Analysis of variance designs for model output. *Computer Physics Communications*, 117(1):35–43, 1999.
- [56] N. Simone, M. Stettler, S. Eastham, and S. Barrett. Aviation Emissions Inventory Code (AEIC) User Manual (R1). Technical report, 2013.
- [57] M. Stettler, A. Boies, A. Petzold, and S. Barrett. Global civil aviation black carbon emissions. *Environmental Science and Technology*, 47(18):10397–10404, 2013.
- [58] K. Seymour, M. Held, G. Georges, and K. Boulouchos. Fuel Estimation in Air Transportation: Modeling global fuel consumption for commercial aviation. *Transportation Research Part D: Transport and Environment*, 88(October):102528, 2020.
- [59] EUROCONTROL. Environmental Assessment: European ATM Network Fuel Inefficiency Study. 2020.
- [60] J. Leones, M. Polaina Morales, L. D'Alto, P. Escalonilla, D. Ferrer Herrer, M. Bravo, F. Càmara, A. Martínez Mateo, B. Namee, S. Wang, A. Grover, and P. Plantholt. Advanced Flight Efficiency Key Performance Indicators to support Air Traffic Analytics: Assessment of European flight efficiency using ADS-B data. 2018.
- [61] EUROCONTROL. R&D Data Release - Metadata, 2020.
- [62] I. Fuller, J.C. Hustache, and T. Kettunen. Flight Efficiency and its Impact on the Environment 2003 Study. 2003.

-
- [63] T. Kettunen, J.C. Hustache, I. Fuller, Howell D., and D. Knorr. Flight Efficiency Studies In Europe And The United States. 2005.
- [64] T. Reynolds. Development of flight inefficiency metrics for environmental performance assessment of ATM. *Proceedings of the 8th USA/Europe Air Traffic Management Research and Development Seminar, ATM 2009*, pages 440–449, 2009.
- [65] F. Dekking, C. Kraaikamp, H. Lopuhaä, and L. Meester. *A Modern Introduction to Probability and Statistics*. 2005.
- [66] Federal Aviation Administration. Aviation Environmental Design Tool (AEDT) 3d: Technical Manual. Technical Report March, FAA, 2021.
- [67] B. Kim, G. Fleming, J. Lee, I. Waitz, J. Clarke, S. Balasubramanian, A. Malwitz, K. Klima, M. Locke, C. Holsclaw, L. Maurice, and M. Gupta. System for assessing Aviation’s Global Emissions (SAGE), Part 1: Model description and inventory results. *Transportation Research Part D: Transport and Environment*, 12(5):325–346, 2007.
- [68] EUROCONTROL. European Aviation Fuel Burn and Emissions Inventory System for the European Environment Agency. 2018.
- [69] International Civil Aviation Organization. Annual Report 2020, 2020.